SYNTHESIS AND OXIDATION KINETICS OF TRANSITION METAL COMPLEXES

RHONDA LUCAS

INFORMATION TO USERS

This manuscript has been reproduced from the microfilm master. UMI films the text directly from the original or copy submitted. Thus, some thesis and dissertation copies are in typewriter face, while others may be from any type of computer printer.

The quality of this reproduction is dependent upon the quality of the copy submitted. Broken or indistinct print, colored or poor quality illustrations and photographs, print bleedthrough, substandard margins, and improper alignment can adversely affect reproduction.

In the unlikely event that the author did not send UMI a complete manuscript and there are missing pages, these will be noted. Also, if unauthorized copyright material had to be removed, a note will indicate the deletion.

Oversize materials (e.g., maps, drawings, charts) are reproduced by sectioning the original, beginning at the upper left-hand corner and continuing from left to right in equal sections with small overlaps.

ProQuest Information and Learning
300 North Zeeb Road, Ann Arbor, MI 48106-1346 USA
800-521-0600

Synthesis and Oxidation Kinetics of Transition Metal Complexes

by

Rhonda Lucas

A thesis submitted to the School of Graduate Studies in partial fulfilment of the requirements for the degree of Master of Science.

Department of Chemistry
Memorial University of Newfoundland

September 2001

Abstract

The nickel (II) complexes of the deprotonated pendant-arm macrocycles 5,5,7,12,12,14-hexamethyl-1,4,8,11-tetraazacyclotetradecane-1,8-diacetic acid (L_1) and 5,12 dimethyl - 7, 14-diphenyl-1,4,8,11 tetraazacyclotetradecane-1,8-diacetic acid (L_2) have been prepared. The oxidation kinetics of these complexes with peroxodisulfate have been studied. Enthalpies and entropies of activation for Ni(II)L_1 are 39.5 ± 5.3 kJ.mol^{-1} and -115 ± 5 J.K^{-1}. mol^{-1}; and for Ni(II)L_2 the corresponding values are 42.8 ± 5.1 kJ.mol^{-1} and -115 ± 5 J.K^{-1}. mol^{-1}. Outer-sphere oxidation of Ni(II)L_1 by bis - (triazacyclononane)nickel (III), $[Ni(III)(tacn)_2]^{3+}$, has been studied and a self-exchange rate constant for the $[Ni(II)L_1]^{0,+}$ system has been estimated at 55 mol^{-1} dm^3 s^{-1}.

The *rac*-Ni(II)L_2 complex and *meso*-Co(III)L_1^+ have been structurally characterized by X-ray crystallography. The *rac*-Ni(II)L_2 complex shows a distorted *cis*-geometry about the metal while the *meso*-Co(III)L_1^+ complex show a *trans* octahedral geometry.

Acknowledgments

I would like to thank all those who assisted me in the completion of this study. I thank my parents, for their endless support and encouragement. Thank-you to Dr. Robert Haines for his time and assistance. I thank my supervisory committee, Dr. Peter Pickup and Dr. Bob Lucas, who have gone beyond the duties of a supervisory committee. Thank-you to David Miller for providing the X-ray crystallograpy data and Dean Hutchings for his assistance with the electrochemistry. I would also like to acknowledge the Natural Sciences and Engineering Research Council of Canada for their financial support, as well as the School of Graduate Studies and the Chemistry Department of Memorial University.

Table of Contents

List of Tables

List of Figures

List of Appendices

Chapter 1: Introduction

1.1. Macrocycles and Pendant Arm Macrocycles.

Extensive studies have been carried out on the synthesis and characterization of metal complexes of macrocyclic ligands. A macrocyclic ligand is a polydentate ligand in which several donor atoms form parts of a large ring such as the porphyrin ring system found complexed with iron at the oxygen binding site of hemoglobin.[1] In this case, the donor atoms consist of four nitrogen atoms. Another such example is chlorophyll a. Although there are nitrogen donors in both these cases, oxygen and sulfur donor atoms, and combinations thereof, are also common.[2,3]

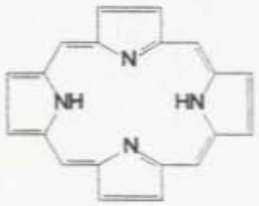

Porphyrin Ring

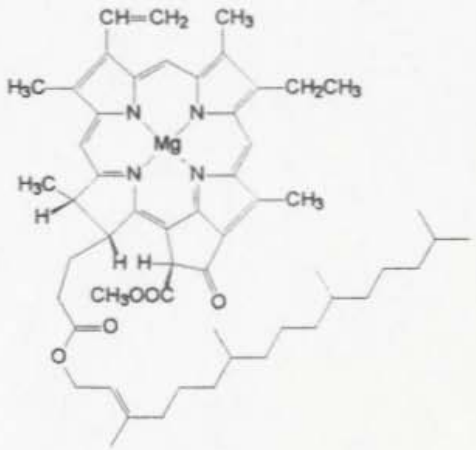

Chlorophyll a

Macrocycles are studied because of their interesting properties, including the selectivity shown by some of the ligands for metal complexation and the high stability of many of

their metal complexes. For example, the Ni^{2+} complex of 1,4,8,11-tetraazacyclotetradecane (cyclam) (I) is fully stable in 10 mol/L $HClO_4$, whereas the Ni^{2+} complex of the analogous acyclic ligand, 1,4,8,11-tetraazaundecane (II), dissociates with a half-life of approximately 170 ms in 6.1 M HCl.[4]

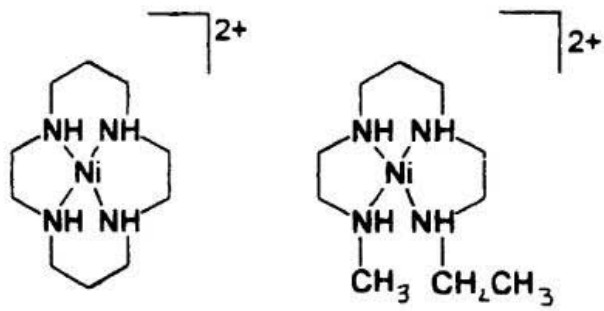

(I) (II)

The high thermodynamic stability of macrocyclic complexes is known as the macrocyclic effect, whereby there is an enhancement of complex stability when a macrocyclic ligand replaces a comparable open-chain ligand.[5] For example, the potassium complex of the crown ether, cyclo-$(CH_2CH_2O)_6$ has a formation constant 10^4 times larger than that of $CH_3O(CH_2\ CH_2O)_5CH_3$. The macrocyclic effect is thought to be due primarily to entropy factors although steric strain, and different conformations of the ligand also have an effect.

In most macrocyclic ligands described in the literature, the coordinating atoms are an integral part of the cyclic structure. There are, however, a few macrocyclic ligands which, besides the donor groups of the ring, have additional ligating groups attached to a side chain.[2, 6, 7] These ligands are commonly referred to as pendant-arm macrocycles. These macrocyclic complexes with functional groups have been synthesized in order to investigate how the functional groups affect the properties of the macrocyclic complexes. Functionalization can modify or introduce new properties into a complex. It can, for example, lead to more stable or more selective complexation or to complexation with faster kinetics.[5] It can also affect the coordination geometry of metal ions or thermodynamically enhance the metal-based redox processes.[8] Pendant-arm macrocycles have found applications in tumor targeting,[9] ion selectivity[10] and electrocatalysis.[5, 11]

Polyazamacrocycles containing mainly nitrogen ring donor atoms are frequently functionalized. Tetraazamacrocycles, i.e, those which have four nitrogen donors, are capable of producing strong ligand fields, yet have the inherent disadvantage of not being able to completely coordinate the majority of transition metal ions which prefer coordination numbers of six.[12] By increasing the ring size and the number of atoms or by appending coordinating groups to the periphery of the macrocycles, one can gain insight into the ability of the macrocycle to coordinate transition metal ions. These additional groups may coordinate to the central metal thereby increasing the ligating ability of the macrocycle. Functionalization is commonly achieved using a nitrogen atom of the

macrocycle as an attachment point. For instance, amine, hydroxyl, amide, carboxylic and nitrite functional groups have been attached to the side chains of the coordinated nitrogen donors.[13] Some of these donors coordinate metal ions intramolecularly at the axial position forming 5 or 6 membered chelate rings.[14]

Most functionalized macrocyclic complexes have been synthesized by inserting the metal ions into the free ligands which have first been prepared by rather elaborate multi-step procedures. Synthetic routes toward incompletely N-alkylated aza macrocycles are more complicated than the synthesis of the completely N-substituted relatives. Examples of mono-, di-, tri- and tetra- derivatives can be found in the literature.[15, 16] The range of mono- to tetra- functionalized ligands depends on the ratio of macrocycle to functional group used in the synthesis.

Tetraaza-pendant-arm macrocycles have important applications in medicinal chemistry. In radioimmunotherapy, a sterilizing dose of radiation is delivered selectively to the tumor stem cells.[9] In this treatment it is essential that a radiolabelled antibody be stable *in vivo* over a period of days. Pendant-arm macrocyclic complexes, because of their slow rate of metal dissociation and their slow acid dependent decomplexation, show encouraging results in addressing this issue.[16, 17] The majority of studies in this area are being performed on tetraazamacrocycles with carboxylate pendant-arms[18], however, amine, nitro and pyridyl functionalities are also being investigated.[19,16] Figures 1.1 to 1.4 show the structures of some pendant arm ligands from the literature.

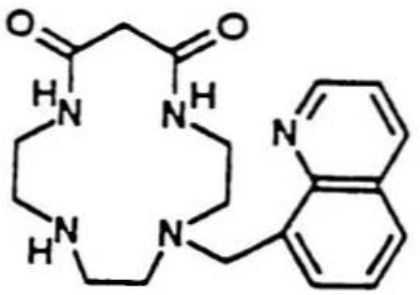

Fig. 1.1. 4-(quinolin-8-ylmethyl)-1,4,7,10-tetraazacyclotridecane-11,13-dione.

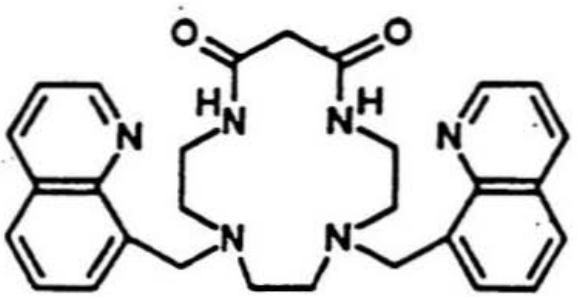

Fig. 1.2. 4,7-bis(quinolin-8-ylmethyl)-1,4,7,10-tetraazacyclotridecane-11,13-dione.

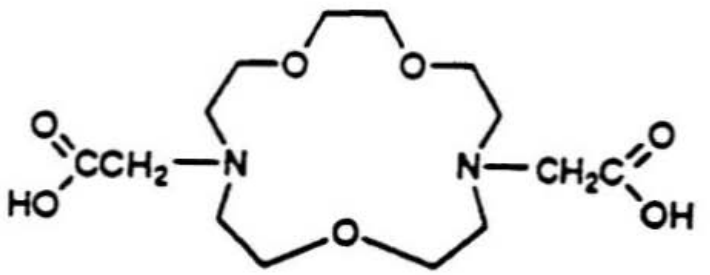

Fig.1.3. 1,4,10-trioxa-7,13-diazacyclopentadecane-N,N^{1}-diacetic acid.

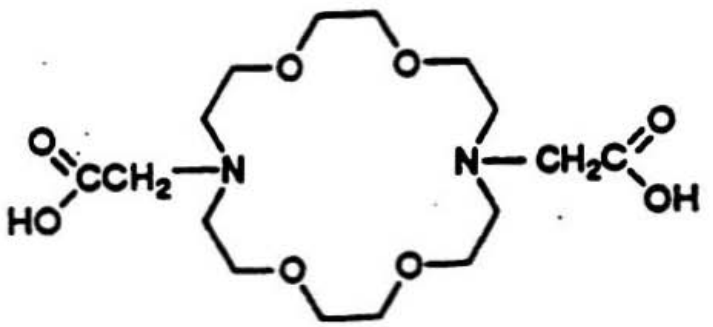

Fig.1.4. 1,4,10,13-trioxa-7,16-diazacyclopentadecane-N,N^{1}-diacetic acid.

1.2. Reaction Kinetics

Kinetic measurements provide important tools for assessing the reactivity of pendant-arm macrocycles. Kinetics is the area of chemistry concerned with the speed of the process whereby a system changes from one state to another. The primary use of kinetics is in the study of reaction mechanisms. Kinetics allows the determination of the experimental rate law for a reaction which is in turn related to the elementary processes or steps of the reaction. The rate law is useful to the mechanist in two ways. First, the kinetic order often suggests the number of molecules involved in the rate determining step of the mechanism. Second, the characteristic rate of a reaction can be determined from its rate law. Rate constants, which are part of the rate law, prove useful for comparison of rates of analogous reactions. Any proposed mechanism should, therefore, be consistent with the rate law.

Kinetic studies are also useful for obtaining knowledge about the activation parameters of a reaction. That reaction rates increase with increasing temperature has long been known on a purely empirical basis. For many reactions it is found that the rate constant varies with temperature according to

$$k = A\exp(-\frac{E_a}{RT}) \qquad \text{Eqn. 1.1}$$

where E_a is the activation energy, the constant A being the pre-exponential or frequency factor, k the rate constant, T the absolute temperature, and R the ideal gas constant. The

frequency factor, A, expresses the rate at which molecules approach close enough to interact. The exponential term expresses the proportion of interactions that have enough energy to overcome the activation-energy barrier.

Equation 1.1, known as the Arrhenius equation, can be validated by simple thermodynamic arguments.[20] The implication of this equation for experimental studies is that the temperature of the reaction mixture must be held as constant as possible throughout the course of the reaction, otherwise the observed reaction rate will be a meaningless average of rates at different temperatures. The Arrhenius equation is usually not followed precisely over a very wide temperature range, in which case more sophisticated treatments are required. Equation 1.1 can be rewritten as the following linear expression:

$$\ln k = \ln A - \frac{E_a}{RT} \qquad \text{Eqn. 1.2}$$

Examination of this expression indicates that a plot of ln k versus T^{-1} should be linear with a slope equal to $-E_a / R$ and a vertical intercept equal to ln A.

A temperature dependence study can be performed whereby the observed rate constant, k_{obs} is determined over a range of temperatures. Using this information, the values of E_a and A can be determined. From these values, activation parameters can be calculated. The sign and magnitude of such parameters can help determine the type of mechanism by which

the reaction proceeds.

The connection between activation parameters and kinetic results is given by Transition State Theory. Consider the following equilibrium between the reactants, A and B, and the activated complex:

$$A + B \rightleftharpoons [AB]^{\ddagger} \rightarrow products$$

The activated complex is treated as an equilibrium species, and an equilibrium constant is defined:

$$K_c^{\ddagger} = \frac{[AB]^{\ddagger}}{[A][B]} \qquad \text{Eqn. 1.3}$$

If we define f, the transmission factor, as the probability that the activated complex will, once formed, go over to the product state, then the specific bimolecular rate constant is:

$$k_{obs} = fK_c^{\ddagger} \qquad \text{Eqn. 1.4}$$

Based on statistical mechanics, the transmission factor f is:

$$f = \frac{k_b T}{h} \qquad \text{Eqn. 1.5}$$

where k_b is Boltzman's constant and h is Planck's constant. Substituting equation 1.5 into

equation 1.4 yields an expression for the observed rate constant, k_{obs}, for a second-order reaction:

$$k_{obs} = k_b \frac{TK_c^*}{h} \qquad \text{Eqn. 1.6}$$

The standard free energy for the formation of the activated complex can be separated into enthalpic and entropic contributions with:

$$\Delta G^* = \Delta H^* - T\Delta S^* \qquad \text{Eqn. 1.7}$$

The standard free-energy change is related to the equilibrium constant by:

$$\Delta G^* = -RT\ln K_c^* \qquad \text{Eqn. 1.8}$$

Using this, with equations 1.6, and 1.7 gives:

$$k_{obs} = k_b \frac{T}{h} \exp\left(\frac{-\Delta G^*}{RT}\right) \qquad \text{Eqn. 1.9}$$

$$k_{obs} = \frac{k_b T}{h} \exp\left(\frac{\Delta S^{\neq}}{R}\right) \exp\left(\frac{-\Delta H^{\neq}}{RT}\right) \qquad \text{Eqn. 1.10}$$

By rearranging equation 1.10 and taking the natural logarithm (ln), we arrive at the Eyring equation:

$$\ln\frac{k_{obs}}{T} = \ln\frac{k_b}{h} + \Delta\frac{S^{\neq}}{R} - \Delta\frac{H^{\neq}}{RT} \qquad \text{Eqn 1.11}$$

Hence, plotting ln (k_{obs}/T) versus 1/T will give a slope equal to $-\Delta H^{\neq}/R$ and an intercept equal to ln (k_b /h) $+\Delta S^{\neq}/R$. Hence, from an Eyring plot,

$$\Delta H^{\neq} = -R(Slope) \qquad \text{Eqn.1.12}$$

$$\Delta S^{\neq} = R(intercept - \ln\frac{k_b}{h}) \qquad \text{Eqn 1.13}$$

Using these equations, and the Arrhenius equation, the Arrhenius parameters for a solution reaction are shown to be:

$$E_a = \Delta H^{\neq} + RT \qquad \text{Eqn. 1.14}$$

$$A = \frac{ek_b T}{h} \exp\left(\frac{\Delta S^*}{R}\right) \qquad \text{Eqn. 1.15}$$

For a reaction, A + B → products, carried out under pseudo-first-order conditions (excess B), that is first order in A, the rate law is:

$$\frac{-d[A]}{dt} = k_{obs}[A] \qquad \text{Eqn. 1.16}$$

This rearranges into:

$$\frac{-d[A]}{[A]} = k_{obs}\,dt \qquad \text{Eqn 1.17}$$

which can be integrated directly. Noting that at time t = 0 the concentration of A is $[A]_0$ and that at a later time t it is $[A]_t$, we have

$$\int \frac{d[A]}{[A]} = \int k_{obs}\,dt \qquad \text{Eqn. 1.18}$$

$$\ln[A]_t - \ln[A]_0 = k_{obs}t$$

Based on this equation, a plot of ln $[A]_t$ versus time should give a straight line with a slope equal to the first-order rate constant, k_{obs}.

The relationship between concentration at time t and absorbance is given by Beer's law:

$$D = bc\epsilon$$

where D is absorbance, b is pathlength, c is molar concentration, and ϵ is the molar absorptivity. Using Beer's law, along with equation 1.14, we see that absorbance is related to the observed rate constant as follows:

$$\ln(D_\infty - D_t) = k_{obs}t \qquad \text{Eqn. 1.19}$$

When experimentally determining rate constants, it is important to keep a constant ionic strength. Ionic strength is a useful measure of the total concentration of ions in a solution, and is defined as

$$\mu = \frac{1}{2}\sum c_i z_i^2 \qquad \text{Eqn. 1.20}$$

where μ is the ionic strength, c_i is the concentration of the ith species, and z_i is its charge. The sum extends over all ions in solution. It is necessary to keep ionic strength constant when determining rate constants since rate constants are dependent on activity coefficients which are in turn influenced by the ionic strength.[20] The relationship between activity

coefficients and rate constants is given by transition-state theory. For a bimolecular reaction of the following type:

$$A + B \rightleftharpoons (A - - - B)^{*} \rightarrow Products \qquad \text{Eqn. 1.21}$$

transition -state theory predicts that the rate is given by

$$Rate = \frac{kTK^{*}}{h}\frac{\gamma_A \gamma_B}{\gamma^{*}}[A][B] = k[A][B] \qquad \text{Eqn. 1.22}$$

where γ_A, γ_B, and γ^{*} are the activity coefficients of the reactants and transition state, respectively. The relationship between activity coefficients (γ_i) and μ is given by the Debye-Hückel limiting law, which applies for $\mu \leq 0.01$ M:

$$\log\gamma_i = -Az_i^2\mu^{\frac{1}{2}} \qquad \text{Eqn. 1.23}$$

where A is a constant for a given solvent and z_i is the charge of the ion. Thus, by maintaining a constant ionic strength, variation of the activity coefficients with reagent concentrations is eliminated. A fixed ionic strength can be achieved by the addition of some "inert electrolyte" such as potassium nitrate or potassium sulfate.

1.3. Peroxodisulphate Kinetics

For a number of years now there have been a significant number of kinetic studies on redox reactions involving the peroxodisulphate anion, $S_2O_8^{2-}$, and transition metal complexes.[21] Peroxodisulphate is often chosen as an oxidizing agent since it is a very strong two-electron oxidant with a redox potential of 2.2 V versus the standard hydrogen electrode. As a result of this high redox potential, the peroxodisulphate anion is capable of oxidizing transition metal complexes to higher oxidation states. In particular it can smoothly oxidize Ni(II) to the tervalent state. Furthermore, oxidation by peroxodisulphate is a relatively slow process and therefore, reaction kinetics can readily be studied by conventional means.

The oxidation of Ni(II) complexes to Ni(III) by a variety of oxidants has been shown to proceed via an outer-sphere mechanism.[21] An outer sphere mechanism is one in which there is little interaction between the oxidant and the reductant at the time of electron transfer and both species go through the process with their coordination shells intact. A common example of an outer sphere reaction is given in eqn 1.24.[22]

$$^{*}[Mn^{VII}O_4]^{-} + [Mn^{VI}O_4]^{2-} \rightarrow {}^{*}[Mn^{VI}O_4]^{2-} + [Mn^{VII}O_4]^{-} \qquad \text{Eqn 1.24}$$

Transition metal oxidations, however, can also proceed via an inner-sphere mechanism. In this case the electron transfer occurs via a bridging ligand. The classical "Taube reaction," eqn. 1.25, is a particularly well-examined case of such an inner-sphere electron transfer

pathway.

$$Cr(OH_2)_6^{2+} + Co(NH_3)_5Cl^{2+} \rightarrow Cr(OH_2)_5Cl^{2+} + Co(OH_2)_6^{2+} - 5NH_3^{+} \qquad \text{Eqn. 1. 25}$$

Characteristics of this mechanism are rapid electron transfer and a trapping of the bridging ligand in the first coordination sphere of the oxidized species. In the "Taube reaction," replacing chloride by a ligand that is incapable of bridging (eg., NH_3), results in a relatively slow outer-sphere electron transfer process and the ligand does not appear in the oxidized product.

In order for inner-sphere electron transfer to occur there must clearly be a bridging ligand present. Such a ligand must contain at least two pairs of unshared electrons which are necessary for simultaneous bonding to the oxidizing and reducing centers. Even when these criteria are met, however, an outer-sphere electron transfer may still occur. Other factors must also be considered. For example, the bridge must be an effective mediator for electron transfer. Also, the type of electron transfer reaction which occurs depends on the affinity of the reductant for the bridging ligand. The preference of a reductant for a particular bridging ligand is reflected in the hard or soft nature of both the metal center and the ligand. A hard metal such as Fe^{3+}, for example, will be more likely to bridge with a hard base such as F^- rather than Br^-. The opposite would be true for a soft acid such as Cr^{2+}.

A wide range of bridging ligands are known, such as the halide ions, pseudohalide ions, hydroxide ion, and carboxylate ions. Carboxylate pendant-arm macrocycles that have the

appendages coordinated to a central transition metal ion may provide an inner-sphere pathway for electron transfer to or from other metal centers. Carboxylate groups, being hard bases, have the potential to form bridges with iron(III) metal centers, which are hard acids. Electron transfer from a transition metal in a macrocyclic complex to iron(III) has important industrial implications. Such behavior has application in reductive dissolution of iron(III)-bearing ferrites, which constitute corrosion films found in industrial boilers and nuclear reactors. The focus of this thesis is to study the behavior of various pendant arm macrocycles so as to help determine their potential for providing an inner sphere pathway suitable for electron transfer.

1.4. Stopped Flow Kinetics

Electron transfer reactions usually occur with half lives of milliseconds to seconds. The stopped-flow method is generally used to study such fast reactions which can be defined as those with half-lives of less than one second. The half life of a reaction, $\tau_{1/2}$, is related to the rate constant as follows:

$$k_{obs} = \frac{\ln 2}{\tau_{1/2}} \qquad \text{Eqn. 1.26}$$

Stopped flow kinetics are identical to those in a normal static batch reaction as it is the change in concentration with time of a particular component of the solution that is measured. Thus, data analysis is the same. Stopped flow kinetics are used in this study to examine the reactivity of pendant-arm macrocycles.

Chapter 2: Experimental

2.1. Synthesis

All chemicals were analytical grade and were not purified further. A list of solvents and chemicals used, along with their source and purity is given in table 2.1 and 2.2. Infrared spectra were recorded on a Bomem Michelson Fourier Transform spectrometer. Elemental analyses were performed by the University of Saskatchewan.

Table 2.1. Solvents used, Source of Solvents and Purity of Solvents.

Solvent	Source	Purity
Acetone	Fisher	Certified ACS, ≥99.5%
Dichloromethane	Aldrich	ACS. spec., 99.5%
DMF	Anachemia	ACS. spec.
Ethanol	Commercial Alcohol	95%
Ether	BDH	99%
Methanol	Fisher	ACS, ≥99%

Table 2.2. Chemicals Used, Source of Chemicals and Purity of Chemicals

Chemical	Source	Purity
Amberlite IRA-400 ion exchange resein	Aldrich	
Bromoacetic acid	Sigma	ACS Reagent, 99%
Cobalt(II) chloride	Mallinckrodt	100.0 %
Diethylenetriamine	Fisher	≥98%
Ethylenediamine	Sigma	
Hydrochloric acid	Fisher	ACS., 95 -98%
Hydrobromic acid	Fisher	Certified ACS, 47 - 79 %
Lithium hydroxide, anhydrous	Fisher	Laboratory grade
Nickel(II) chloride	BDH	AnalaR, 98.0%
Nickel(II) perchlorate	ALFA	
Perchloric acid	BDH	Certified ACS, 60 %
Potassium carbonate	Sigma	ACS Reagent, ≥99.0 %
Potassium peroxodisulfate	Fisher	Certified ACS, ≥99.0 %
Potassium sulfate	BDH	ACS Reagent, ≥99.0 %
Sodium carbonate	Sigma	ACS , 99.95 - 100.05%
Sodium hydroxide	BDH	ACS Reagent, ≥97.0 %
Sodium hydride, dry	Aldrich	95%
Sodium tetrahydroborate	BDH	ACS Reagent, ≥99.5 %
Sulfuric acid (conc.)	Fisher	ACS., 95 -98%
p-toluenesulphonyl chloride	Sigma	99%
Triethylamine	Anachemia	98%

Fisher Certified ACS grade potassium peroxodisulfate was purified so as to obtain reproducible, clean kinetics. This was accomplished by first washing several times with distilled water, then recrystallizing four times from cold water, rinsing with ice-water and drying over P_4O_{10} in vacuo.

I. Synthesis of 5,5,7,12,12,14-hexamethyl-1,4,8,11-tetraazacyclotetradecane-4,11-diacetic acid (L_1).

The ligand L_1 was prepared according to a modification of the literature preparation using the following scheme:[23, 24, 25]

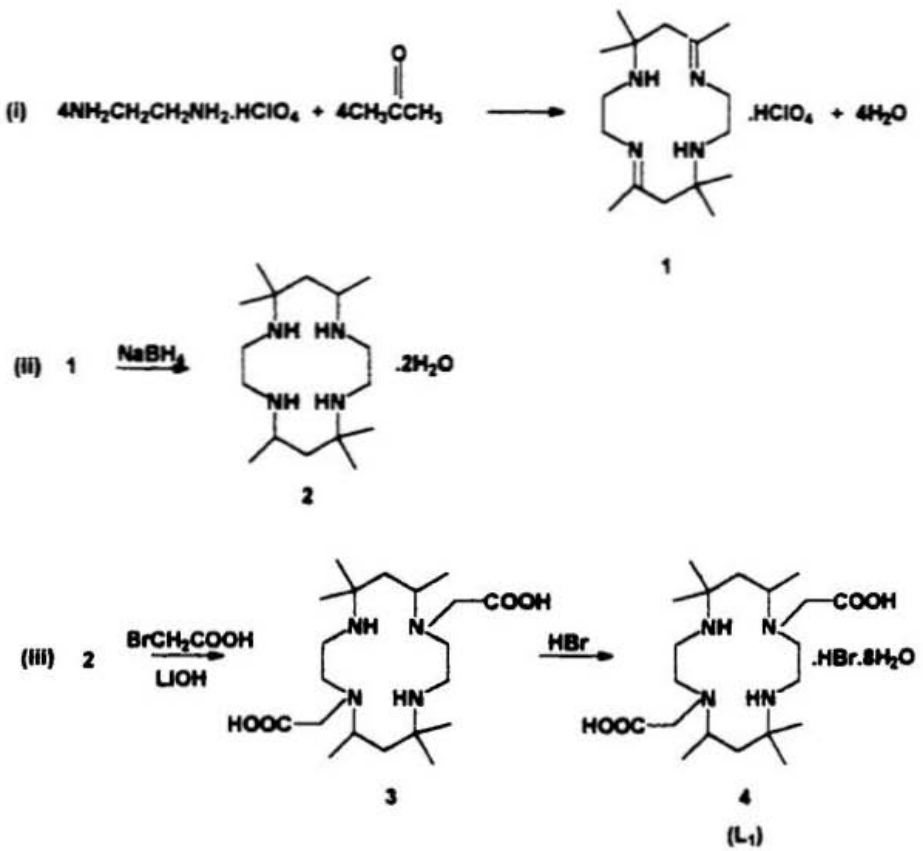

The modifications to the literature procedure were for the most part quite simple modifications of conditions, that resulted in slightly better yields. Reaction (iii) used a greater excess of bromoacetic acid over ligand 2 than did the literature, so as to ensure the di-substituted product.

Method

*Reaction (i): 5,7,7,12,14,14-Hexamethyl-1,4,8,11-tetraazacyclotetradecadiene diperchlorate, **1**:*

To 500 mL of anhydrous acetone was added 20 g (0.33 mol) of ethylenediamine. The solution was stirred while 55 g (0.33 mol) of 60% perchloric acid was added slowly from a dropping funnel over a 30-minute period. An orange-brown color developed and the solution became hot. Following addition of the acid, the solution was stirred rapidly and was cooled to room temperature. The white crystalline product was isolated by suction filtration and washed thoroughly with cold acetone. The yield of 5,7,7,12,14,14-hexamethyl-1,4,8,11-tetraazacylcotetradecadiene diperchlorate was 50 g (73%).

*Reaction (ii): meso-(5,5,7,12,12,14-hexamethyl-1,4,8,11-tetraazacyclotetradecane) dihydrate, **2**:*

To 250 mL of methanol was added 50 g (0.11 mol) of **1**. The solution was stirred and 9.5 g (0.32 mol) of sodium tetrahydroborate and 8.2 g (0.21 mol) of sodium hydroxide were added in alternate portions over a one-hour period. The solution was stirred at room

temperature for a one-hour period and then heated to reflux for fifteen minutes. After cooling, 25 g of sodium hydroxide in 50 mL of water was added and the solution was stirred until precipitation of the product was complete. The white product was then collected by filtration, washed with cold water and air-dried.

The product was then dissolved in 300 mL of methanol, refluxed and filtered. The filtrate was diluted to 300 mL with methanol and the solution was refluxed again. Water (200 mL) was added to the hot solution, which was then stirred and cooled to room temperature. The white solid was collected by filtration, washed with cold water and dried over P_4O_{10}. The yield was 50 g (85%). m.p. 144 - 146,°C, lit. m.p. 146 - 148°C.

Reaction (iii): 5,5,7,12,12,14-hexamethyl-1,4,8,11-tetraazacyclotetradecane-$N^{I}N^{III}$-diacetic acid, **4***:*

To 41.7 g (0.300 mol) of bromoacetic acid in 150 mL of water was added 12.0 g (0.300 mol) of NaOH in 100 mL of cold water, while maintaining the temperature below 5°C. To the mixture were added 32.0 g (0.0500 mol) of **2** in 250 mL of methanol and 31.8 g (0.300 mol) of Na_2CO_3. The mixture was stirred and the temperature was maintained at 65°C for 48 h. The reaction mixture was then cooled and filtered. The filtrate was concentrated to 100 mL and acidified to pH 3 with hydrobromic acid.. The solution was cooled for 24 h. A white precipitate formed and was collected by filtration to yield 21 g (60%) of ligand L_1. m.p. 256 -259°C, lit. m.p. 258 - 260°C. IR: 3400 (OH), 2800 - 2900 (NH_2^+), 1730 (COOH) (KBr discs).

II. Synthesis of Ni(II)L_1·2HCl.H_2O

$$NiCl_2.6H_2O + L_1 \xrightarrow{NaOH} NiL_1.2HCl.H_2O$$

To 350 mg (0.500 mmol) of L_1 dissolved in 20 mL of water was added 238 mg (1.00 mmol) of $NiCl_2 \cdot 6H_2O$. The pH was adjusted to pH 5 with 0.1 mol/L NaOH and the mixture was heated to reflux for 24 h. The solution was concentrated to approximately 10 mL and violet crystals formed. These were collected and air dried to yield 197 mg of product (70%). *Anal.* Found: C 43.78, H 7.77, N 10.94. Calcd. for $NiC_{20}H_{18}N_4O_4.2HCl.H_2O$: C43.82, H 7.72, N 10.22 %. IR (KBr cm^{-1}): 3396 (OH), 3124 (NH), 1623 (COO^-).

III. Synthesis of Co(III)L_1· Cl

$$CoCl_2.6H_2O + L_1 \xrightarrow{NaOH} CoL_1.Cl$$

To 350 mg (0.5 mmol) of L_1 dissolved in 20 mL of water, was added 238 mg (1.0 mmol) of $CoCl_2 \cdot 6H_2O$ and the pH was adjusted to pH 5 with 0.1 mol/L NaOH. The mixture was heated to reflux for several days. The mixture was concentrated in volume to approximately 10 mL and red crystals formed. These crystals were then dissolved in boiling water, filtered and cooled to yield the final product. IR (KBr cm^{-1}): 3430 (OH), 3149 (NH), 1649 (COO^-).

IV. Synthesis of 5,12 dimethyl - 7, 14-diphenyl-1,4,8,11 tetraazacyclotetradecane-1,8-diacetic acid (L_2).

The ligand L_2 was prepared according to a modification of the literature preparation using the following scheme:[23, 26, 27]

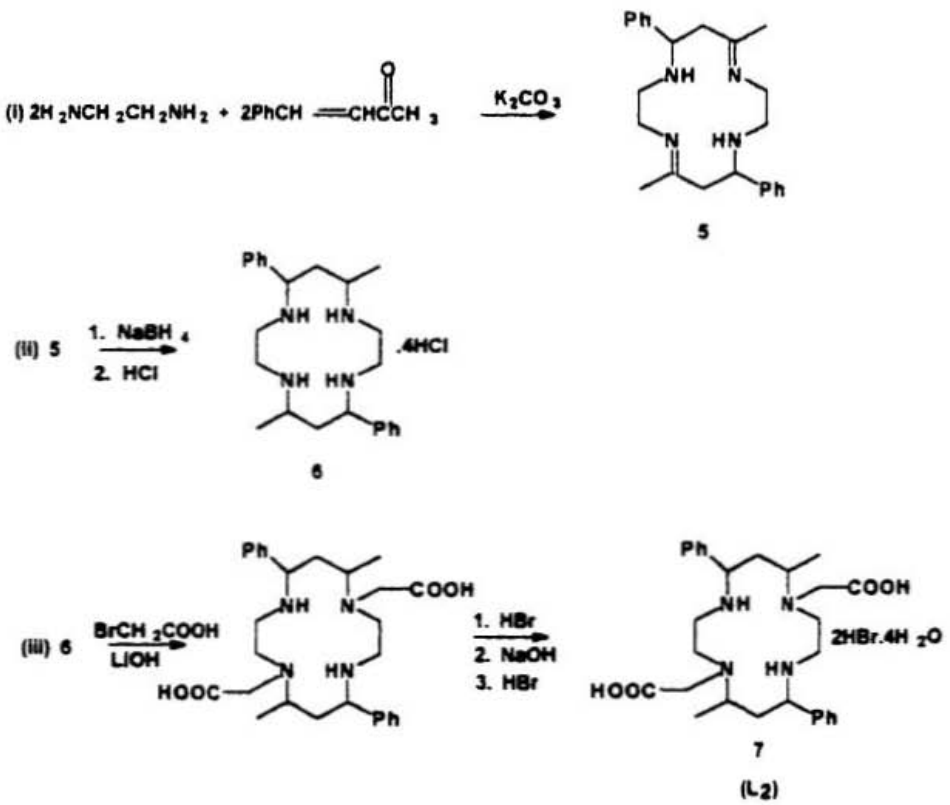

Reaction (i) 5,12-Dimethyl-7,14-diphenyl-1,4,8,11-tetraazacyclotetradeca-1,8-diene, ***5****:*

To 14.6 g of benzylidene-acetone (0.100 mol) was added 6.0 g of ethylenediamine (0.10 mol), and 10 g of potassium carbonate. The mixture was heated to reflux for three hours. The mixture was then filtered to remove the potassium carbonate. The filtrate slowly solidified, was suspended in ether and cooled. The white crystals that formed were collected by filtration and washed with ether. The yield was 30 g (67%).

Reaction (ii): 5,12-Dimethyl-7,14-diphenyl-1,4,8,11-tetraazacyclotetradecane ***6****:*

To 2.5 g (0.060 mol) of ligand **5** dissolved in methanol, was added over a 30 minute period, 4.5 g (0.12 mol) of sodium tetrahydroborate. The solution was left standing for 2 hours and then filtered. Hydrochloric acid (11.6 mol/L) was added to the filtrate and the mixture was cooled for 2 hours, after which time a white precipitate formed. The precipitate was collected by filtration, washed with cold methanol and dried. The yield was 2.4 g (53 %).

Reaction (iii):5,12-Dimethyl-7,14-diphenyl-1,4,8,11-tetraazacyclotetradecane-1,8-diacetic acid, $\mathbf{L_2}$*:*

To 16.7 g (0.120 mol) of bromoacetic acid in 100 mL of methanol was added 6.72 g (0.120 mol) of KOH in 200 mL of methanol. Anhydrous sodium carbonate, 12.70 g (0.12 mol), and 19.0 g (0.0500 mol) of ligand **6** were added to the mixture which was then stirred at 60°C for 48 hours. The mixture was then cooled and filtered. The filtrate was evaporated to dryness and the residue was dissolved in 50 mL of water and then filtered. The filtrate was

then acidified to pH 5 with dilute hydrochloric acid. A white solid formed which was collected by filtration and washed with a 50:50 water / ethanol mixture. The solid was then dissolved in 20 mL of dilute NaOH and 20 mL of concentrated hydrochloric acid was added. A white precipitate formed and the mixture was stirred for 24 hours. The solid was collected by filtration and washed with cold water. The yield was 24 g (40%). IR: 3410 (OH), 2700 - 2900 (NH_2), 1700 (COOH).

V. Synthesis of Ni(II)$L_2 \cdot 3H_2O$

$$NiCl_2.6H_2O + L_2 \xrightarrow{NaOH} NiL_2.3H_2O$$

To 350 mg (0.500 mmol) of L_2 dissolved in 20 mL of water was added 238 mg (1.00 mmol) of $NiCl_2 \cdot 6H_2O$. The pH was adjusted to pH 5 with 0.1 mol/L NaOH and the mixture was heated at reflux for 24 h. The solution was concentrated to approximately 5 mL and violet crystals precipitated. The crystals were collected and air dried to give 177 mg (60%) of yield. *Anal.* Found: C 57.20, H 7.21, N 9.72. Calcd. for $NiC_{28}H_{42}N_4O_6$ (trihydrate): C 57.06, H 7.18, N 9.51 %. IR (KBr cm^{-1}): 3448 (OH), 3232 (NH), 1604 (COO^-).

VI. Synthesis of 1,4,7-triazacyclononane

The ligand L_3 was synthesized according to a modification of the literature preparation[28] using the following scheme:

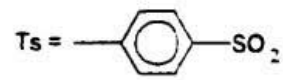

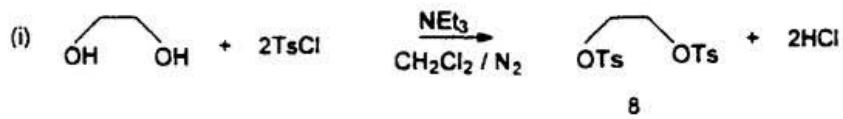

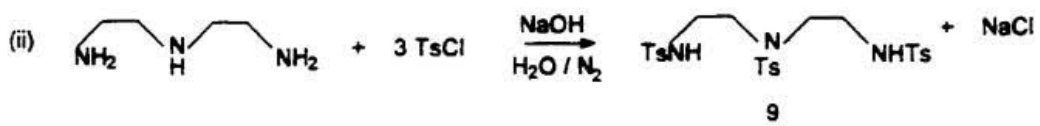

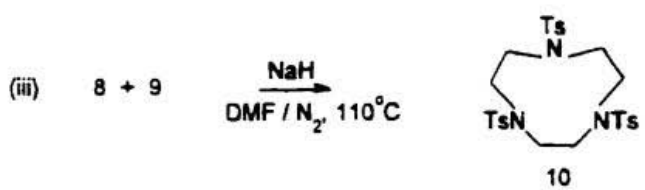

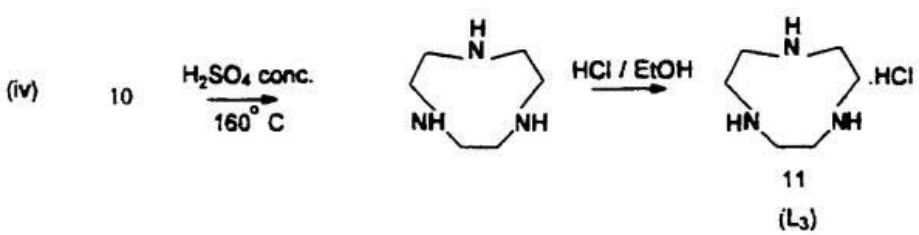

The modifications to the literature method were minor resulting in similar yields but under more convenient conditions. Reaction (i) used triethylamine as a base rather than dry pyridine as suggested by the literature, giving a comparable yield. Also, reactions (i) to (iii) were performed under a stream of dry N_2.

Reaction (i): Ditosylate of 1,2-ethanediol, ***8***:

To 400 mL of dry CH_2Cl_2, was added 11.3 mL (1.20 mol) of 1,2-ethanediol. The solution was cooled to 0° C and 50 mL of NEt_3 was added. A solution containing 76 g (0.40 mol) of p-toluenesulphonyl chloride dissolved in 200 mL of dry CH_2Cl_2 was slowly added from a dropping funnel over a 30-minute period. The mixture was stirred for 20 minutes, after which time the NEt_3HCl was filtered off. The remaining filtrate was washed with an equivalent volume of 2 $mol.L^{-1}$ HCl, four equal volumes of water and finally an equal volume of saturated Na_2CO_3. The CH_2Cl_2 layers were combined and dried over Na_2SO_4. Evaporation of the solvent under reduced pressure gave a white solid which was then recrystallized from acetone to yield 110 g (74 %) of product. m.p. 123 - 126°C, lit. m.p. 123 - 125°C.

Reaction (ii): N,N', N''-tritosyldiethylenetriamine, **9**:

To 20 g (0.50 mol) of NaOH dissolved in 200 mL of water, was added 15.3 mL (0.14 mol) of diethylenetriamine. The mixture was stirred as 100 g (0.52 mol) of p-toluenesulfonyl chloride in 500 mL of anhydrous Et_2O was added dropwise over a period of 60 minutes.

The resulting thick, white mixture was stirred for thirty minutes and then filtered. The white solid was added to boiling methanol and stirred for 40 minutes. The mixture was then suction filtered to yield a white solid that was dried over P_4O_{10} under vacuum overnight. Yield: 54 g (68%). m.p. 171 - 175°C, lit. m.p. 173 - 175°C.

Reaction (iii): 1,4,7-tritosyl-1,4,7-triazacyclononane, ***10***:

To 54 g (0.10 mol) of **9**, was added 500 mL of dry DMF. Carefully, 4.8 g (~0.2 mol) of 95 % NaH powder was added. The solution was then heated to 110°C at which time 38 g (0.10 mol) of **8**, dissolved in 200 mL of dry DMF, was added to the solution with stirring. The resulting yellow solution was cooled to room temperature and was then poured into 2 L of ice cold water. The beige solid formed was collected by filtration and washed with 300 mL of water and dried over P_4O_{10} under vacuum to yield 50 g (91 %) of product.

Reaction (iv): 1,4,7,triazacyclononane trihydrochloride: **L_3.HCl** (tacn):

To 100 mL of concentrated H_2SO_4 was added 50 g (0.084 mmol) of **10** at 160°C. Following addition, a black solution formed which was cooled to room temperature. Over a 30 minute period, 400 mL of cold ethanol was added to the solution. A 400 mL quantity of Et_2O was then added, producing a grey precipitate. The precipitate was dissolved in 100 mL of boiling water and activated charcoal was added. A hot gravity filtration was performed to yield a light yellow solution. Removal of approximately 95 mL of solvent produced an oily residue, to which 25 mL of concentrated HCl was added, followed by

75 mL of cold absolute ethanol. A light yellow solid formed which was collected by filtration and washed with modest amounts of cold ethanol. The product was then recrystallized from water to yield a white solid, 15 g (74%), m.p. 271 - 277°C, lit. m.p. 271 - 277°C.

VII. Synthesis of $[Ni(tacn)_2](ClO_4)_2$

The Ni(II) complex was prepared as per the literature method.[29] The reaction was performed as follows:

$$Ni(ClO_4)_2.6H_2O + L_3 \xrightarrow{NaOH} [Ni(tacn)_2](ClO_4)_2$$

To 25 mL of methanol was added 2.19 g (6.0 mmol) of nickel(II) perchlorate hexahydrate, resulting in a dark green solution. A solution containing 2.88 g (1.21 mmol) of L_3 in 30 mL of water was added to the green solution. The mixture was cooled to 5°C and 35 mL of 1.0 mol $.L^{-1}$ NaOH was added dropwise with stirring. The solution progressed from a green color to deep blue, to a light purple color upon complete addition of base. Upon cooling, purple crystals appeared. The product was recrystallized from a 50/50 methanol/water mixture and washed with diethyl ether. The UV-vis spectrum corresponded with that found for the perchlorate salt in the literature, with a molar absorbtivity of $\epsilon = 6.13 \pm 0.08$ L.mol^{-1}.cm^{-1} at 510 nm.

VIII. Preparation of $[Ni(tacn)_2]^{3+}$

$$2[Ni(tacn)_2]^{2+} + S_2O_8^{2-} \rightarrow 2\,[Ni(tacn)_2]^{3+} + 2SO_4^{2-}$$

A 67.6 mg (0.25 mmol) quantity of potassium peroxodisulfate was dissolved in 25 mL of water. This solution was added dropwise, with stirring, to 306 mg (0.60 mmol) of $[Ni(tacn)_2]^{2+}$ dissolved in 25 mL of water. The solution was kept in an ice bath and kept in the dark in a foil wrapped flask until required for kinetic experiments. Experiments were performed in a dimly lit room. An excess of $[Ni(tacn)_2]^{2+}$ was used to ensure complete reaction of the peroxodisulfate. The $[Ni(tacn)_2]^{3+}$ was characterized by its UV/Visible spectrum ($\epsilon = 8000 M^{-1}cm^{-1}$). The Ni(III) concentration was determined by UV/Visible spectroscopy using Beer's laws.

2.2. Crystallography

Crystallography was performed by Mr. David Miller at Memorial University. The data were collected at a temperature of 26 ± 1°C on a Rigaku AFC6S diffractometer (MoK_α radiation, graphite monochromator) in the ω-2θ scan mode to $2\theta_{max}$ = 50.1 °. Lorentz and polarization corrections were applied. The structure was solved by direct methods[30, 31] using the TEXSAN [32] crystallographic software package. Refined parameters were calculated using anisotropic thermal parameters for non-hydrogen atoms and isotropic factors for all hydrogen atoms. Neutral atom scattering factors were taken from Cromer and Waber.[33] Details of each individual crystal structure and specific parameters are provided where appropriate. The following crystallographic tables are reported in Appendices 1 and 2:

Positional and Thermal Parameters (Table A1.a).

General Temperature Factor Expressions, U's (Table A1.b).

Bond Distances (Table A1.c).

Intramolecular Bond Angles (Table A1.d).

Torsion Angles (Table A1.e).

Atomic Coordinates and Equivalent Isotropic Displacement Parameters (Table A2.a).

Bond Lengths and Angles (Table A2.b).

Anisotropic Displacement Parameters (Table A2.c).

Hydrogen Coordinates and Isotropic Displacement Parameters (Table A2.d).

2.3. Kinetic Measurements

Absorbance changes as a function of time were measured using a Beckman DU-65 spectrometer. Data were collected using Kinetics Soft-Pac software on an IBM personal computer. An initial cell blank was obtained using deionized water in a 1 cm path length quartz cuvette. All kinetic experiments were run under pseudo first-order conditions, using a minimum tenfold excess of peroxodisulfate. Due to the low solubility of the neutral complexes in water, all kinetics measurements were performed in 20% by volume aqueous ethanol. The concentrations of $Ni(II)L_1$ and $Ni(II)L_2$ were both 1.00×10^{-4} mol·L^{-1}. A constant ionic strength of 9.00×10^{-3} mol·L^{-1} was maintained using potassium sulfate. The reactants present in each cell and their concentrations are listed in Table 2.3.

Table 2.3. Concentration and Volume of Reactants in Each Cell for the $Ni(II)L_1$ and $Ni(II)L_2$ / Peroxodisulfate system.

Cell Number	$[K_2S_2O_8]$ (mmol/L)	Vol. of $K_2S_2O_8$ (μL)	$[K_2SO_4]$ (mmol/L)	Vol. of K_2SO_4 (μL)	$[Ni(II)L_1]$ (mmol/L)	Vol. of Ni(II)L (mL)	Vol. of H_2O (mL)
1	2.00	60	4.00	60	0.0400	1.200	1.680
2	3.00	90	3.00	45	0.0400	1.200	1.665
3	4.00	120	2.00	30	0.0400	1.200	1.650
4	5.00	150	1.00	15	0.0400	1.200	1.635
5	6.00	180	0	0	0.0400	1.200	1.620

The concentration of the stock $K_2S_2O_8$ solution was 0.100 mol/L. The concentration of the stock K_2SO_4 solution was 0.200 mol/L.

The general method used was to place the Ni(II)L solution and the potassium sulfate solution in the cuvette by means of micropipettes. The cuvette was placed in the thermostated cell compartment of the spectrometer. The pre-thermostated peroxodisulfate was then micropipetted into the cuvette. The cuvette was then capped, inverted and then repositioned in the cell compartment of the spectrometer. In this way, reagents were added, mixed, the cover of the cell compartment replaced and data collection initiated within ten to fifteen seconds. There was approximately one minute when the readings were unreliable due to a combination of factors such as bubbles rising through the solution and stabilization of the spectrometer to new light conditions. The absorbance values obtained for the first minute of the reaction were therefore omitted. Subsequent readings, however were strictly dependent on the absorption of the solution under consideration.

Absorbances were measured at a wavelength of 403 nm for $Ni(II)L_1$ and at 430 nm for $Ni(II)L_2$. For each given temperature and concentration, first-order rate constants, k_{obs}, were calculated from the slopes of the linear regression plots of $\ln(D_\infty - D_t)$ versus time, according to equation 1.19. For any given set of conditions, the reported value of k_{obs} is the mean of repetitive measurements that produced results consistent within 1%. When conducting the temperature dependence studies, temperatures were maintained constant to $\pm$ 0.1°C.

2.4. Stopped-Flow Kinetics

The stopped-flow apparatus (Tri-Tech dynamics) consisted of two sample compartments, A and B, as shown in figure 2.1. Jets of the two reacting solutions are forced rapidly into a mixing chamber (M) and the mixed solution flows into a third syringe, the piston of which is suddenly stopped by coming up against an external stop. Mixing of the reactants in this way allows the mixing time to be reduced to 10 ms. Conventional methods for studying kinetics usually have a mixing time of at least 0.1 s.

Close to the mixing chamber there is an observation point O, where measurement via the detection system is made. Changes in absorbance versus time were measured using a monochromatic light source passing through the observation chamber. Transmitted light passes to a photomultiplier tube via an optical fibre. Changes in transmitted light with time are followed using a time-based oscilloscope.

Initially, the sample containers, A and B, were filled with deionized water which was flushed through the apparatus several times. Following this, the containers were filled with various combinations of solutions as described in Tables 2.4 and 2.5.

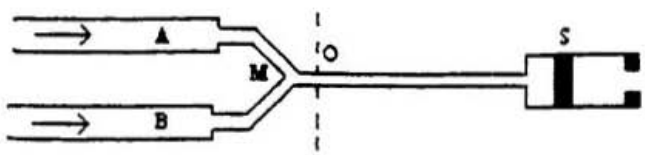

Figure 2.1

Table 2.4. Concentrations of $[Ni(tacn)_2]^{3+}$ in the $[Ni(tacn)_2]^{3+}$/ Ni(II)L_1 System.

Solution	$[Ni(tacn)_2]^{3+}$ (mol/L)	$[NaClO_4]$ (mol/L)	$[HClO_4]$ (mol/L)
A1	1.00×10^{-3}	0.100	0
A2	2.00×10^{-3}	0.100	0
A3	2.00×10^{-3}	0	0.100
A4	2.00×10^{-3}	0.050	0.050
A5	1.50×10^{-3}	0.100	0
A6	2.00×10^{-3}	0.100	0
A7	2.50×10^{-3}	0.100	0
A8	3.00×10^{-3}	0.100	0

Table 2.5. Concentrations of Ni(II)L_1 in the $[Ni(tacn)_2]^{3+}$ / Ni(II)L_1 System.

Solution	$[NiL_1]$ (mol/L)	$[NaClO_4]$ (mol/L)	$[HClO_4]$ (mol/L)
B1	1.00×10^{-4}	0.100	0
B2	2.00×10^{-4}	0.100	0
B3	2.00×10^{-4}	0	0.100
B4	2.00×10^{-4}	0.050	0.050

The concentrations reported in Tables 2.4 and 2.5 are those found in the sample chambers. The actual concentrations in the reaction are half of those in the sample compartments due to 50:50 dilution upon mixing. A stock solution of $[Ni(tacn)_2]^{3+}$ was

prepared as described in section 2.1, and its concentration determined by UV/Visible spectroscopy.

All experiments were run under pseudo first-order conditions, using a minimum tenfold excess of $[Ni(tacn)_2]^{3+}$. A constant ionic strength of 0.100 mol/L was maintained using sodium perchlorate.

The temperature in the sample chamber was controlled by a Haake circulating water bath. The exact temperature at the point of mixing was measured by a digital thermometer. Prior to use, each solution was placed in the circulating water bath for approximately five minutes to allow for temperature equilibration . Each solution was then poured directly into its appropriate compartment.

The change in absorbance was measured at a wavelength of 420 nm. For each given temperature and concentration, first-order rate constants, k_{obs}, were calculated. For each particular set of conditions, the reported value of k_{obs} is the mean of repetitive measurements that produced results consistent within 1%. When conducting the temperature dependence studies, temperatures were maintained constant to ± 0.1°C.

2.5. Cyclic Voltammetry

Cyclic voltammograms of Ni(II)L_1 and Ni(II)L_2 were measured using a Princeton Applied Research model 482 fast-scanning electrochemical apparatus, in aqueous 0.10 M trifluoromethanesulphonic acid, under an argon atmosphere. A 1 mm diameter Pt disk working electrode, a platinum counter electrode and a Ag/AgCl (sat. KCl) reference electrode were used.

Chapter 3: Results

3.1. Crystallography

$Ni(II)L_2$

Diffraction quality crystals of $NiL_2 \cdot 3H_2O$ were obtained by slow evaporation from aqueous ethanol. The purple crystals were mounted on a glass fiber and centered on a Rigaku AFCC6S diffractometer. The cell was refined using 23 centered reflections in the range $2\theta = 25$ -37°. Intensity measurements were carried out with MoKα radiation, $\lambda = 0.71069$ Å. The asymmetric unit consisted of the neutral complex and three water molecules of crystallization. One water site was fully occupied and two were partially occupied. Data reduction yielded 3841 reflections with $I>2\sigma(I)$, which were used for solution and refinement of the structure.

The structure was solved by direct methods using TEXSAN.[32] Refined parameters were calculated using anisotropic thermal parameters for non-hydrogen atoms and isotropic factors for all hydrogen atoms. A summary of crystal data is given in Table 3.1. Atomic positional parameters are given in Table 3.2, bond lengths are given in Table 3.3 and bond angles are given in Table 3.4.

The crystal was found to have three waters of crystallization in the structure. These waters occur in channels between the complexes. Two are strongly hydrogen bonded with each other, but none are hydrogen-bonded to either the nitrogens or the oxygens of the macrocyclic ligand. The nickel atom in the complex is octahedrally coordinated to the four nitrogen atoms in the macrocycle and two oxygen atoms of the appended carboxylato- groups. This is achieved by the folding of the macrocycle which allows both of the carboxylic oxygen atoms to coordinate in a cis-arrangement. A diagram of the complex is shown in Figure 3.1.

Table 3.1. Experimental crystallographic data for Ni(II)$L_2 \cdot 3H_2O$

Empirical Formula	$C_{28}H_{42}N_4O_6Ni$
Crystal colour, habit	purple, irregular
Formula Weight	589.36
Crystal System	monoclinic
Space Group	$P2_1/c$
a(Å)	12.981(8)
b(Å)	16.474(6)
c(Å)	14.262(7)
β(°)	98.81(4)
V(Å^3)	3014(5)
D_{calc} (g cm^{-3})	1.299
Z value	4
Crystal dimensions (mm)	0.250x0.150x0.400
Diffractometer	Rigaku, AFC6S
Radiation	MoKα (0.71069 Å)
2θ range for unit cell determination	24.9 - 36.7 °
Absorption coefficient, μ	6.88 cm^{-1}
F_{000}	1256
Reflections collected	5797
Reflections with I > 2.00σ(I)	3841
No. parameters	334
Solution Method	TEXSAN
Goodness of fit	3.39
R	0.059
R_w	0.067

$R = \Sigma \mid |F_o| - |F_c| \mid / \Sigma |F_o| R_w = [(\Sigma w (|F_o| - |F_c|)^2 / \Sigma w F_o^2)]^{1/2}$

Table 3.2. Positional Parameters and B(eq) values for Ni(II)$L_2 \cdot 3H_2O$ Coordination Sphere.

atom	x	y	z	B(eq)
Ni(1)	0.75914(6)	0.22878(5)	0.22054(5)	2.61(3)
O(1)	0.6731(3)	0.2686(3)	0.0946(3)	3.5(2)
O(2)	0.8693(3)	0.1936(2)	0.1355(3)	3.4(2)
O(3)	0.7119(3)	0.3446(3)	-0.0251(3)	4.2(2)
O(4)	0.8958(3)	0.0960(3)	0.0340(3)	4.6(2)
N(1)	0.6490(3)	0.2611(3)	0.3070(3)	2.8(2)
N(2)	0.7066(4)	0.1104(3)	0.1952(3)	2.8(2)
N(3)	0.8559(4)	0.1844(3)	0.3397(3)	2.9(2)
N(4)	0.8031(4)	0.3502(3)	0.2268(3)	2.8(2)

Table 3.3 Selected bond distances (Å) for Ni(II)$L_2 \cdot 3H_2O$ Coordination Sphere.

Bond	Distance
Ni(1)-O(1)	2.072 (4)
Ni(1)-O(2)	2.093 (4)
Ni(1)-N(1)	2.094 (5)
Ni(1) -N(2)	2.080 (5)
Ni(1) -N(3)	2.084 (5)
Ni(1)-N(4)	2.078 (5)

Table 3.4 Selected bond angles (°) for Ni(II)$L_2 \cdot 3H_2O$ Coordination Sphere

Bonds	Angle
O(1)-Ni(1)-O(2)	84.9 (2)
O(1)-Ni(1)-N(1)	96.0 (2)
O(1)-Ni(1)-N(2)	91.6 (2)
O(1)-Ni(1)-N(3)	174.6 (2)
O(1)-Ni(1)-N(4)	80.8 (2)
O(2)-Ni(1)-N(1)	178.6 (2)
O(2)-Ni(1)-N(2)	82.8 (2)
O(2)-Ni(1)-N(3)	89.7 (2)
O(2)-Ni(1)-N(4)	94.8 (2)
N(1)-Ni(1)-N(2)	96.0 (2)
N(1)-Ni(1)-N(3)	89.4 (2)
N(1)-Ni(1)-N(4)	86.5 (2)
N(2)-Ni(1)-N(3)	87.3 (2)
N(2)-Ni(1)-N(4)	172.2 (2)
N(3)-Ni(1)-N(4)	100.1 (2)

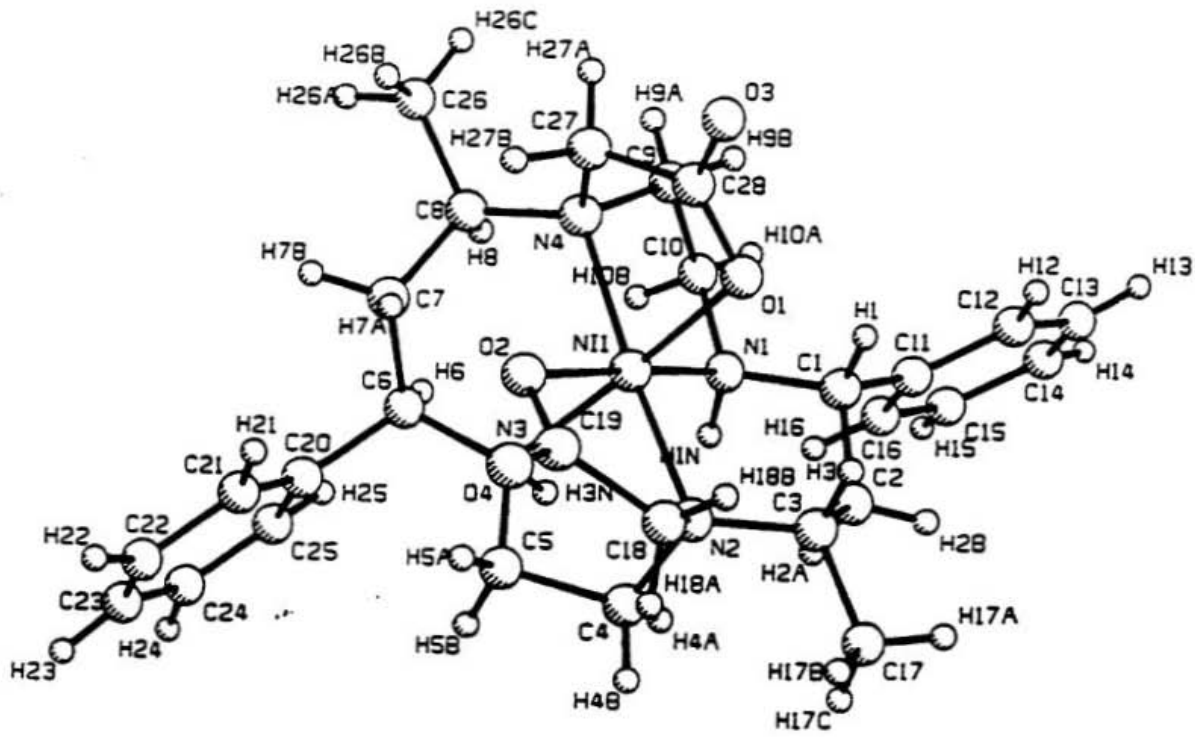

Fig. 3.1. PLUTO Diagram of the NiL_2 Complex.

[Co(III)L_1] X

Diffraction quality crystals of [Co(III)L_1]X (where X is Cl^- or Br^-) were obtained under a controlled rate of evaporation of an aqueous solution of the complex in a 80°C bath for two days. The red crystals were mounted on a glass fiber and centered on the diffractometer. The cell was refined using centered reflections in the range θ = 1.72 to 28.33°. Intensity measurements were carried out with MoKα radiation, λ = 0.71073 Å. The asymmetric unit cell consisted of the complex with a one plus charge and portions of counter halide ions. The crystal contained half a bromide ion and half a chloride ion trapped in the asymmetric unit. Data reduction yielded 16420 reflections with $I>2\sigma(I)$, which were used for solution and refinement of the structure.

The structure was solved by direct methods.[32] Refined parameters were calculated using anisotropic thermal parameters for non-hydrogen atoms and isotropic factors for all hydrogen atoms. A summary of crystal data is given in Table 3.5. Atomic positional parameters are given in Table 3.6 and selected bond lengths and angles are given in Table 3.7

The cobalt atom in the complex is six coordinated to the four nitrogen atoms in the macrocycle and two oxygen atoms of the appended carboxylato- groups. The complex shows a distorted trans-octahedral geometry with four amino nitrogens in a plane and two apical carboxylato- oxygen donors. The molecule has a center of symmetry at the cobalt with the result that the pairs of methyl and carboxylato- groups are each *trans*. An ORTEP diagram of the complex is shown in Figure 3.2.

Table 3.5. Experimental crystallographic data for $[Co(III)L_1]^-$

Empirical formula	$C_{20}\ H_{38}\ Br_{0.57}\ Cl_{0.44}\ Co\ N_4\ O_4$
Formula weight	518.53
Temperature	298(2) K
Wavelength	0.71073 Å
Crystal system	Monoclinic
Space group	P2(1)/c
Unit cell dimensions	a = 12.7163(3) Å α = 90 deg.
	b = 15.8224(3) Å β = 111.597(1) deg.
	c = 14.0899(3) Å γ = 90 deg.
Volume	2635.9(1) $Å^3$
Z value	4
Density (calculated)	1.307 Mg/m^3
Absorption coefficient	1.589 mm^{-1}
F(000)	1090
Crystal size	0.20 x 0.20 x 0.20 mm
Theta range for data collection	1.72 to 28.33 deg.
Limiting indices	-16<=h<=16, -20<=k<=21, -9<=l<=18
Reflections collected	16420
Independent reflections	6325 [R(int) = 0.0305]
Max. and min. transmission	0.801471 and 0.578717
Refinement method	Full-matrix least-squares on F^2
Data	6325
Restraints	1
Parameter	285
Goodness-of-fit on F^2	1.104
Final R indices [I>2sigma(I)]	R = 0.0688, R_w = 0.2329
R indices (all data)	R = 0.0983, R_w = 0.2538
Largest diff. peak and hole	0.875 and -0.726 e.$Å^3$

Table 3.6. Positional Parameters and B(eq) values for $[CoL_1]^+$ Coordination Sphere.

atom	x	y	z	B(eq)
Co	10000	5000	10000	23(1)
O(1)	11176(3)	5379(2)	9600(3)	28(1)
O(2)	12112(3)	6527(2)	9438(4)	46(1)
N(1)	8831(3)	5301(3)	8622(3)	29(1)
N(2)	9888(3)	6187(2)	10448(3)	30(1
N(1A)	5941(3)	10810(3)	6103(3)	30(1)
N(2A)	5722(3)	9056(3)	5973(3)	29(1)

Table 3.7 Selected bond distances (Å) for $[CoL_1]^+$ Coordination Sphere.

Bond	Distance
Co-O(1A)	1.880(3)
Co-O(1)	1.880(3)
Co-N(2A)	2.004(4)
Co-N(2)	2.004(4)
Co-N(1)	2.020 (4)
Co-N(1A)	2.020(4)

Table 3.8 Selected bond angles (°) for $[CoL_1]^+$ Coordination Sphere.

Bonds	Angle
O(1A)-Co-O(1)	180.0
O(1A)-Co-N(2A)	87.3(2)
O(1)-Co-N(2A)	92.7(2)
O(1A)-Co-N(2)	92.7(2)
O(1)-Co-N(2)	87.3(2)
N(2A)-Co-N(2)	179.998(1)
O(1A)-Co-N(1)	88.7(2)
O(1)-Co-N(1)	91.3(2)
N(2A)-Co-N(1)	91.8(2)
N(2)-Co-N(1)	88.2(2)
O(1A)-Co-N(1A)	91.3(2)
O(1)-Co-N(1A)	88.7(2)
N(2A)-Co-N(1A)	88.2(2)
N(2)-Co-N(1A)	91.8(2)
N(1)-Co-N(1A)	179.998(1)

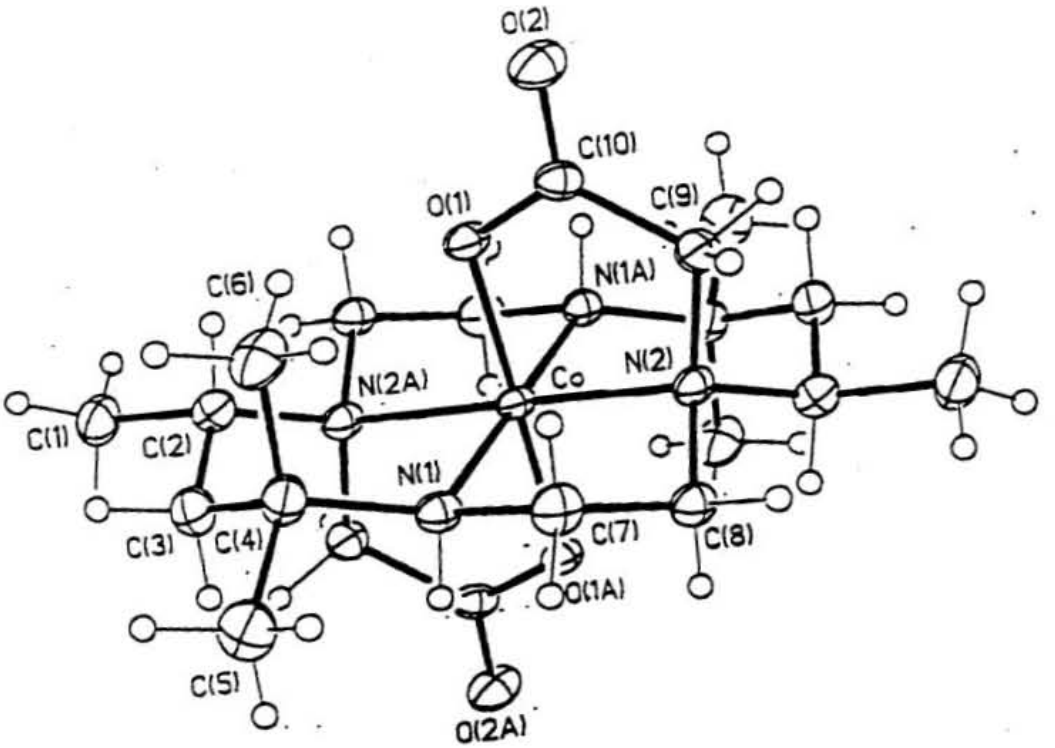

Fig. 3.2. ORTEP Diagram of the $[CoL_1]^+$ Cation.

3.2. Peroxodisulfate Kinetics

The Ni(II)L_1 and Ni(II)L_2 complexes were oxidized smoothly to the tervalent state by peroxodisulphate in 20% by volume aqueous ethanol. Figure 3.3 shows the UV/Visible spectral changes during the oxidation of Ni(II)L_1. A strong peak at 300 nm (ϵ = 8000 mol^{-1} dm^3 cm^{-1}), with a shoulder at 400 nm (ϵ = 6000 mol^{-1} dm^3 cm^{-1}) is characteristic of nickel(III) polyazamacrocycles. Excellent first-order kinetics were observed over at least five half-lives for the appearance of the nickel(III) products. Addition of the radical scavenger allyl acetate had no effect on the reaction rates. It has been shown that sulfate radicals will react quickly with allyl acetate.[34] Peroxodisulfate, however, does not react directly with allyl acetate. In this experiment, the presence of 0.024 - 0.17 mol/L allyl acetate, caused reaction rates to differ by less than 3 %. The presence of sulfate radicals would have caused a dramatic increase in the reaction kinetics. This demonstrates the lack of participation of sulfate radicals in the kinetics of the reactions. The overall reaction corresponds to:

$$2[Ni(II)L] + S_2O_8^{2-} \rightarrow 2[Ni(III)L]^{\cdot} + 2SO_4^{2-}$$

where Ni(II)L refers to either Ni(II)L_1 or Ni(II)L_2.

Figure 3.4 shows a typical change in absorbance as a function of time for the oxidation of Ni(II)L_1 by 0.0040 mol L^{-1} $S_2O_8^{2-}$ at a temperature 288.4 K and a wavelength of 403 nm. The increase in absorbance corresponds to the formation of the Ni(III)L_1 complex. Figure 3.5 shows a linear regression plot of the data shown in Figure 3.4. From the slope of the linear regression plot, the value of k_{obs} can be determined according to equation 1.19.

The observed pseudo first-order rate constant, k_{obs}, and second-order rate constants, k_2, for the Ni(II)L_1 / peroxodisulfate systems are given in Table 3.9, while those for the

$Ni(II)L_2$ / peroxodisulfate system are given in Table 3.10. The values of the second-order rate constants were determined using linear regression plots of the k_{obs} versus $[S_2O_8^{2-}]$ data.

Doubling the concentration of Ni(II)L increases the rate twofold. Furthermore, doubling the concentration of $S_2O_8^{2-}$ also causes the rate to double. Reducing the concentration of each reactant to half its original value causes the rate to decrease by half. These observations indicate that the reaction is first order in both Ni(II)L and $S_2O_8^{2-}$.

Figures 3.6 and 3.7 are graphical depictions of the dependence of the observed pseudo first-order rate constants on peroxodisulfate concentration at various temperatures. These figures illustrate that the reactions have well-behaved first-order dependence on the peroxodisulfate concentration. Based on this observation, the rate of the reaction:

$$2[Ni(II)L] + S_2O_8^{2-} \rightarrow 2[Ni(III)L]^{+} + 2SO_4^{2-} \qquad \text{Eqn. 3.1}$$

is given as follows:

$$\text{Rate} = \frac{-d[Ni(II)L]}{2dt} = k_2[Ni(II)L][S_2O_8^{2-}]$$

Figures 3.8 is an Arrhenius plot for the oxidation of $Ni(II)L_1$ by peroxodisulfate. Using such graphs and equation 1.2, the Arrhenius activation energy for the oxidation of the $Ni(II)L_1$ and $Ni(II)L_2$ by peroxodisulfate can be calculated. The values were determined to be 40.7 ± 5.4 kJ mol^{-1} and 45.3 ± 6.3 kJ mol^{-1}, respectively. Using the Eyring equation, the activation enthalpy and entropy of reaction can be calculated. The Eyring plot for the $Ni(II)L_1$ / $S_2O_8^{2-}$ system is shown in Figure 3.9.

Enthalpy and entropy are related by the Eyring equation, as follows:

$$\ln(\frac{k_2}{T}) = \ln(\frac{k_b}{h}) + \frac{\Delta S^*}{R} - \frac{\Delta H^*}{RT}$$

The experimentally determined activation enthalpy and entropy for the $Ni(II)L_1$ complex were 39.5 ± 5.3 kJ.mol^{-1} and -115 ± 5 J.K^{-1}.mol^{-1}, respectively. For the $Ni(II)L_2$ complex, the acitvation enthalpy was 42.8 ± 5.1 kJ.mol^{-1} and the activation entropy was -115 ± 5 J.K^{-1}.mol^{-1}.

Table 3.9: Observed Pseudo First-order Rate Constants, k_{obs}, and the Second-order Rate Constants, k_2, for the Oxidation of Ni(II)L_1 by Peroxodisulfate.

	$10^3[K_2S_2O_8]$ (mol/L)					
	2	3	4	5	6	
T(K)	10^3 x k_{obs} (s^{-1})					k_2 (mol $L^{-1}s^{-1}$)
288.4	7.85	13	15.5	21.5	24.2	4.11
294.2	9.83	14.5	20	27	36.7	5.54
297.9	12.2	20.1	24.2	31.7	38.4	6.34
302.1	14.6	24.4	35	44.6	59.1	9.11
307.6	23.0	30.9	44.8	53.4	75.8	11.6

Table 3.10: Observed Pseudo First-order Rate Constants, k_{obs}, and the Second-order Rate Constants, k_2, for the Oxidation of Ni(II)L_2 by Peroxodisulfate.

	$10^3[K_2S_2O_8]$ (mol/L)					
	2	3	4	5	6	
T(K)	10^3 x k_{obs} (s^{-1})					k_2 (mol $L^{-1}s^{-1}$)
292.7	3.03	4.09	6.16	7.12	-------	0.145
296.2	4.53	3.89	5.7	7.38	8.17	0.144
299.5	4.78	5.65	9.18	12.1	15.1	0.239
302.8	5.26	6.91	10.7	13.2	15.5	0.262
309.8	7.52	11.2	14.4	19.0	-------	0.373

3.3 Stopped -Flow Kinetics

Addition of the colorless peroxodisulfate solution to the pink $[Ni(tacn)_2]^{2+}$ solution resulted in a deep yellow solution, indicating the formation of the $[Ni(tacn)_2]^{3+}$ species, as follows:

$$2\,[Ni(tacn)_2]^{2+} + S_2O_8^{2-} \rightarrow 2\,[Ni(tacn)_2]^{3+} + 2SO_4^{2-}$$

Combining this yellow solution with the pink colored $Ni(II)L_1$ solution produced an orange solution with a distinct absorbance increase at λ = 420 nm. The reaction is given by :

$$Ni(II)L_1 + [Ni(tacn)_2]^{3+} \rightarrow [Ni(III)L_1]^{+} + [Ni(tacn)_2]^{2+} \qquad \text{Eqn. 3.2}$$

The above reaction was studied by stopped-flow kinetics. The reaction half-life was measured, from which k_{obs} was determined according to eqn. 1.23, as described earlier. The observed first-order rate constants, k_{obs}, and second-order rate constant, k_2, for the oxidation of $Ni(II)L_1$, as a function of temperature and $[Ni(tacn)_2]^{3+}$ concentrations are given in Table 3.11. Table 3.12 contains the observed rate constants as a function of acid, $Ni(II)L_1$, $[Ni(tacn)_2]^{3+}$ and sodium perchlorate concentrations. From these results it is clear that halving the concentration of $Ni(II)L_1$ halves the observed rate constant. The same is true when the concentration of $[Ni(tacn)_2]^{3+}$ is halved. This indicates that the reaction is first-order in both $Ni(II)L_1$ and $[Ni(tacn)_2]^{3+}$. Addition of $NaClO_4$, to maintain a constant ionic strength, has no effect on the reaction rate. Sodium perchlorate present in concentrations of 0.050 mol/L and 0.100 mol/L gives rates that differ by less than 1 %. The

reaction rate was found to be independent of acid concentration between 0.050 and 0.100 mol/L, giving an overall simple second-order rate law:

$$\text{Rate} = \frac{-d[Ni(II)L_1]}{dt} = k_2 [Ni(tacn)_2^{3+}] [Ni(II)L_1]$$

Values for the second-order rate constants were determined using linear regression plots of the k_{obs} versus $[Ni(tacn)_2]^{3+}$ concentration data. Figure 3.10 is a graphical depiction of the dependence of the observed first-order rate constants on $[Ni(tacn)_2]^{3+}$ at various temperatures. Figure 3.11 is an Arrhenius plot for the oxidation of $Ni(II)L_1$ by $[Ni(tacn)_2]^{3+}$. Using this graph and equation 1.2, the Arrhenius activation energy for the oxidation of $Ni(II)L_1$ by $[Ni(tacn)_2]^{3+}$ can be calculated. The value was determined to be 32.8 ± 0.1 kJ mol^{-1}. The Eyring equation was used to calculate the activation enthalpy and entropy of reaction. The values were 30.3 ± 1.2 kJ mol^{-1} and -132 ± 20 J K^{-1} mol^{-1}. The Eyring plot is shown in Figure 3.12.

Table 3.11: Observed Pseudo First-order Rate Constants, k_{obs}, and the Second-order Rate Constants, k_2, for the Oxidation of Ni(II)L_1 by $[Ni(tacn)_2]^{3+}$.

	10^3 $[Ni(tacn)_2^{3+}]$ (mol/L)					
	0.5	0.75	1	1.25	2.5	
T(K)	10^3 x k_{obs} (s^{-1})					k_2 (mol $L^{-1}s^{-1}$)
290.1	1.25	1.89	2.37	3	3.42	1.18
294.6	1.66	2.36	3.24	4.37	4.86	1.65
298	1.95	2.63	3.63	4.66	5.75	1.87
301.2	2.03	2.76	3.83	4.93	6.27	2
304.6	2.5	2.88	4.31	5.75	7.67	2.47

Table 3.12. Observed Pseudo First-order Rate Constants, k_{obs}, as a Function of Concentration for the oxidation of Ni(II)L_1 by $[Ni(tacn)_2]^{3+}$.

$[HClO_4]$ (mol/L)	$[Ni(tacn)_2^{3+}]$ (mol/L)	Ni(II)L_1 (mol/L)	$[NaClO_4]$ (mol/L)	k_{obs} (s^{-1})
0	1.00×10^{-3}	1.00×10^{-3}	0.1	2.37×10^{-3}
0	1.00×10^{-3}	0.50×10^{-3}	0.1	1.20×10^{-3}
0	0.50×10^{-3}	1.00×10^{-3}	0.1	1.18×10^{-3}
0.05	1.00×10^{-3}	1.00×10^{-3}	0.05	1.28×10^{-3}
0.1	1.00×10^{-3}	1.00×10^{-3}	0	2.43×10^{-3}

3.4. Electrochemistry

Figures 3.13 and 3.14 show cyclic voltammograms for Ni(II)L_1 and Ni(II)L_2, measured at various scan rates (50-200 mV/s), between 0 and 1.0 V (vs Ag/AgCl reference electrode). It is clear that the complexes undergo clean, reversible one-electron oxidations to the nickel(III) forms. The values of the formal potential, $E^{\circ\prime}$, for Ni(II)L_1 and Ni(II)L_2 respectively are 0.72 V and 0.77V (vs Ag/AgCl reference electrode) with peak separations of 64 ± 4 mV. The anodic and cathodic peak separations were independent of scan rate. While both voltammograms exhibit reversibility, information regarding geometry and coordination change cannot be inferred. Rate constants for rearrangement and ligand substitution would be very fast and beyond the time scale of the scan rates used.

Fig. 3.3 Absorbance vs. Wavelength for the Oxidation of Ni(II)L_1 by 0.00400 mol/L $S_2O_8^{2-}$ at 288.4K.

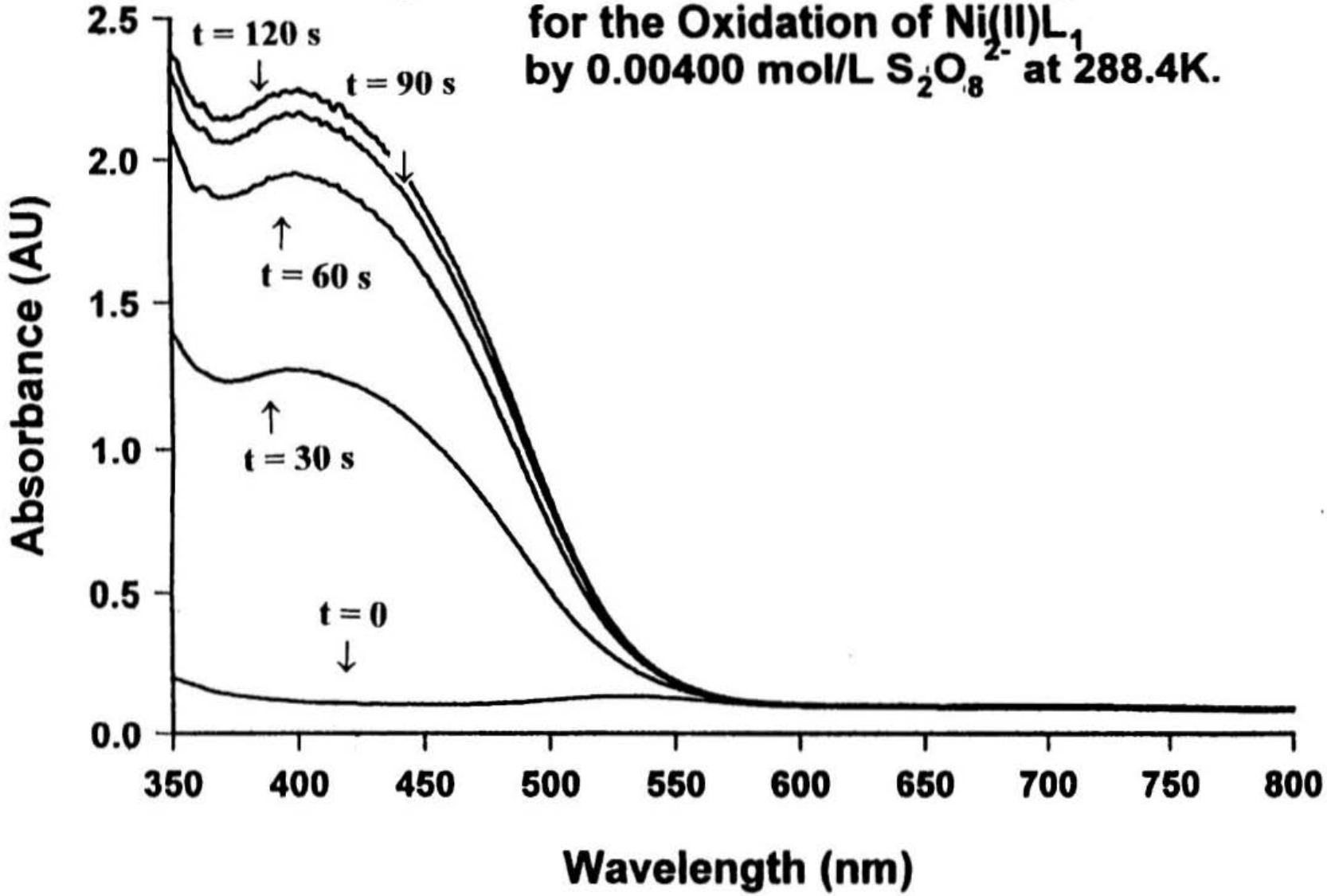

Fig. 3.4. Absorbance at 403 nm as a Function of Time for the Oxidation of $Ni(II)L_1$ by 0.00400 mol/L $S_2O_8^{2-}$ at 288.4 K.

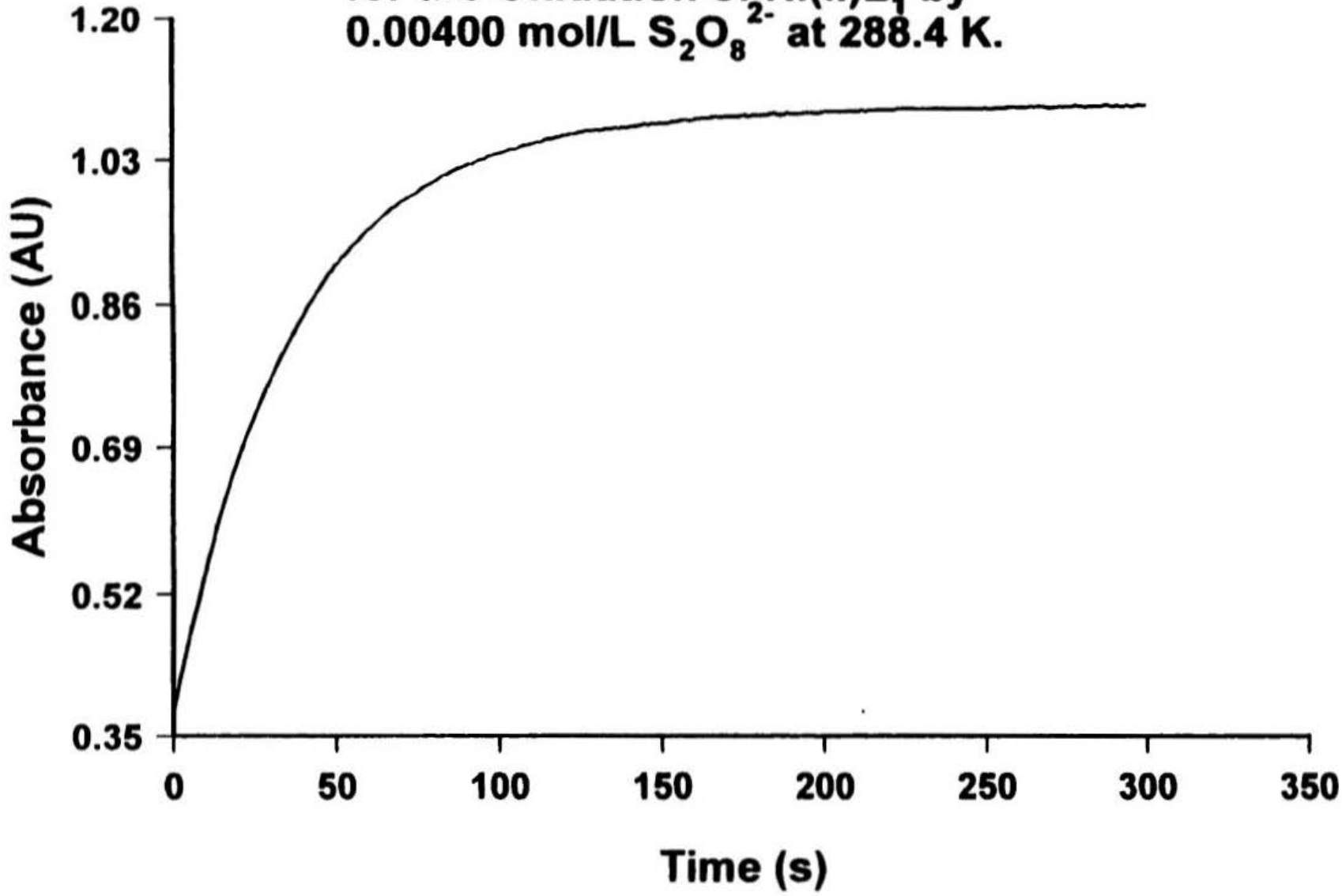

Fig. 3.5. Linear Regression Plot for the Oxidation of Ni(II)L_1 by 0.00400 mol/L $S_2O_8^{2-}$ at 288.4 K.

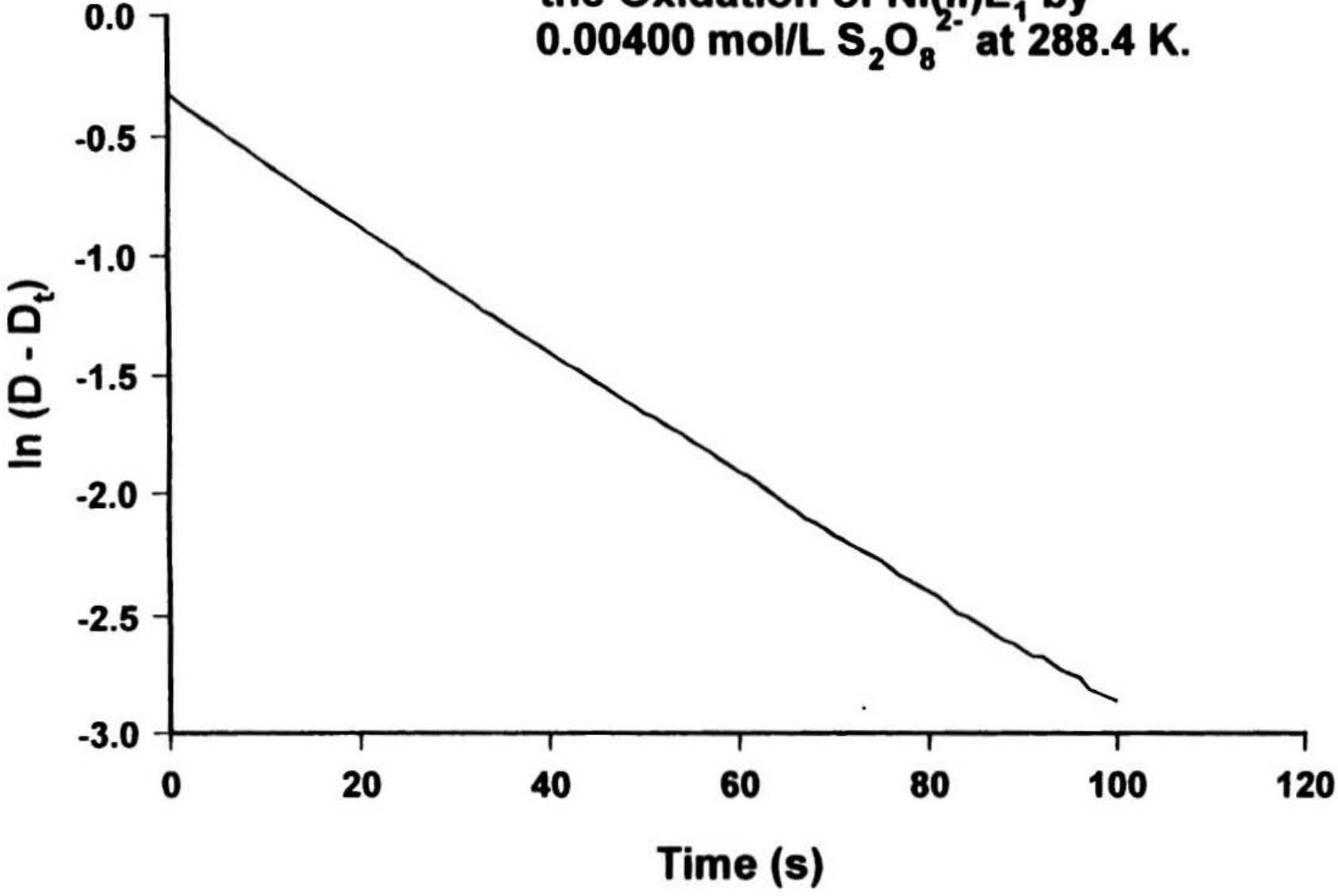

Fig. 3.6. Rate Constant as a Function of Temperature and Concentration for Ni(II)L_1.

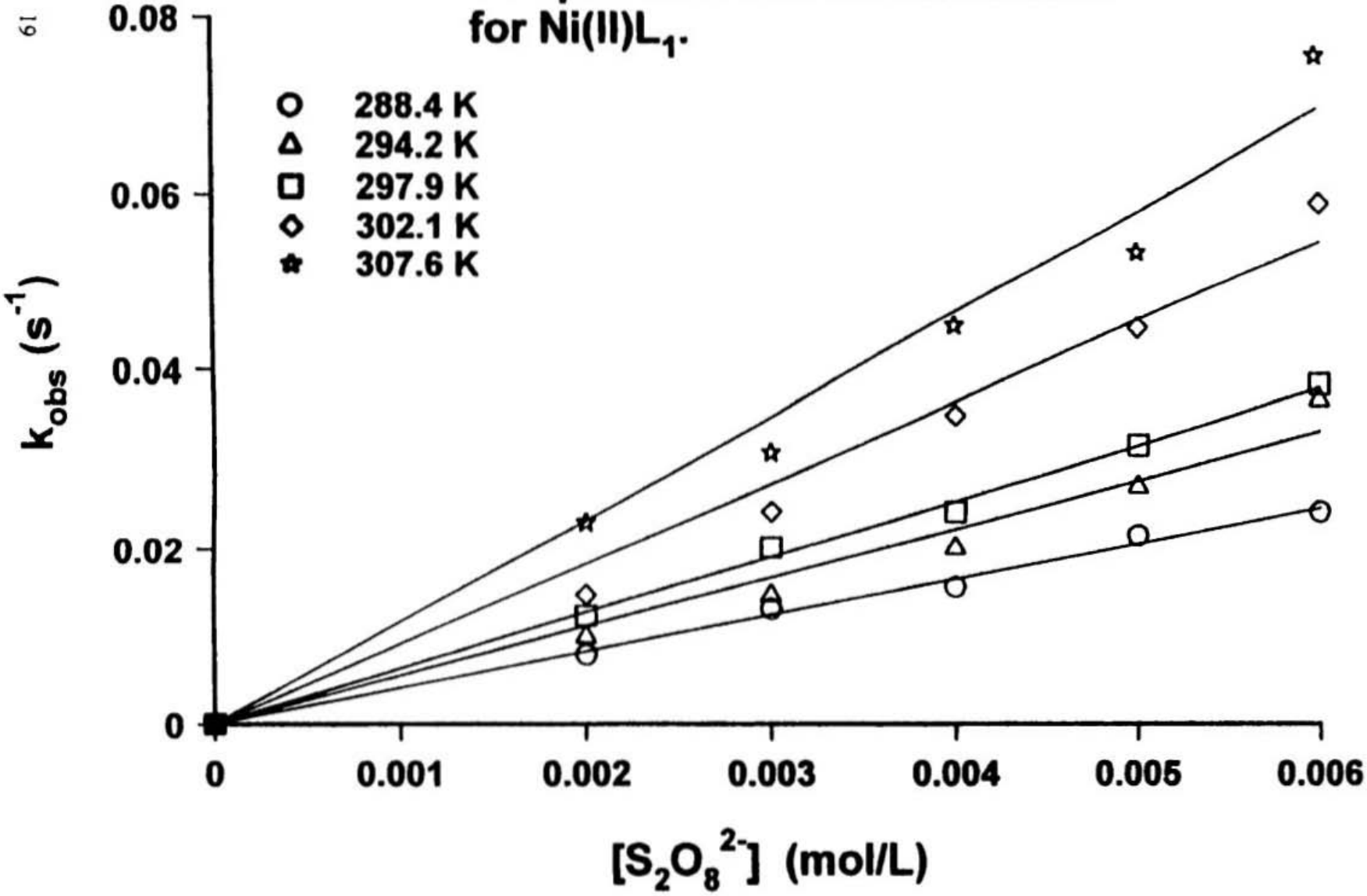

Fig. 3.7. Rate constant as a Function of Temperature and Concentration for Ni(II)L_2.

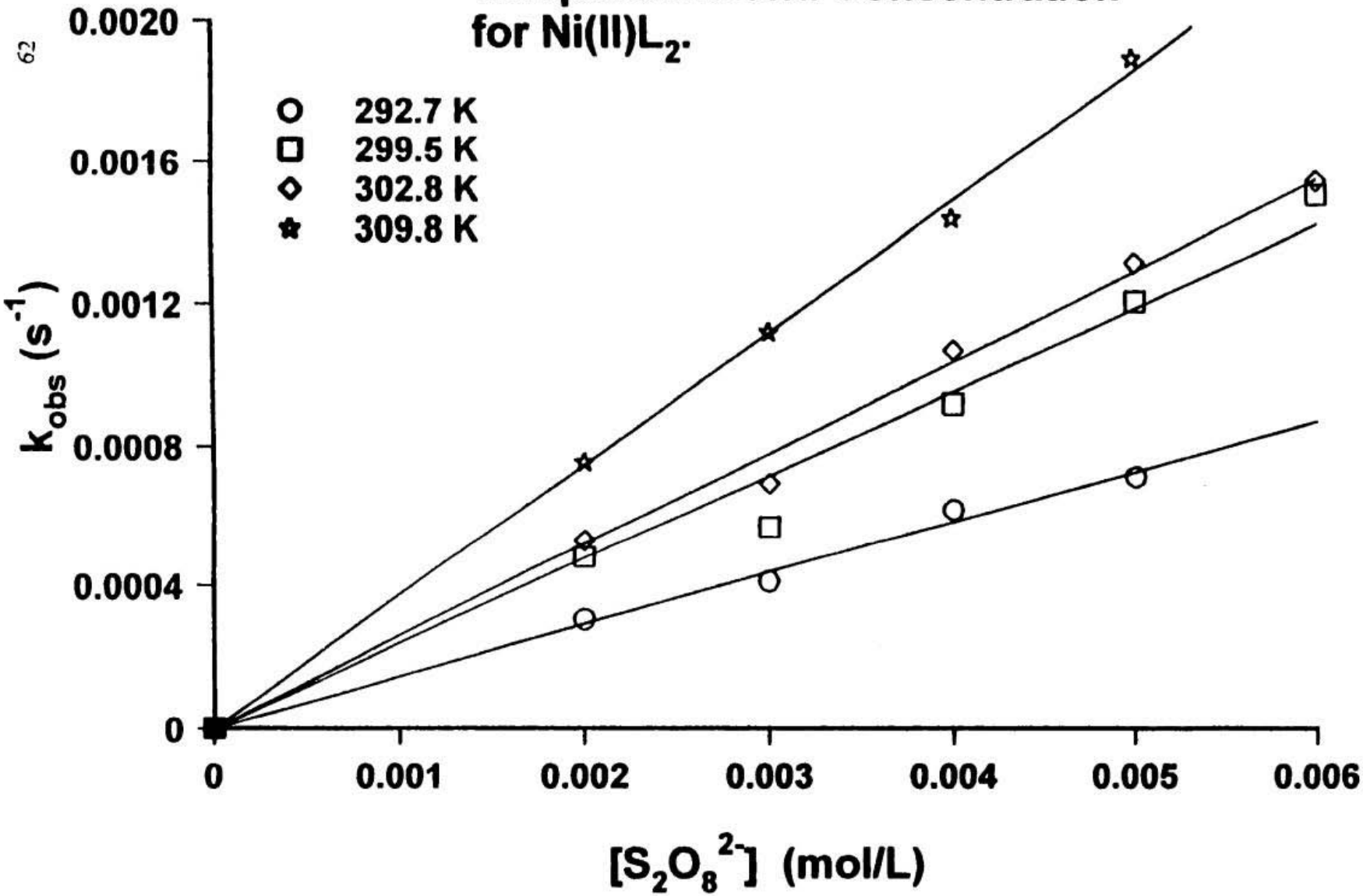

Fig. 3.8. Arrhenius Plot for Ni(II)L_1 Oxidation by $S_2O_8^{2-}$.

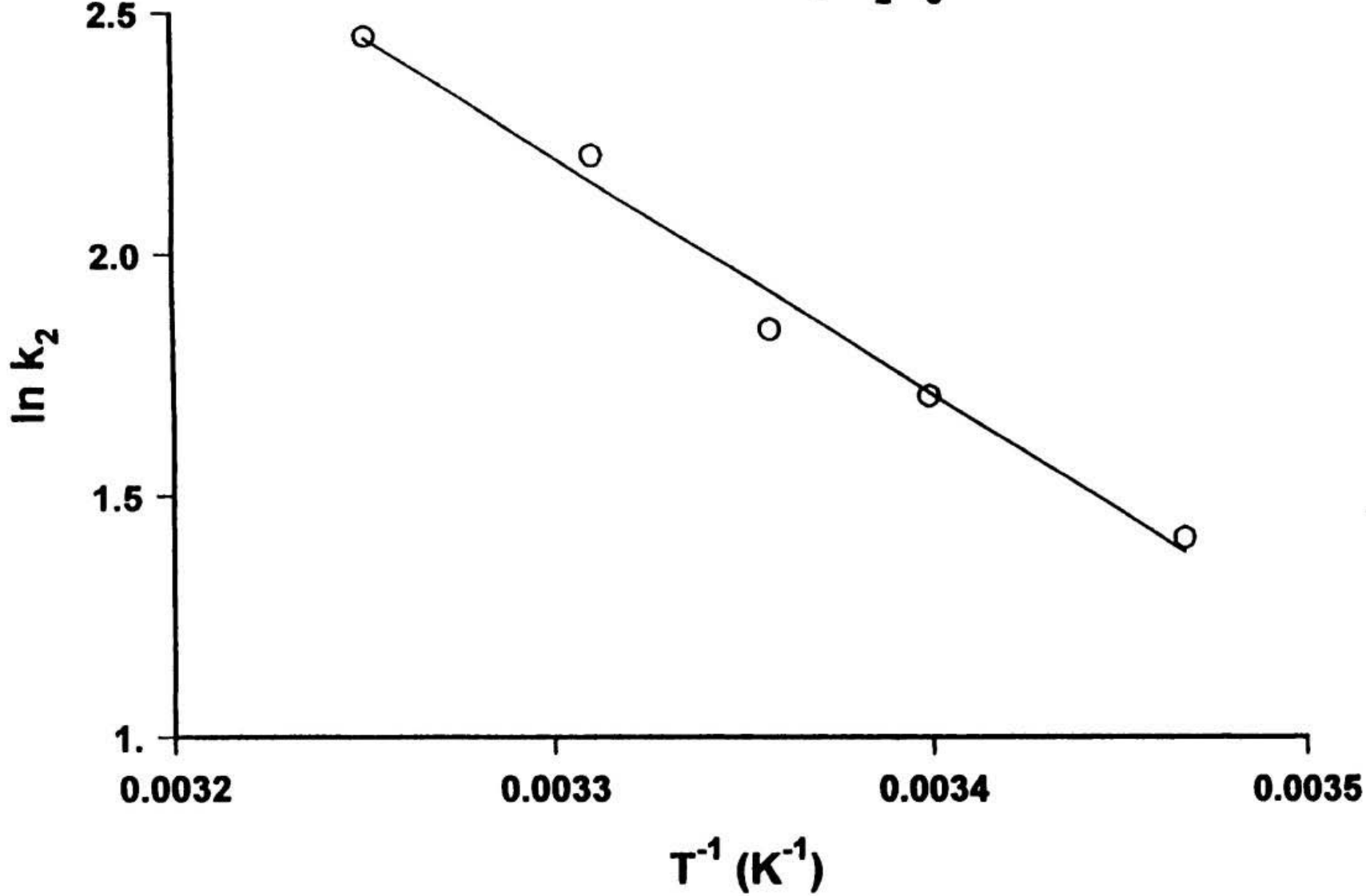

Fig. 3.9. Eyring Plot for Ni(II)L_1 Oxidation by $S_2O_8^{2-}$.

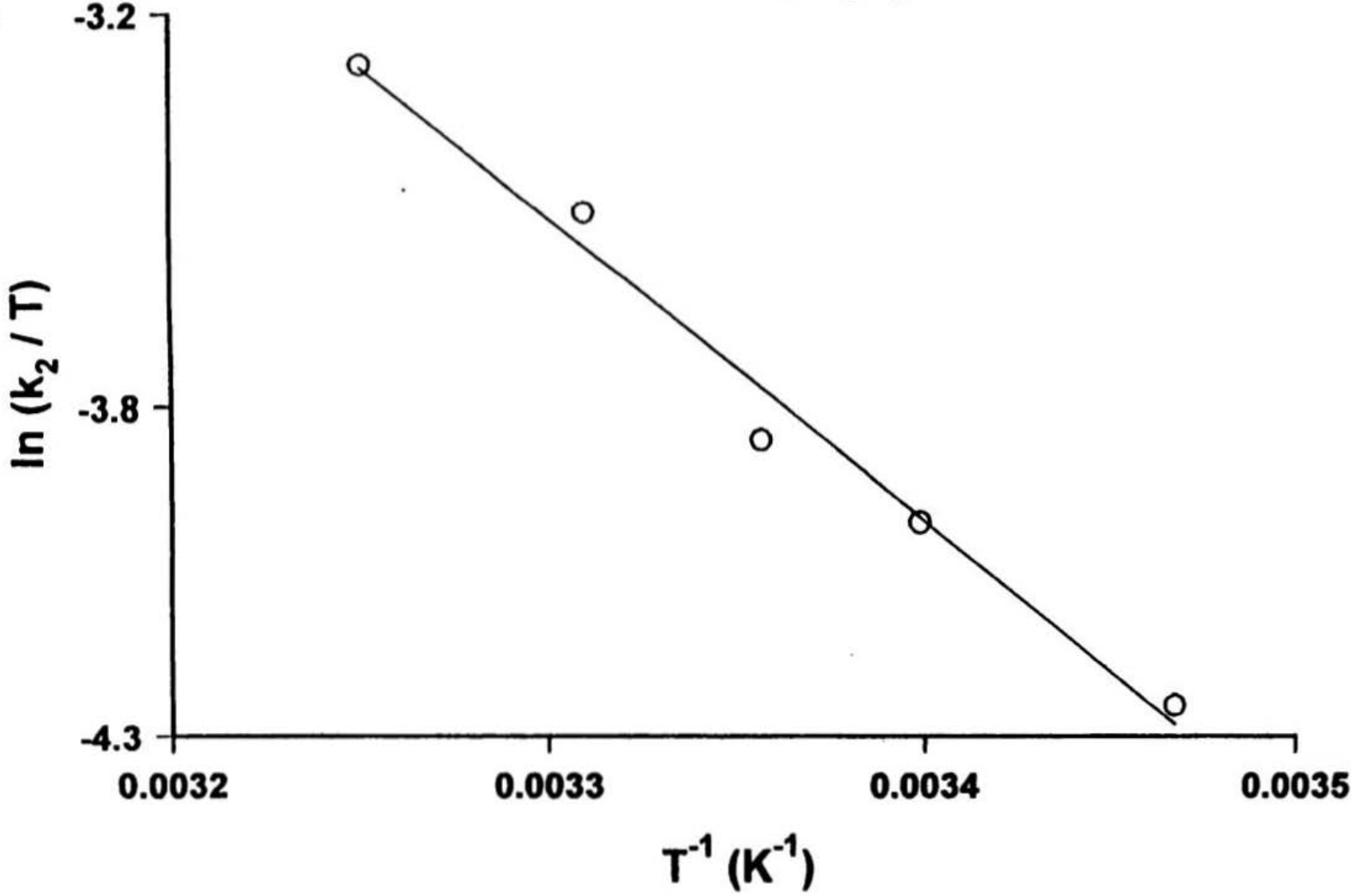

Fig. 3.10. Rate Constant as a Function of Temperature and Concentration for $Ni(II)L_1$ Oxidation by $Ni(tacn)_2^{3+}$.

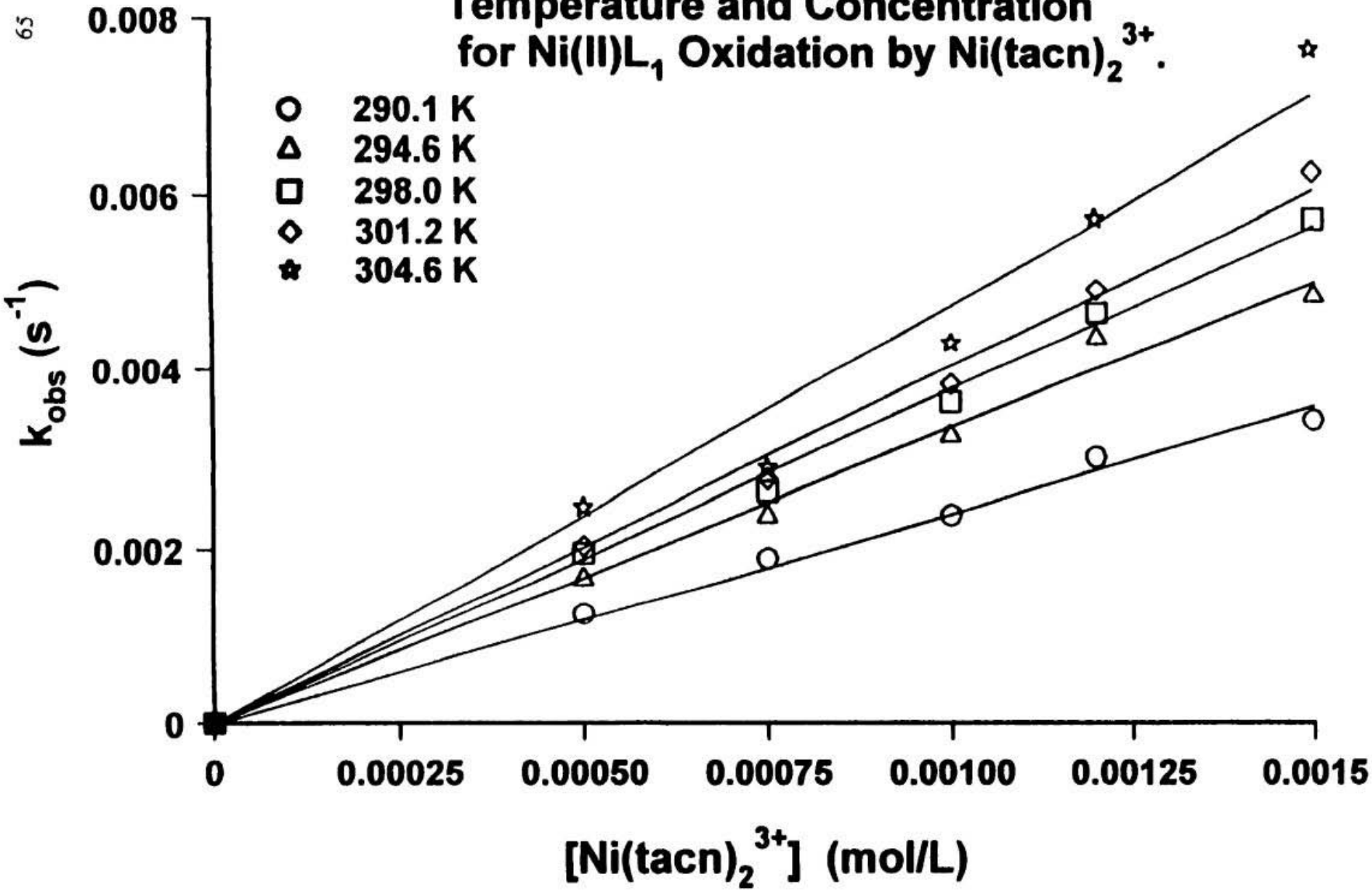

Fig. 3.11. Arrhenius Plot for $Ni(II)L_1$ Oxidation by $Ni(tacn)_2^{3+}$.

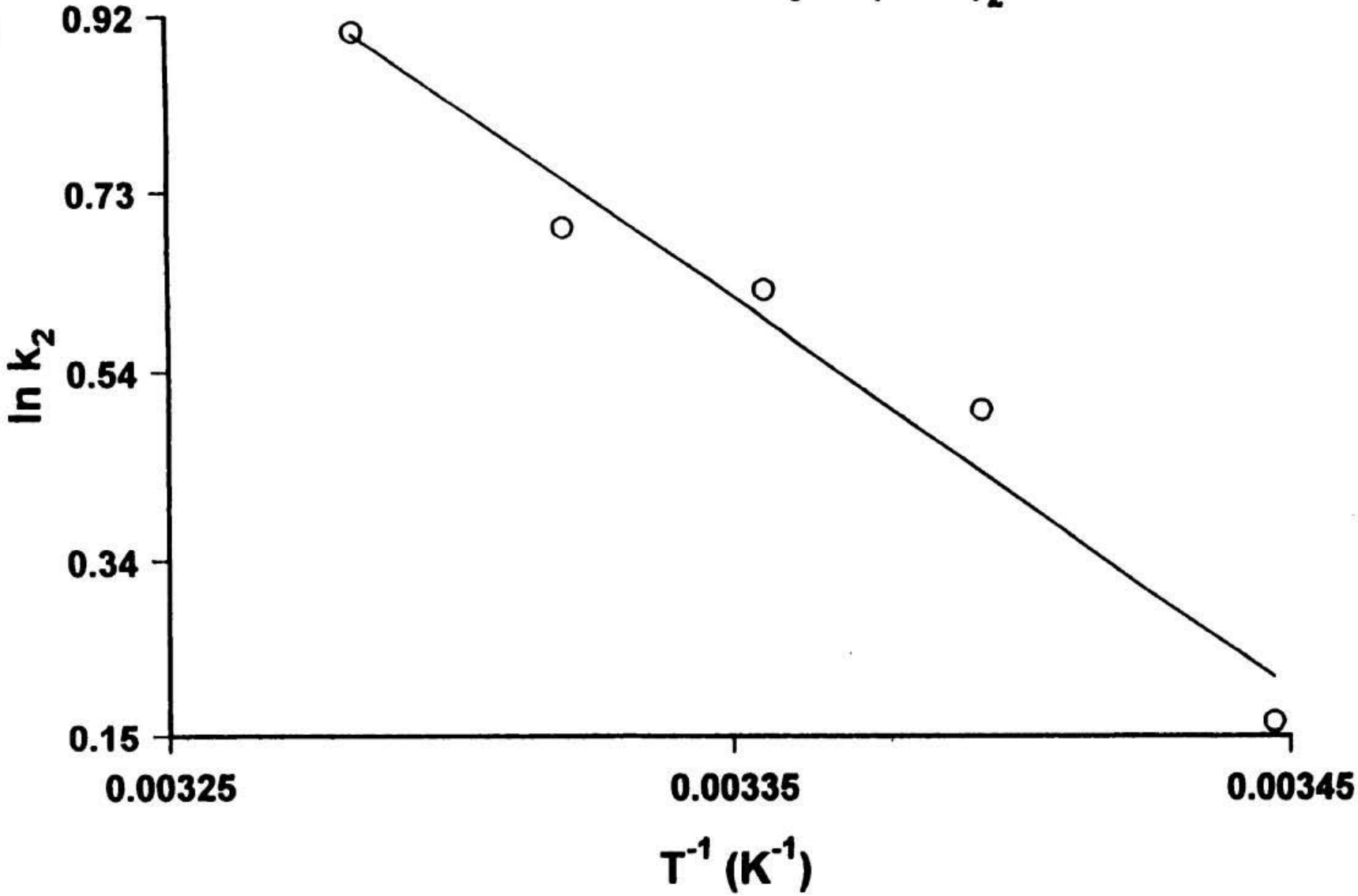

Fig. 3.12. Eyring Plot for Ni(II)L_1 Oxidation by $Ni(tacn)_2^{3+}$.

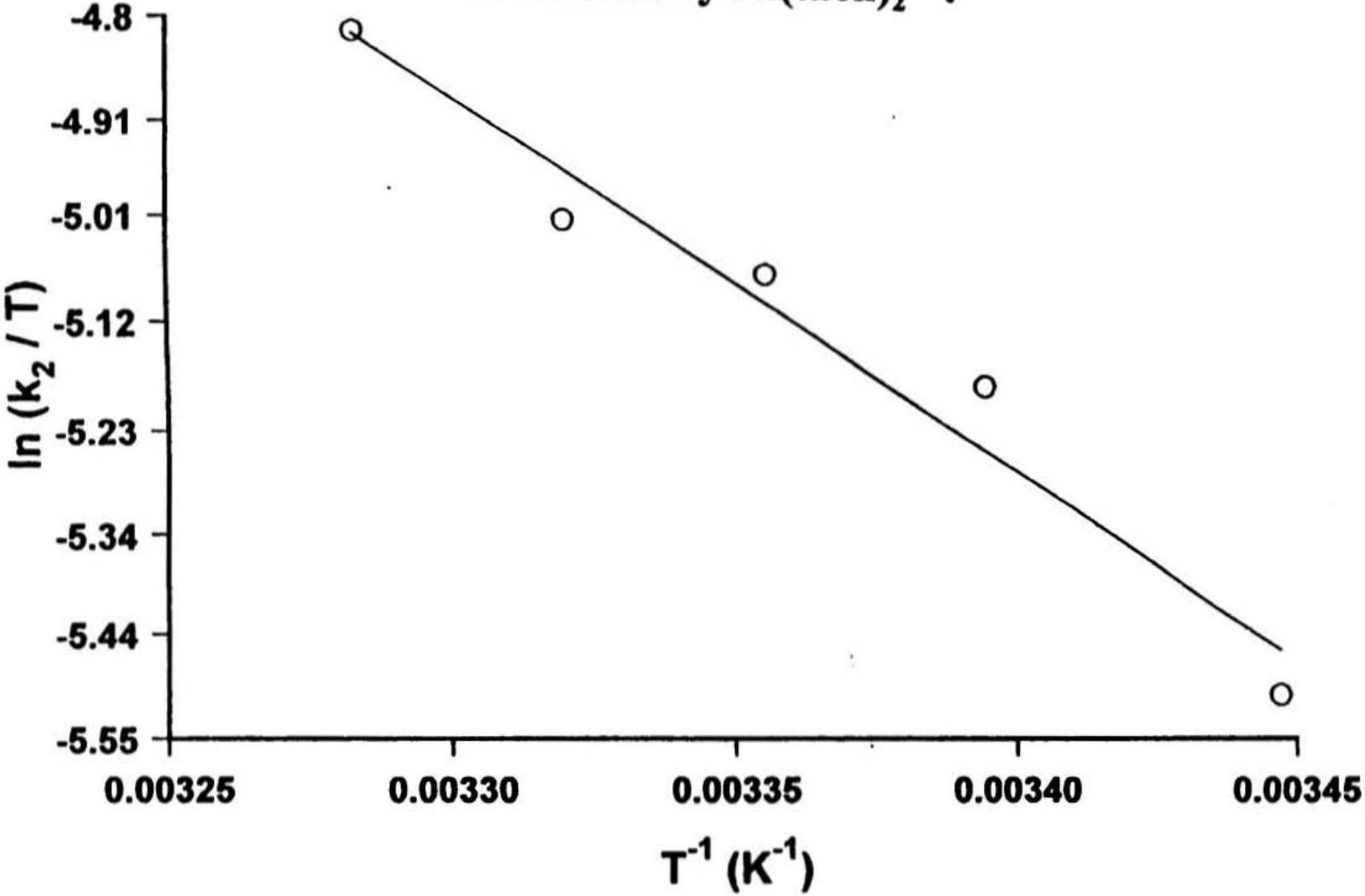

Fig. 3.13. Cyclic Voltammograms for $Ni(II)L_1$

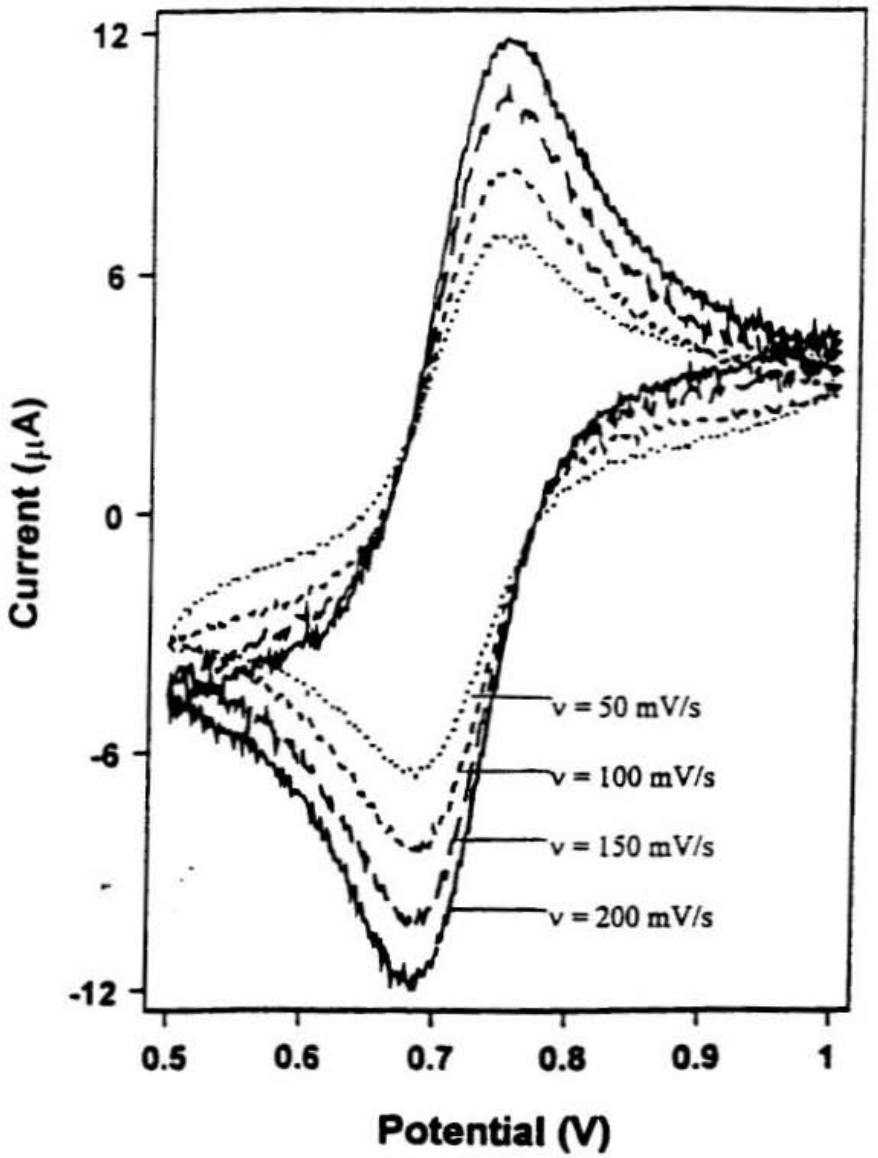

Fig. 3.14. Cyclic voltammogram for $Ni(II)L_2$

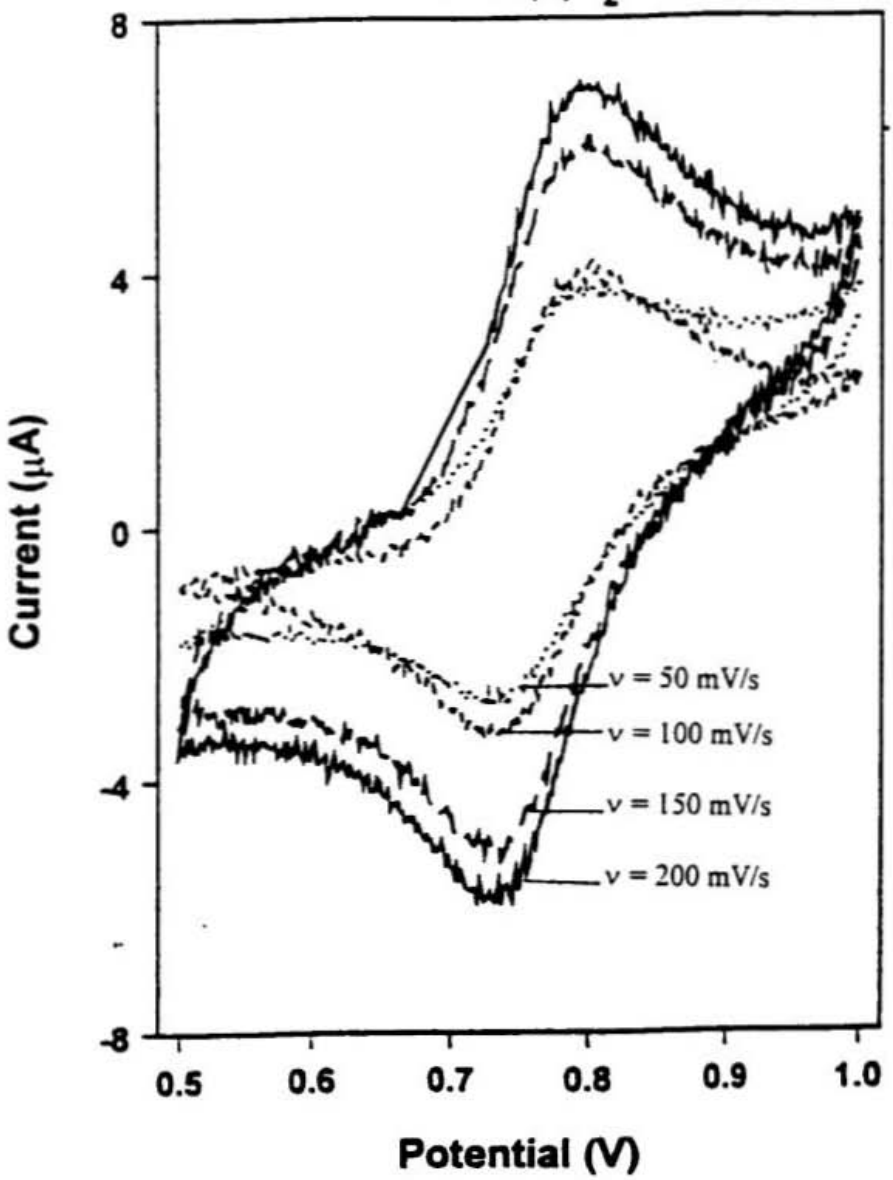

Chapter 4: Discussion

4.1. Synthesis

The alkylation of C-*meso* - 5,5,7,12,12,14- hexamethyl-1,4,8,11-tetraazacyclotetradecane (tet-a) with a large excess of bromoacetic acid in alkaline methanol medium gave only the di-N-substituted product. No tri-substituted or per-substituted product was formed as might be expected, that is the alkylation of tet-a is stereospecific. This phenomenon is probably due to the steric hindrance caused by methyl substituents in the environment of the unsubstituted amine groups. In the case of 5,12-dimethyl-7,14-diphenyl-1,4,8,11-tetraazacyclotetradecane, the nitrogens in the 1 and 8 positions are less sterically hindered than those in tet-a since the phenyl group is less bulky than two methyl groups. As a result alkylation can lead to tri-N-substituted and per-N-substituted products. By controlling the ratio of ligand and bromoacetic acid the di-N-substituted product can be prepared.

The functionalized ligands, L_1 and L_2, in principle, occur in several configurations arising from the presence of chirally substituted nitrogen centers as well as asymmetric carbon atoms present in the macrocyclic ligand. In the ligand L_1, the chiral carbon atoms occur at positions 7 and 14. This leads to two non-interconvertible diastereomeric forms, C-*meso* and C-*racemic*. The two chiral carbons of the *meso* form are of opposite configurations, R and S, while the two asymmetric carbons within each enantiomeric form of the racemate are of the same R or S configuration. When complexed to a metal, 20 isomers are possible, assuming the chelate ring conformers are analogous to those predicted to be the most strain

free in the systems studies by Tobe and coworkers.[35]

Tobe and coworkers[35] have discussed the stereochemistry of the corresponding unsubstituted macrocycle (cyclam).

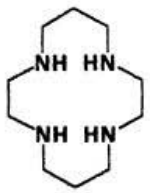

Cyclam

When coordinated to a metal, each nitrogen in the cyclam ligand is an asymmetric center and five distinct non-enantiomeric combinations can be produced. Bosnich et al.[35] discuss these combinations in terms of the direction in which the N-H bond points when the nitrogens are coordinated to the corners of a square. The five forms can be represented diagrammatically as follows:

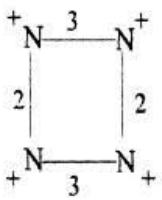

I

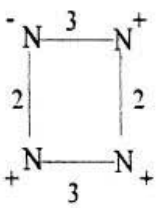

II

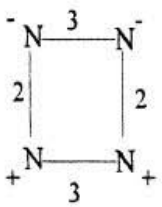

III

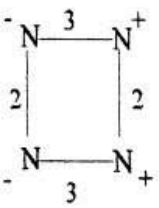

IV

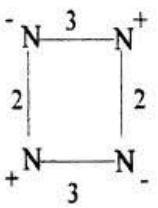

V

In these diagrams the plus refers to a hydrogen that points above the plane and a minus to one that points below. The number of carbon atoms in the linking chains are also shown. In theory, each of these trans forms can be converted to one or two cis analogs by displacing a nitrogen along an edge of the octahedron. Some of these forms, however, are sterically impossible and others are somewhat strained. Some idealized structures, based on the amount of strain are shown in Figure 4.1

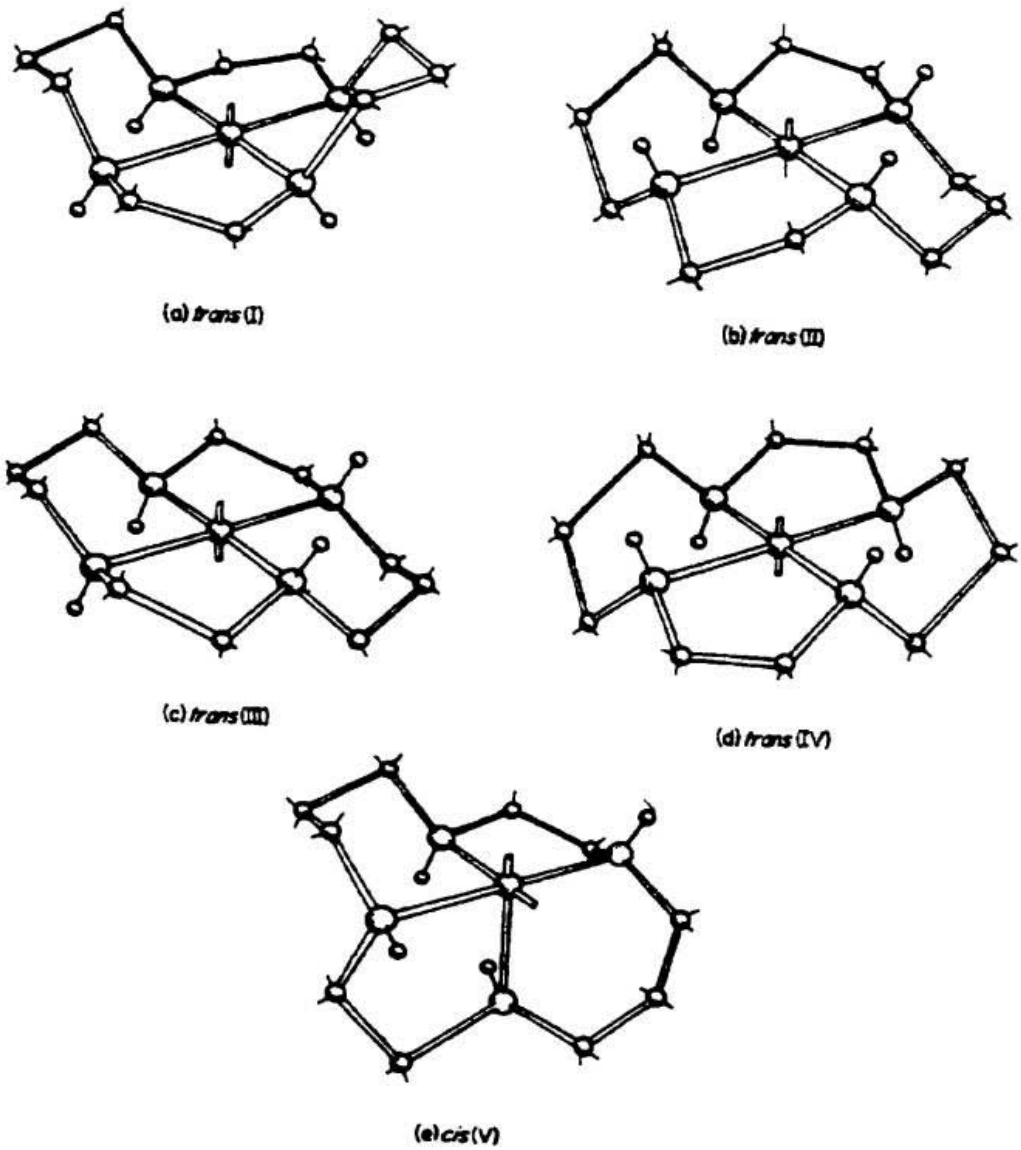

Figure 4.1. Idealized structures of the strain-free octahedral complexes of 1,4,8,11-tetraazacyclotetradecane.

In the ligand L_2, there are four chiral carbons, occurring at positions 5, 7, 12, and 14. This results in a number of possible diastereomers arising from the asymmetry of the carbon atoms as well as the asymmetry of the four nitrogens and their various combinations. It has been shown by Chen et al., that the *C-meso* $Cu(II)L_2$, complex has the trans (III) configuration as in Figure 4.2. [27]

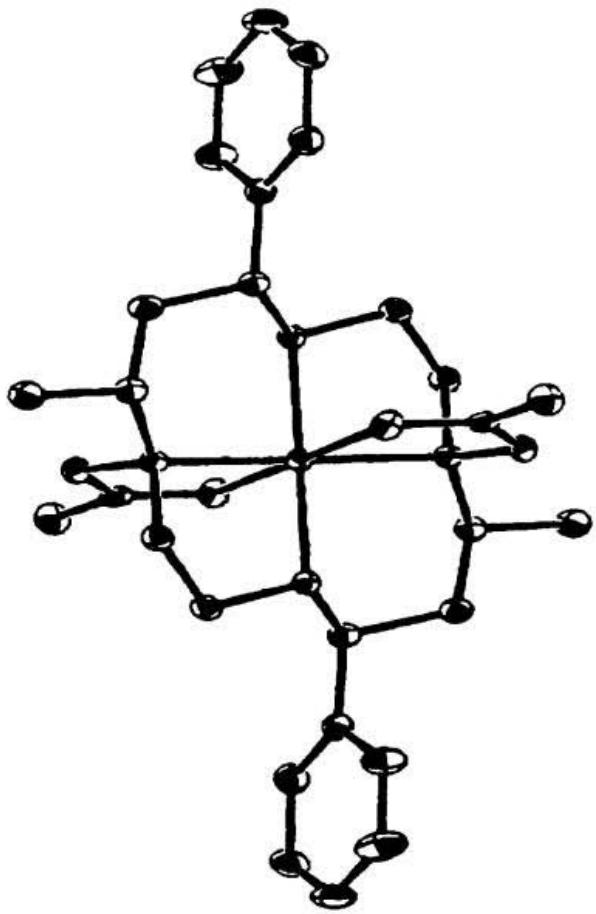

Figure 4.2. Structural representation of CuL_2 with hydrogen atoms omitted.

The metal atom in each complex is coordinated to the four nitrogen atoms in the macrocycle and two oxygen atoms of the appended carboxylato groups. The crystal structure of the Ni(II) complex of ligand L_1 has been published by Ji-De et al., and is shown to exist in the cis (V) configuration.[25]

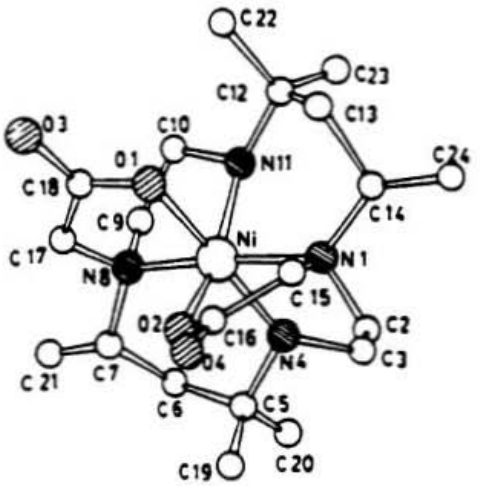

Figure 4.3. Structural representation of NiL_1.

This coordination is achieved by folding the macrocycle, which allows both of the carboxylic oxygen atoms to coordinate in a cis-arrangement. Both groups suggest that the different stereochemistry exhibited by the two tetraazamacrocyclic complexes is probably due to the fact that the two macrocycles prefer different basic conformations when they coordinate to metal ions. A later study by Belsky and coworkers, has shown the $Cu(II)L_1$ complex to have a trans configuration (Figure 4.4).[36] This fact has been cited as evidence to contradict the suggestion that the cis structure is attributed to the stereochemical pattern of the ligand. Based on the crystal structure of $Cu(II)L_1$, it would appear that the cis/trans phenomenon is dependent on the nature of the metal rather than the ligand.

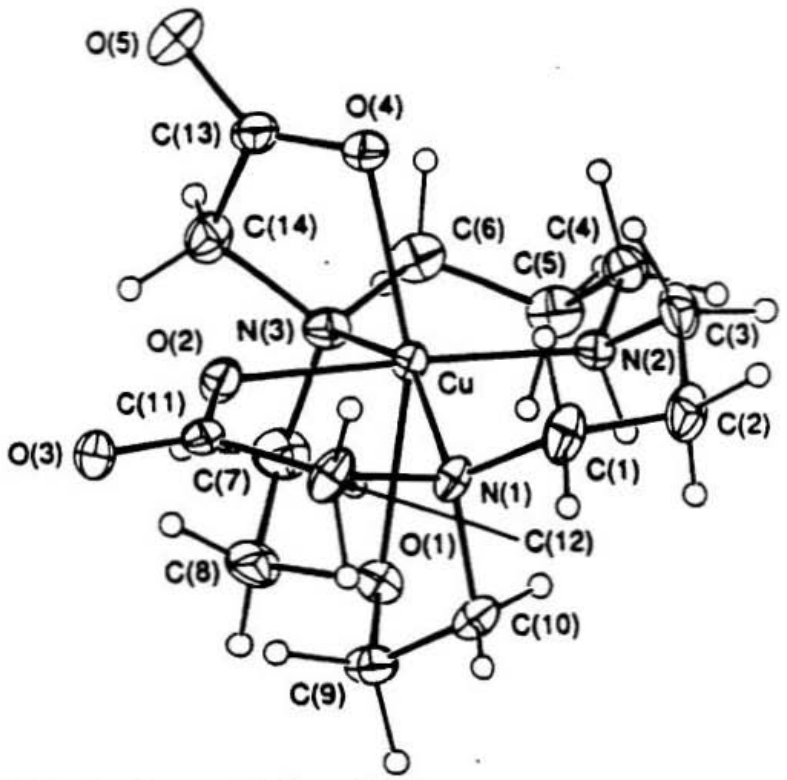

Figure 4.4. Structural representation of CuL_1.

The parent macrocycle of L_1 is 5,5,7,12,12,14-hexamethyl-1,4,8,11-tetraazacyclotetradecane (**2**). It was first prepared by Curtis and it is shown below:[37]

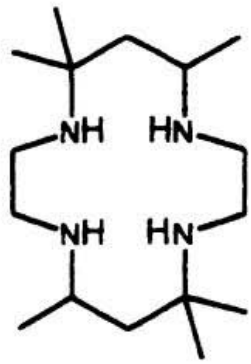

2

This macrocycle is identical to L_1 in all respects except for the absence of the two carboxylato pendant arms. Consequently, as with L_1, **2** has both meso and racemic forms that are traditionally labeled tet a and tet b, respectively. Curtis found that the *meso* ligand, tet a, can only coordinate with its four donor atoms arrayed in a single plane. Tet b, however, can coordinate in this fashion or it can form octahedral metal complexes of the type [M (tet a)A], where A is a bidentate ligand , in which the tetramine has buckled into a cis arrangement.

Curtis explains this observation on the basis of symmetry and steric arguments. He infers that the *meso* form has both axial co-ordination sites equally crowded by the *gem*-dimethyl groups, and thus, forms *trans* derivatives. In the *racemic* form, both *gem* dimethyl groups are on the same side of the molecular plane. This causes one of the axial sites to be blocked

and as a result, a *cis* arrangement can be observed. Given the similarities between L_1 and **2**, one would expect Curtis' reasoning to hold for the metal complexes of both ligands. If this were the case, one would predict the *meso* forms of ML_1 to have a *trans* configuration, regardless of the nature of the metal. The reported crystal structure of C-meso Ni(II)L_1, however, has the *cis* configuration. This fact appears to be in contradiction to Curtis' argument. However, closer inspection of the Ni(II)L_1 crystal structure has shown it to be the *racemic* isomer and not the *meso* isomer as reported. This finding further supports Curtis' theory.

Given the similarities between L_1, L_2, and **2**, one would expect that any cis / trans phenomena observed for the metal complexes of L_2 could be explained using the same arguments. The copper(II) complex of *C-meso* L_2 has been shown by Chen et al.,[27] to have a *trans* configuration. Given these facts, we predicted that the *racemic* isomers of L_2 should have a *cis* configuration when complexed to a metal. To test this prediction the Ni(II) complex of C-*rac* L_2 was prepared and a crystallographic analysis was performed. The results supported our prediction as the complex was shown to have a *cis* arrangement. The structure of NiL_2 is illustrated in Figure 3.1. The crystal was found to have three waters of crystallization in the structure. These waters occur in channels between the complexes. Two are strongly hydrogen bonded with each other, but none are hydrogen-bonded to either the nitrogens or the oxygens of the macrocyclic ligand. Both pendant carboxylato arms are coordinated to the central nickel(II) ion in a slightly distorted *cis*-octahedral arrangement. Ni - N (secondary) (2.094 Å) distances are slightly longer than Ni - N (tertiary) (2.078 Å).

This is also true for the *cis*- form of NiL_1. In that complex the Ni-N bonds were shorter (2.072, 2.0173 Å) for the tertiary nitrogens than the secondary ones (2.091, 2.107Å). This could possibly be due to the electron-attracting inductive effect of the carboxylato groups. The Ni-O bonds were quite different from each other (2.199, 2.065 Å). On inspection of the geometry about the metal centre, it may be surmised that this difference is in part due to strain in the macrocycle on coordination to the metal. For example, the N-Ni-O angles, that would be 180° for a perfectly octahedral centre, are in fact 176.78° and 163.06°. For the *cis*-NiL_2 structure, there is much less distortion from octahedral geometry, evidenced by the equatorial O-Ni-N angles of 178.6° and 174.6°.

Ji-De et al.[25] have also reported the structure of the aquonickel(II) complex of a mono-carboxylato- analogue of L_1. That complex takes up a trans-(III) configuration, with four nitrogens in a square plane and the carboxylato- and aqua- ligands in axial positions. In that case the Ni-N bonds were all similar (2.097, 2.093, 2.070 and 2.103 Å), and the Ni-O length (for the carboxylato- arm) was 2.065 Å, with only minor deviations from octahedral geometry. The mean Ni(II)-N bond length for octahedral NiN_6 moieties has been reported to be 2.081 ± 0.026 Å.[38] Hence the bond lengths reported here for $Ni(II)L_2$ are not unusual.

Further evidence to support our theory on the *cis/trans* phenomena is provided by the geometry of the cobalt complex of L_1. The *meso* form of $[Co(III)\,L_1]^+$ was synthesized and was found to have a distorted *trans* octahedral geometry, as predicted. The complex has four amino nitrogens in a plane and two apical carboxylate oxygen donors. The molecule has a center of symmetry at Co 1 with the result that the methyl and carboxylato groups are

each *trans*. The O-Co-O and N-Co-N angles are all 180°, as for a perfectly octahedral center. As with the *cis*-Ni complexes, the Co(II)L_1 has Co-N bonds that are shorter (2.004, 2.007 Å) for the tertiary nitrogens than the secondary ones (2.020, 2.030 Å).

The Ni(II)L_1 complex used for kinetic studies in this work has a *trans*-(III) conformation,[39] similar to $[CoL_1]^+$ and the Cu(II)L_2 complexes.[25]

4.2. Peroxodisulfate Kinetics

Redox reactions involving metal ions or organic reductants and peroxodisulfate usually proceed via fission of the peroxo bond.[21] This step may be assisted by the presence of a metal ion. A common mechanistic scheme for the oxidation of a cationic complex $[ML]^{n+}$ by $S_2O_8^{2-}$ is described as follows:

Step 1

$$[ML]^{n+} + S_2O_8^{2-} \overset{K_{ip}}{\rightleftharpoons} \underset{\text{ion pair}}{\{ML^{n+}, S_2O_8^{2-}\}}$$

Step 2

$$\{ML^{n+}, S_2O_8^{2-}\} \overset{k_1}{\rightarrow} [ML]^{(n+1)+} + SO_4^{\cdot-} + SO_4^{2-}$$

Step 3

$$[ML]^{n+} + SO_4^{\cdot-} \overset{fast}{\rightarrow} [ML]^{(n+1)+} + SO_4^{2-}$$

Overall Reaction

$$2[ML]^{n+} + S_2O_8^{2-} \rightarrow 2[ML]^{(n+1)+} + 2SO_4^{2-}$$

The first step in the mechanism consists of an equilibrium whereby the reactant cation and anion form an ion-pair. Step 2 involves cleavage of the peroxo bond followed by outer-sphere electron transfer from nickel(II) to peroxodisulfate. In the third step the sulfate radical produced in step 2 reacts with a second cation molecule. The second step is

considered the rate determining step since it is much slower than both the ion-pairing and the step involving the $SO_4^{\cdot-}$ radical. It has been shown that nickel(II) complexes of neutral square planar macrocycles, coordinate sulfate ion when undergoing oxidation, forming the $[Ni(III)L(SO_4)]^+$ cation.[40] There are no vacant coordination sites at the metal in this present study, thereby eliminating the possibility of sulfato-adduct formation.

Considering the overall reaction, a relatively simple overall second-order rate law is obtained

$$\text{Rate} = \frac{+1/2\, d[ML]^{2+}}{dt} \qquad \text{Eqn. 4.1}$$

$$= k_r [M(II)_{tot}] [S_2O_8^{2-}]$$

where $[M(II)_{tot}]$ is the total metal concentration given by:

$$[M(II)_{tot}] = [ML^{2+}] + [\{ML^{2+}, S_2O_8^{2-}\}] \qquad \text{Eqn. 4.2}$$

The expression in 4.1 must be equivalent to the reaction rate indicated by the rate determining step:

$$\text{Rate} = 2k_r [\{ML^{2+}, S_2O_8^{2-}\}] \qquad \text{Eqn. 4.3}$$

Using the reaction in step 1, an expression for K_{ip} can be obtained:

$$K_{ip} = \frac{[\{ML^{2+}, S_2O_8^{2-}\}]}{[S_2O_8^{2-}]\,[ML^{2+}]} \qquad \text{Eqn. 4.4}$$

Rearrangement of 4.4 gives:

$$[ML^{2-}] = \frac{[\{ML^{2-}, S_2O_8^{2-}\}]}{[S_2O_8^{2-}]\,K_{ip}} \qquad \text{Eqn. 4.5}$$

Substitution of equation 4.5 into equation 4.2 yields:

$$[M(II)_{tot}] = \frac{[\{ML^{2-}, S_2O_8^{2-}\}]\,(K_{ip}([S_2O_8^{2-}] + 1))}{K_{ip}\,[S_2O_8^{2-}]} \qquad \text{Eqn. 4.6}$$

Rearrangement of equation 4.6 gives:

$$[\{ML^{2-}, S_2O_8^{2-}\}] = \frac{[M(II)_{tot}]\,K_{ip}\,[S_2O_8^{2-}]}{(K_{ip}([S_2O_8^{2-}] + 1)} \qquad \text{Eqn. 4.7}$$

Substitution of equation 4.7 into equation 4.3 yields:

$$\text{Rate} = \{2k_r K_{ip}/(1 + K_{ip}[S_2O_8^{2-}]\}\,[S_2O_8^{2-}][ML^{n-}]$$

If the ion pairing constant is sufficiently large, such a rate law is expected to show curvature in the dependence of the observed first-order rate constant on peroxodisulfate concentration. In the present system, where $[ML]^{n-}$ represents [NiL], no curvature in the k_{obs} vs $[S_2O_8^{2-}]$ plots was seen. This suggests that the ion-pairing constant is small. This is to be expected since we have a 2- anion with a neutral metal complex. The ion-pairing constant can be

estimated using the Eigen-Fuoss equation[41], as follows:

$$K_{ip} = (4\pi N\sigma^3/3000)\exp(-w(\sigma)/RT)$$

where

$$w(\sigma) = Z_M Z_L e^2/(D_s\sigma(1+\beta\sigma I^{1/2}))$$

In these expressions, σ is the sum of the radii of the reactants, Z_M and Z_L are the charges on the reactants, D_S is the solvent dielectric constant and $\beta = (8\pi Ne^2/1000D_skT)^{1/2}$. Using the Eigen-Fuoss equation an ion-pairing constant of 4.2×10^{-15} M^{-1} has been estimated for the Ni(II)L / peroxodisulfate systems. This is consistent with the literature values. Ion-pairing constants of a Fe(III)/Cr(II) and Fe(II)/Mn(III) electron transfer reactions have been shown to be 9.93×10^{-3} M^{-1} and 2.39×10^{-2} M^{-1}, respectively. The charges of the reactants in these examples are significantly higher than those of this study. This difference in charge accounts for the variation observed. Due to the small ion-pairing constants observed in this study, the approximation $(1 + K_{ip}[S_2O_8^{2-}]) \sim 1$ is valid over the range of oxidant concentrations used. Hence, the rate law simplifies to :

$$\text{Rate} = k_{obs}[NiL]$$

$$= 2k_sK_{ip}[S_2O_8^{2-}][NiL]$$

The activation parameters determined in this study for $Ni(II)L_1$ and $Ni(II)L_2$ are consistent with those for the reaction of other transition metal complexes with peroxodisulfate.[42] The second order rate constants for the two complexes, which differ nearly 100 fold, may be attributed to the differences in redox potentials. $Ni(II)L_1$ has a redox potential that is lower by 50 mV. The activation entropies are negative which is consistent with the overall reaction as expressed in equation 3.1. According to this equation the reaction produces four charged species for every three charged species it consumes. By increasing the number of charged species in the aqueous solution, the solution becomes more organized due to electrostriction of the solvent. This increase in organization is reflected in a negative entropy value. Table 4.1 lists the enthalpy and entropy values for oxidation of various metal complexes by peroxodisulfate.[42]

Sutin, Ehrenson and Bruswhig have derived analytical expressions for interpreting the activation parameters for an outer-sphere electron-transfer mechanism.[43] While such mathematical models are applicable to the Ni(II) systems under study, they are not practical to apply since $\Delta G^0 \neq 0$. For the self-exchange study, where $\Delta G^0 = 0$, such models are applied.

Table 4.1. Enthalpy and Entropy Values for Oxidation of Various Metal Complexes by Persoxodisulfate.

Complex	$\Delta H^{\ddagger}$ (kJ mol^{-1})	$\Delta S^{\ddagger}$ (J K^{-1} mol^{-1})
Cu(dioxocyclam)	35	-132
Ni(5,5,7,12,12,14-hexamethyl-1,4,8,11-tetraazacyclotetradecane-1,8-diacetic acid)	40	-115
Ni(5,12 dimethyl - 7, 14-diphenyl-1,4,8,11 tetraazacylotetradecane-1,8-diacetic acid)	43	-115
$[Fe(2,2^{1},6^{1},2^{11}\text{-terpyridyl})_3]^{2+}$	42	-100
Co(nitrilotriacetate)	65	-99
$[Ni(pyane)]^{2+}$	69	-30
$[Co(iminodiacetate)]^{2-}$	87	-32

4.3 Stopped-Flow Kinetics

$[Ni(tacn)_2]^{3+}$ is well known as an outer-sphere oxidant, whose redox reactions do not display acid dependence, unless the reductant undergoes protonation/deprotonation.[44] For this reason, $[Ni(tacn)_2]^{3+}$ is a useful oxidant to study the mechanism of electron-transfer from the nickel(II) pendant-arm macrocycles that are being studied. The general outer-sphere mechanism for the NiL_1 and $[Ni(tacn)_2]^{3+}$ reaction mechanism is a follows:

$$M_O^1 + M_r \rightleftharpoons M_o^1 M_R$$

$$M_o^1 M_R \rightarrow M_R^1 M_o$$

$$M_R^1 M_o \rightarrow M_R^1 + M_o$$

The first step in the mechanism consists of diffusion of the two reagents together to form the outer sphere adduct. The second, rate determining step, involves electron transfer to yield the products. The outer sphere mechanism is ensured in the reaction

between NiL_1 and $[Ni(tacn)_2]^{3+}$ because of the substitutionally inert nature of $[Ni(tacn)_2]^{3+}$. Although NiL_1 has two potential bridging ligands, the lower energy outer sphere mechanism will be followed. The rate determining step in this reaction is usually the electron transfer step. When comparing the reaction rates for NiL_1 oxidation with $[Ni(tacn)_2]^{3+}$ versus $S_2O_8^{2-}$ there is a significant difference. Clearly this is because the faster reaction has a transition state requiring less energy. The rate determining step of the NiL_1 / $S_2O_8^{2-}$ system involves bond cleavage. The peroxo bond must be broken before electron transer may occur. This requires more energy than electron transfer in the NiL_1 / $[Ni(tacn)_2]^{3+}$ system, where bond making or breaking does not take place. This is reflected in the differing activation energies of 32.8 ± 0.1 kJ mol^{-1} and 40.7 ± 5.4 kJ mol^{-1}.

Both $Ni(II)L_1$ and $Ni(II)L_2$ are high-spin six coordinate and hence, paramagnetic. As a result, it is not possible to measure the self-exchange rates for the complexes by the usual NMR or epr methods.[45] However, self-exchange rates can be estimated using Marcus Theory.[46]

For an outer-sphere electron transfer mechanism, the rate constant for the cross-reaction k_{12} is related to the rate constants for the self-exchange rates of the components, k_{11} and k_{22}, and the equilibrium constant K_{12} by the expression $k_{12} = (k_{11}\, k_{22}\, K_{12} f_{12})^{1/2} w_{12}$,

where

$$\ln f_{12} = \frac{[\ln K_{12} + (w_{12}-w_{21})/RT]^2}{4[\ln (k_{11} k_{22}/A_{11}A_{22}) + (w_{11} + w_{22})/RT]}$$

$$w_{12}' = \exp[(-w_{12} + w_{21} - w_{11} - w_{22})/2RT]$$

$$w_{ij} = \frac{Z_iZ_je^2}{D_s\sigma_{ij}(1 + \beta\sigma_{ij}(\mu^{1/2}))}$$

$$A_{ij} = \frac{4\pi N\sigma^2 \upsilon b \gamma r \exp(-w(\sigma)/RT)}{1000}$$

In these expressions, w_{ij} is the work required to bring the ions i and j (with charges Z_i and Z_j respectively) to the separation distance σ_{ij}. This distance is assumed to be equal to the sum of the radii of the ions i and j; β ($= 8\pi Ne^2/1000D_skT)^{1/2}$; υb is the nuclear frequency that destroys an activated complex configuration; and γr is the thickness of the reaction layer (~ 0.8Å); D_s is the dielectric constant of the medium. In the present reaction, where Ni(II)L_1 is neutral, the work terms will be negligible, so w_{12}' becomes unity . Hence $k_{12} = (k_{11} k_{22} K_{12} f_{12})^{1/2}$. The term f is usually assumed to be 1, hence k_{11} is calculated as $(k_{12}^2 / k_{22} K_{22})$. The value of k_{22}, the self-exchange rate for $[Ni(tacn)_2]^{3+}$ has been determined to be 6×10^3 s^{-1}.[28, 47] From the electrode potentials of Ni(II)L_1 and $[Ni(tacn)_2]^{2+}$, the K_{12} value is calculated to be 43. Hence the self-exchange rate for

$[NiL^1]^{0\,\cdot-}$ is calculated to be 55 $mol^{-1}\ dm^3\ s^{-1}$. This value is low compared to six-coordinate $[Ni(LL)_3]^{2+3+}$ systems, where LL represents the bidentate ligands tacn, 2,2'-bipyridyl (bipy) and 1,-10 phenanthroline (phen), and their substituted derivatives.[48] The self exchange rates for these tris-bidentate chelate complexes have been estimated as 1500 $mol^{-1}\ dm^3\ s^{-1}$ for LL = bipy and phen.[48] The self-exchange rate for $[Ni(cyclam)]^{2+3+}$ has also been measured at 2000 $mol^{-1}\ dm^3\ s^{-1}$.[49] The value for $[NiL^1]^{0\,\cdot-}$ estimated here is one to two orders of magnitude lower than other nickel systems, which has been considered as "not unreasonable".[50] Interestingly, the self-exchange rate for a nickel complex containing a deprotonated tripeptide has been estimated at 450 $mol^{-1}\ dm^3\ s^{-1}$,[51] which is much closer to that for $[NiL^1]^{0\,\cdot-}$. We have assumed the reaction to be adiabatic, where the transmission coefficient, κ_{12} is unity. Any non-adiabatic behaviour ($\kappa_{12} < 1$) would result in a higher calculated value for the self-exchange rate.

The reorganization energies of the self-exchange electron transfer can be calculated using the following equation[43]:

$$\lambda/4 = \Delta G^0 + \Delta G^{\neq}$$

where λ is the reorganization energy. Since $\Delta G^0 = 0$, for a self-exchange reaction, this equation simplifies to:

$$\lambda/4 = \Delta G^{\neq}$$

Using an expression for the rate constant, $\Delta G^{\neq}$ can be determined.[52]

$$k = Z\exp(\Delta G^{\neq}/RT)$$

where Z is taken to be the collision frequency between reaction partners and is often set at the gas-phase collision frequency, ~10^{11} L mol^{-1} s^{-1}. Using the experimental self exchange rate constant for $[NiL^1]^{0/+}$, the reorganization energy for the electron transfer is estimated to be 211.4 $KJ.mol^{-1}$. This value is similar to that found for a series of hexaquo ions. The reorganization energies for the series $Fe^{2+/3+}$, $Cr^{2+/3+}$, $Mn^{2+/3+}$, $V^{2+/3+}$, $Co^{2+/3+}$ were 202.3 $kJ.mol^{-1}$, 334.8 $KJ.mol^{-1}$, 314.3 $kJ.mol^{-1}$, 263.2 $kJ.mol^{-1}$, 216.2 $kJ.mol^{-1}$.[52]

Conclusion

The purpose of this study was to examine pendant-arm macrocyles and determine their suitability as bridging ligands for inner-sphere reactions. While no inner-sphere reactions were found or examined in this study, greater insight has been gained into the behavior of the particular macrocycles researched. Exploration on the redox properties of these complexes with cationic oxidants, with application as inner-sphere reducing agents for reductive dissolution of transition metal oxides, is ongoing.

List of References

1. D.F. Shriver, P.W. Atkins, and C.H. Langsford, Inorganic Chemistry, 2nd Edition; W.H. Freeman and Company: New York, 240 (1994).

2. A. McAuley and S. Subramanian, *Inorg. Chem.*, **30**, 371 (1991).

3. V.K. Manchanda, P.K. Mohapatia, C. Zhu and R.M. Izatt., *J. Chem. Soc. Dalton Trans.*, 1583 (1995).

4. M.R. Oberholzer, L.C. Siegfried, T.A. Kaden, *Inorg. Chim. Acta.*, **246**, 41 (1996).

5. S. Chaves, R. Delgado, M.T. Duarte, J.A.L. Silvia, V. Felix, M. De, C.T. Carronda, *J. Chem. Soc. Dalton Trans.*, 2579 (1992).

6. P.J. Davies, M.R. Taylor, K.D. Wainwright, P. Harriott, P.A. Duckworth, *Inorg. Chim. Acta*, **246**, 1 (1996).

7. R. Zhang and D.H. Busch, *Inorg. Chem.*, **32**, 4970 (1993).

8. X. Bu, D. An, Y.Chen, M. Shionoya, E. Kimura, *J. Chem. Soc. Datlton Trans.*, 2289 (1995).

9. J.P.L. Cox, K.J. Jankowski, R. Kataky, D. Parker, N.R.A. Beeley, B.A. Boyce, M.A.W. Eaton, K. Miller, A.T. Millian, A. Harrison and C. Walker, *J. Chem. Soc., Chem. Commun.*, 797 (1989).

10. E. Kimura, T. Koike and M. Takahashi, *J. Chem. Soc., Chem. Commun.*, 385 (1985).

11. J.P. Collin, J.P. Sauvage, *J. Chem. Soc., Chem. Comm.*, 1075 (1987).

12. I. Meunier, A.K. Mishra, B. Hanquet, P. Cocolios, and R. Guilard, *Can. J. Chem.*, **73**, 685 (1995).

13. M.P. Suh, B.Y. Shim and T.S. Yoon, *Inorg. Chem.*, **33**, 5509 (1994).

14. P.V. Berhardt, and G.A. Lawrance, *Coor. Chem. Rev.*, **104**, 297 (1990).

15. X.H. Bu, D.A. An, Y.T. Chen, M. Shionoya, and E. Kimura, *J. Chem. Soc. Dalton Trans.*, 2289 (1995).

16. J. R. Morphy, D. Parker, R. Kataly, A. Harrison, M.A.W. Eaton, A.T. Millian, A. Phipps and C. Walker, *J. Chem. Soc., Chem. Comm.*, 792 (1989).

17. A.S. Craig, I.M. Helps, K.J. Jankowski, D. Parker, N.R.A. Beily, B.A. Boyce, R.K. Rhind, and A. Phipps, *J. Chem. Soc., Chem. Comm.*, 794 (1989).

18. A.D. Sherry, R.D. Brown, C. Geralds, S.H. Koenig, K.T. Kuan, M. Spiller, *Inorg. Chem.*, **28**, 620 (1989).

19. J.R. Morphy, D. Parker, R. Alexander, A. Bains, A.F. Curre, M.A. Eaton, A. Harrison, A. Millian, A. Phipps, S.K. Shind, R. Titmas, D. Weaterhby, *J. Chem. Soc., Chem. Comm.*, 157 (1988).

20. R. Chang, *Chemistry*, 4th edition, McGraw-Hill, Inc., NewYork (1991).

21. R. I. Haines and S.J. Northcott, *Can. J. Chem.*, 2785 (1992).

22. R.A. Henderson, The Mechanisms of Reactions at Transition Metal Sites, Oxford University Press, (1993).

23. M. Tait, D.H. Busch and N.F. Curtis, *Inorganic Syntheses*, **18** (1978).

24. M. Jaacobi, D. Meyerstein and J. Libie, *Inorg. Chem.*, **18**, 429 (1979).

25. X. Ji-De, N. Shi-Sheng and L. Yu-Juan, *Inorg. Chim. Acta*, **111**, 61 (1986).

26. R.W. Hay and P.M. Gidney, *J. Chem. Soc. Dalton Trans.*, 974 (1976).

27. L. Chen, L.K. Thompson, J.N. Bridson, J. Xu, S. Ni and R. Guo, *Can. J. Chem.*, **71**, 1805 (1993).

28. A. McAuley, P.R. Norman and O. Olubuyide, *Inorg. Chem.*, **23**, 1938 (1984).

29. K.A. Kumar, P. Sirawaroop, K.J. Rao and P.V.K. Rao, *Transition Met. Chem. (London)*, **12**, 441 (1987).

30. C.J. Gilmore, *J. Appl. Cryst.*, **17**, 42 (1984).

31. P.T. Beurskens, Technical Report 1984/1, Crystallographic Laboratory, Toernooiveld, 6525 Ed Nijmegan, Netherlands.

32. Texsan-Texray Structure Analysis Package, Molecular Structure Corporation, 1985.

33. D.T. Cromer and J.T. Waber, *International Tables for X-Ray Crystallography*, **IV**, The Kynock Press, Birmingham, England.

34. I.M. Kolthoff, E.J. Meehan, E.M. Carr, *J. Am. Chem. Soc.*, **75**, 1439 (1953).

35. B. Bosnich, C.K. Poon and M.L. Tobe, *Inorg. Chem.*,**4**, 1102 (1965).

36. V.K. Belsky, N.R. Streltsova, E.N. Kuzmina and A.Y. Nazarenko, *Polyhedron*, **12**, 831 (1993).

37. N.F. Curtis, *J. Chem. Soc.*, 1979 (1967).

38. A. McAuley, T. Palmer and T.W. Whitcombe, *Can J. Chem.*, **71**, 1972 (1993).

39. N.F. Curtis, *Coord. Chem. Rev.*, **3**, 3 (1968).

40. E.S. Gore and D.H. Busch, *Inorg. Chem.*, **12**, 1 (1973).

41. D.H. Macartney, *Reviews in Inorganic Chemistry*, **9**, 103 (1988).

42. R.G. Clarke, Synthesis and Oxidation Kinetics of Transition Metal Complexes, Honors Thesis (1995).

43. G.M. Brown, N. Sutin, *J. Am. Chem. Soc.*, **101**, 883 (1979), B.S. Brunschwig, J. Logan, M.D. Newton, N. Sutin, *J. Am. Chem. Soc.*, **102**, 5798 (1980), N. Sutin, M.J. Weaver, *Inorg. Chem.*, **19**, 1096 (1980).

44. A.G. Lapin and A. McAuley, *Adv. Inorg. Chem.*, **32**, 241 (1988).

45. N.B. Lewis, C.D. Coryell and J.W. Irvine, *J. Am. Chem. Soc.*, **386**, (1949).

46. R.A. Marcus, *Ann. Rev. Phys. Chem.*,**15**, 155, (1964); N. Sutin, *Progr. Inog. Chem.*, **30**, 441 (1983); R.A. Marcus and N. Sutin, *Biophys. Acta*, **811**, 265 (1985).

47. A. McAuley, P.R. Norman and O. Olubuyide, *J. Chem. Soc., Dalton Trans.*, 1501 (1984).

48. D.H. Macartney and N. Sutin, *Inorg. Chem.*, **22**, 3530 (1983).

49. A. McAuley, D.H. Macartney and T. Oswald, *J. Chem. Soc. Chem. Commun.*, 274 (1982).

50. D. Astruc, in Electron Transfer and Radical Processes in Transition Metal Chemistry, Wiley-VCH (1995) p. 20.

51. J.F. Wang, K. Kumar and D.W. Margerum, *Inorg Chem.*, **28**, 3481 (1989).

52. K.M. Rosso, J.R. Rustad, *J. Phys. Chem.*, **104**, 6718 (2000).

Table A1.a. Positional Parameters and B (eq) for NiL_2.

atom	x	y	z	B(eq)
H(8)	0.8793	0.3761	0.3578	4.4
H(9A)	0.7246	0.4499	0.2735	4.1
H(9B)	0.6574	0.3977	0.2004	4.1
H(10A)	0.6100	0.3741	0.3532	4.1
H(10B)	0.7224	0.3439	0.3937	4.1
H(12)	0.3602	0.3092	0.1962	5.1
H(13)	0.2247	0.3479	0.2757	6.8
H(14)	0.2360	0.3445	0.4435	6.2
H(15)	0.3923	0.2934	0.5258	6.6
H(16)	0.5285	0.2460	0.4450	5.6
H(17A)	0.4812	0.0188	0.1357	6.2
H(17B)	0.5869	-0.0160	0.1165	6.2
H(17C)	0.5614	-0.0114	0.2220	6.2
H(18A)	0.7630	0.0235	0.1133	4.0
H(18B)	0.6993	0.0928	0.0635	4.0
H(21)	1.1019	0.1634	0.2847	7.4
H(22)	1.2458	0.0899	0.3443	8.7
H(23)	1.2706	0.0602	0.5208	12.5
H(24)	1.1644	0.1064	0.6174	12.3
H(25)	1.0163	0.2098	0.5523	10.2
H(26A)	1.0180	0.4618	0.3193	5.8
H(26B)	0.9890	0.4407	0.2099	5.8
H(26C)	0.9107	0.4950	0.2595	5.8
H(27A)	0.8097	0.4244	0.1136	4.1
H(27B)	0.8808	0.3479	0.1102	4.1

Table A1.a. Positional Parameters and B (eq) for NiL_2.

atom	x	y	z	B(eq)
O(5)	0.1107	0.0730	0.0201	7.7
O(6)	0.2642	0.1130	0.1621	8.0
H(5OA)	0.0389	0.0971	0.0324	9.1
H(5OB)	0.0937	0.0089	-0.0038	9.3
H(6OA)	0.2207	0.1750	0.1589	16.7
H(6OB)	0.1938	0.0929	0.1103	9.5
O(7)	0.5019	0.0239	0.5433	9.4
H(7OA)	0.4862	0.0873	0.5663	11.0
H(7OB)	0.5674	0.0366	0.4979	17.9

Table A1.a. Positional Parameters and B (eq) for NiL_2.

atom	x	y	z	B(eq)
C(17)	0.5497(5)	0.0178(4)	0.1650(6)	5.3(4)
C(18)	0.7490(5)	0.0831(4)	0.1101(4)	3.6(3)
C(19)	0.8465(5)	0.1281(4)	0.0928(4)	3.3(3)
C(20)	1.0465(5)	0.1826(4)	0.4144(6)	4.5(4)
C(21)	1.1107(6)	0.1515(5)	0.3581(7)	6.0(4)
C(22)	1.1997(7)	0.1050(6)	0.3971(9)	7.8(6)
C(23)	1.2146(9)	0.0944(7)	0.491(1)	9.8(8)
C(24)	1.151(1)	0.127(1)	0.553(1)	12(1)
C(25)	1.0675(7)	0.1702(6)	0.5113(6)	7.7(5)
C(26)	0.9554(5)	0.4468(4)	0.2690(5)	4.8(4)
C(27)	0.8103(5)	0.3680(4)	0.1264(4)	3.4(3)
C(28)	0.7249(5)	0.3238(4)	0.0611(4)	3.4(3)
H(1)	0.5311	0.2635	0.1980	3.8
H(1N)	0.6536	0.2278	0.3704	3.3
H(2A)	0.5614	0.1264	0.3215	4.8
H(2B)	0.4665	0.1326	0.2383	4.8
H(3)	0.5678	0.1345	0.1205	4.3
H(3N)	0.8118	0.1813	0.4022	3.5
H(4A)	0.7143	0.0680	0.3323	3.9
H(4B)	0.7594	0.0035	0.2645	3.9
H(5A)	0.9083	0.0906	0.2713	3.7
H(5B)	0.8915	0.0655	0.3724	3.7
H(6)	0.9296	0.2633	0.4303	4.4
H(7A)	0.9806	0.2729	0.2469	4.2
H(7B)	1.0471	0.3212	0.3325	4.2

Table A1a. Positional parameters and B(eq) for NiL_2.

atom	x	y	z	B(eq)
Ni(1)	0.75914(6)	0.22878(5)	0.22054(5)	2.61(3)
O(1)	0.6731(3)	0.2686(3)	0.0946(3)	3.5(2)
O(2)	0.8693(3)	0.1936(2)	0.1355(3)	3.4(2)
O(3)	0.7119(3)	0.3446(3)	-0.0251(3)	4.2(2)
O(4)	0.8958(3)	0.0960(3)	0.0340(3)	4.6(2)
N(1)	0.6490(3)	0.2611(3)	0.3070(3)	2.8(2)
N(2)	0.7066(4)	0.1104(3)	0.1952(3)	2.8(2)
N(3)	0.8559(4)	0.1844(3)	0.3397(3)	2.9(2)
N(4)	0.8031(4)	0.3502(3)	0.2268(3)	2.8(2)
C(1)	0.5421(4)	0.2402(4)	0.2612(4)	3.1(3)
C(2)	0.5354(5)	0.1473(4)	0.2521(5)	3.7(3)
C(3)	0.5893(5)	0.1048(4)	0.1779(4)	3.4(3)
C(4)	0.7576(5)	0.0641(4)	0.2791(4)	3.2(3)
C(5)	0.8662(5)	0.0970(4)	0.3164(4)	3.4(3)
C(6)	0.9527(5)	0.2330(4)	0.3762(4)	3.5(3)
C(7)	0.9764(4)	0.2980(4)	0.3060(4)	3.5(3)
C(8)	0.9015(5)	0.3690(4)	0.2934(4)	3.3(3)
C(9)	0.7122(5)	0.3932(4)	0.2560(4)	3.4(3)
C(10)	0.6699(5)	0.3477(4)	0.3338(4)	3.5(3)
C(11)	0.4558(5)	0.2712(4)	0.3140(5)	3.6(3)
C(12)	0.3643(5)	0.3025(4)	0.2643(5)	4.3(3)
C(13)	0.2837(5)	0.3269(5)	0.3120(6)	5.4(4)
C(14)	0.2928(6)	0.3229(5)	0.4081(6)	5.4(4)
C(15)	0.3837(6)	0.2930(5)	0.4584(5)	5.5(4)
C(16)	0.4652(5)	0.2666(5)	0.4121(5)	4.8(4)

Table A1.b. General Temperature Factor Expressions, U's, for NiL_2.

atom	U11	U22	U33	U12	U13	U23
C(28)	0.055(4)	0.039(4)	0.036(4)	0.006(3)	0.015(3)	0.001(3)
H(1)	0.0478					
H(1N)	0.0418					
H(2A)	0.0606					
H(2B)	0.0606					
H(3)	0.0547					
H(3N)	0.0444					
H(4A)	0.0496					
H(4B)	0.0496					
H(5A)	0.0474					
H(5B)	0.0474					
H(6)	0.0553					
H(7A)	0.0532					
H(7B)	0.0532					
H(8)	0.0562					
H(9A)	0.0522					
H(9B)	0.0522					
H(10A)	0.0513					

Table A1.b. General Temperature Factor Expressions, U's, for NiL_2.

atom	U11	U22	U33	U12	U13	U23
H(10B)	0.0513					
H(12)	0.0647					
H(13)	0.0859					
H(14)	0.0787					
H(15)	0.0839					
H(16)	0.0710					
H(17A)	0.0781					
H(17B)	0.0781					
H(17C)	0.0781					
H(18A)	0.0513					
H(18B)	0.0513					
H(21)	0.0935					
H(22)	0.1105					
H(23)	0.1581					
H(24)	0.1562					
H(25)	0.1287					
H(26A)	0.0737					
H(26B)	0.0737					

Table A1.b. General Temperature Factor Expressions, U's, for NiL_2.

atom	U11	U22	U33	U12	U13	U23
H(26C)	0.0737					
H(27A)	0.0515					
H(27B)	0.0515					
O(5)	0.0974					
O(6)	0.1011					
H(5OA)	0.1154					
H(5OB)	0.1184					
H(6OA)	0.2120					
H(6OB)	0.1199					
O(7)	0.1184					
H(7OA)	0.1393					
H(7OB)	0.2264					

Table A1.b. General Temperature Factor Expressions, U's, for NiL_2.

atom	U11	U22	U33	U12	U13	U23
Ni(1)	0.0340(4)	0.0323(4)	0.0336(4)	-0.0007(4)	0.0079(3)	-0.0006(4)
O(1)	0.048(3)	0.045(3)	0.037(2)	-0.005(2)	0.003(2)	0.004(2)
O(2)	0.047(3)	0.042(3)	0.045(3)	-0.005(2)	0.018(2)	-0.009(2)
O(3)	0.068(3)	0.058(3)	0.037(3)	-0.007(3)	0.013(2)	0.004(2)
O(4)	0.062(3)	0.061(3)	0.056(3)	0.000(3)	0.027(3)	-0.016(3)
N(1)	0.034(3)	0.038(3)	0.035(3)	0.002(2)	0.011(2)	0.001(2)
N(2)	0.034(3)	0.035(3)	0.037(3)	-0.001(2)	0.007(2)	-0.002(2)
N(3)	0.035(3)	0.037(3)	0.037(3)	0.003(2)	0.004(2)	0.002(2)
N(4)	0.038(3)	0.034(3)	0.035(3)	-0.003(2)	0.007(2)	0.001(2)
C(1)	0.036(3)	0.048(4)	0.036(3)	0.002(3)	0.008(3)	-0.002(3)
C(2)	0.036(4)	0.045(4)	0.062(5)	-0.005(3)	0.012(3)	-0.000(4)
C(3)	0.038(4)	0.043(4)	0.047(4)	-0.004(3)	0.005(3)	-0.007(3)
C(4)	0.042(4)	0.035(3)	0.044(4)	-0.001(3)	0.010(3)	0.002(3)
C(5)	0.044(4)	0.039(4)	0.047(4)	0.008(3)	0.010(3)	0.007(3)
C(6)	0.042(4)	0.044(4)	0.046(4)	-0.003(3)	0.000(3)	-0.001(3)
C(7)	0.033(4)	0.049(4)	0.050(4)	-0.007(3)	0.005(3)	-0.005(3)
C(8)	0.043(4)	0.040(4)	0.043(4)	-0.007(3)	0.006(3)	-0.000(3)
C(9)	0.048(4)	0.036(4)	0.047(4)	0.003(3)	0.006(3)	-0.003(3)

Table A1.b. General Temperature Factor Expressions, U's, for NiL_2.

atom	U11	U22	U33	U12	U13	U23
C(10)	0.044(4)	0.043(4)	0.049(4)	0.002(3)	0.015(3)	-0.009(3)
C(11)	0.034(4)	0.042(4)	0.061(4)	-0.001(3)	0.013(3)	-0.003(4)
C(12)	0.042(4)	0.058(5)	0.064(5)	0.003(4)	0.012(4)	0.005(4)
C(13)	0.039(4)	0.070(6)	0.098(7)	0.013(4)	0.012(4)	0.010(5)
C(14)	0.046(5)	0.071(6)	0.095(7)	0.003(4)	0.030(5)	-0.013(5)
C(15)	0.059(5)	0.096(7)	0.059(5)	-0.006(5)	0.026(4)	-0.014(5)
C(16)	0.047(4)	0.086(6)	0.053(4)	0.006(4)	0.015(3)	0.001(4)
C(17)	0.051(5)	0.053(5)	0.095(6)	-0.011(4)	0.009(4)	-0.019(4)
C(18)	0.051(4)	0.044(4)	0.043(4)	-0.002(3)	0.010(3)	-0.011(3)
C(19)	0.050(4)	0.044(4)	0.035(4)	0.007(3)	0.014(3)	0.002(3)
C(20)	0.046(5)	0.047(5)	0.072(5)	-0.006(4)	-0.009(4)	0.005(4)
C(21)	0.051(5)	0.052(5)	0.118(7)	0.003(4)	-0.004(5)	-0.010(5)
C(22)	0.072(7)	0.066(6)	0.15(1)	0.003(5)	-0.017(7)	-0.012(7)
C(23)	0.077(8)	0.081(8)	0.19(2)	-0.005(6)	-0.05(1)	0.03(1)
C(24)	0.11(1)	0.20(2)	0.12(1)	-0.01(1)	-0.031(8)	0.06(1)
C(25)	0.071(6)	0.128(9)	0.084(7)	-0.004(6)	-0.027(5)	0.038(6)
C(26)	0.064(5)	0.047(4)	0.069(5)	-0.018(4)	0.001(4)	0.004(4)
C(27)	0.054(4)	0.036(4)	0.038(4)	-0.011(3)	0.009(3)	0.003(3)

Table A1.c. Bond Distances (Å) for NiL_2.

atom	atom	distance	ADC(*)	atom	atom	distance	ADC(*)
O1	H16	2.628	55404	O4	H25	3.553	55404
O1	H1N	3.169	55404	C3	H15	3.516	55404
O1	H7OA	3.374	55404	C4	H24	3.261	75603
O1	H10B	3.552	55404	C4	H23	3.576	75603
O2	H25	2.877	55404	C5	H26B	3.244	74502
O2	H6	3.222	55404	C5	H26A	3.444	74502
O2	H5OA	3.246	65501	C5	H24	3.519	75603
O3	H3N	1.829	55404	C7	H13	3.418	65501
O3	H1N	1.968	55404	C10	H18B	3.384	4
O3	H4A	2.495	55404	C10	H17A	3.499	65502
O3	H2A	2.742	55404	C12	H6OA	3.047	1
O3	H7OB	2.765	55404	C12	H17C	3.210	65502
O3	H16	2.787	55404	C12	H24	3.422	45404
O3	H5B	3.287	55404	C12	H17B	3.450	65502
O3	H10B	3.324	55404	C13	H4B	3.127	65502
O3	H6	3.478	55404	C13	H7B	3.130	45501
O3	H23	3.558	75502	C13	H24	3.161	45404
O3	H7OA	3.566	55404	C13	H17B	3.168	65502
O4	H5OB	1.791	65503	C13	H6OA	3.339	1
O4	H5OA	1.861	65501	C13	H17C	3.417	65502
O4	H8	2.531	55404	C13	H18A	3.491	65502
O4	H6	2.819	55404	C13	H21	3.563	45501
O4	H10B	2.945	55404	C14	H17B	3.127	65502
O4	H5OB	3.060	65501	C14	H7B	3.207	45501
O4	H26A	3.130	74502	C14	H18A	3.388	65502
O4	H5OA	3.460	65503	C15	H3	3.285	4

Contacts out to 3.60 angstroms. Estimated standard deviations in the least significant figure are given in parentheses.

Table A1.c. Bond Distances (Å) for NiL_2.

atom	atom	distance	ADC(*)	atom	atom	distance	ADC(*)
C15	H17B	3.365	65502	C26	H5OB	3.532	65504
C16	H3	3.471	4	C27	H25	3.283	55404
C17	H10A	3.131	64502	C27	H3N	3.302	55404
C18	H5OB	3.117	65503	C28	H3N	2.682	55404
C18	H10B	3.281	55404	C28	H1N	2.865	55404
C19	H5OB	2.758	65503	C28	H16	3.045	55404
C19	H5OA	2.810	65501	C28	H7OB	3.117	55404
C19	H10B	3.078	55404	C28	H7OA	3.439	55404
C19	H6	3.240	55404	H1	H15	2.968	55404
C19	H26A	3.390	74502	H1	H7OA	3.094	55404
C19	H8	3.443	55404	H2A	H7OB	2.910	1
C19	H25	3.565	55404	H2A	O7	3.319	65603
C21	H26C	3.066	74502	H2B	O6	2.704	1
C21	H6OA	3.392	65501	H2B	H15	3.272	55404
C22	H27A	2.982	74502	H2B	H6OA	3.293	1
C22	H26C	3.057	74502	H2B	H22	3.510	45501
C23	H27A	3.167	74502	H3	H15	2.736	55404
C23	H7OA	3.526	65501	H3	H16	3.164	55404
C23	H7OB	3.543	75603	H3N	H27B	3.003	4
C24	H13	3.197	65504	H3N	H27A	3.484	4
C24	H12	3.310	65504	H4A	H23	2.959	75603
C24	H5B	3.414	75603	H4A	H7OB	3.296	1
C24	H4B	3.436	75603	H4A	H24	3.301	75603
C24	H26B	3.476	4	H4B	H24	2.566	75603
C25	H27B	3.000	4	H4B	H13	2.642	64502
C26	H5A	3.063	75502	H4B	H23	3.316	75603

Contacts out to 3.60 angstroms. Estimated standard deviations in the least significant figure are given in parentheses.

Table A1.c. Bond Distances (Å) for NiL_2.

atom	atom	distance	ADC(*)	atom	atom	distance	ADC(*)
H4B	H26A	3.363	74502	H9B	H7OB	3.137	55404
H4B	H26B	3.392	74502	H9B	H22	3.500	75502
H5A	H26A	2.731	74502	H9B	H17C	3.535	65502
H5A	H26B	2.799	74502	H10A	H17A	2.677	65502
H5A	H26C	2.917	74502	H10A	H17C	2.988	65502
H5B	H26B	2.927	74502	H10A	H18B	3.094	4
H5B	H24	2.932	75603	H10A	H17B	3.215	65502
H5B	H23	3.467	75603	H10B	H18B	2.696	4
H5B	H26A	3.571	74502	H12	H6OA	2.855	1
H5B	H26C	3.600	74502	H12	H24	2.965	45404
H6	H5OA	2.966	65504	H12	H15	3.041	55404
H6	H27B	3.291	4	H12	H7OA	3.154	55404
H7A	H25	2.897	55404	H12	H17C	3.282	65502
H7A	H13	3.367	65501	H12	H23	3.370	45404
H7B	H13	2.596	65501	H12	O6	3.471	1
H7B	H14	2.735	65501	H13	H24	2.395	45404
H7B	H5OA	3.170	65504	H13	H18A	3.290	65502
H7B	O5	3.195	65504	H13	H6OA	3.296	1
H8	H5OB	3.004	65502	H13	H26A	3.409	45501
H8	H5OA	3.019	65504	H13	H26B	3.420	45501
H9A	O6	2.836	65502	H13	H21	3.444	45501
H9A	H22	2.913	75502	H13	H17B	3.495	65502
H9A	H6OB	2.979	65502	H14	O5	2.497	4
H9A	H17A	3.340	65502	H14	H6OB	2.725	4
H9B	H7OA	2.713	55404	H14	H18A	3.058	65502
H9B	O7	3.063	55404	H14	H6OA	3.126	4

Contacts out to 3.60 angstroms. Estimated standard deviations in the least significant figure are given in parentheses.

Table A1.c. Bond Distances (Å) for NiL_2.

atom	atom	distance	ADC(*)	atom	atom	distance	ADC(*)
H14	O6	3.162	4	H22	H6OB	3.302	65501
H14	H5OA	3.175	4	H23	H7OB	2.684	75603
H14	H5OB	3.199	4	H23	H7OA	2.810	65501
H14	H17B	3.449	65502	H23	H27A	3.026	74502
H15	O6	3.148	4	H23	O7	3.030	65501
H15	H6OA	3.183	4	H23	O7	3.508	75603
H15	H6OB	3.543	4	H24	H26B	2.906	4
H15	H17A	3.579	4	H25	H27B	2.264	4
H16	H7OA	3.228	1	H25	H5OA	3.211	65504
H16	H7OB	3.551	1	H25	H26B	3.402	4
H17A	O6	3.288	1	H25	H6OA	3.424	65504
H17A	H17B	3.571	65503	H26A	H5OB	2.609	65504
H17C	H7OA	3.411	65603	H26A	O5	2.988	65504
H17C	O7	3.573	65603	H26A	H5OA	3.163	65504
H18A	H5OB	2.661	65503	H26A	H5OA	3.234	65502
H18A	H26A	3.034	74502	H26A	H5OB	3.286	65502
H18A	O5	3.129	65503	H26A	O5	3.544	65502
H18B	H5OB	3.384	65503	H26C	H6OB	2.944	65502
H21	H6OA	2.545	65501	H26C	O6	3.312	65502
H21	H26C	2.845	74502	H26C	H5OA	3.387	65502
H21	O6	3.051	65501	H26C	O5	3.447	65502
H21	H6OB	3.140	65501	H26C	H5OB	3.501	65502
H22	O6	2.674	65501	H27A	H7OB	3.382	55404
H22	H26C	2.800	74502	O5	H6OB	1.582	1
H22	H27A	2.906	74502	O5	H6OA	2.814	1
H22	H6OA	2.967	65501	O5	H5OB	2.954	3

Contacts out to 3.60 angstroms. Estimated standard deviations in the least significant figure are given in parentheses.

Table A1.c. Bond Distances (Å) for NiL_2.

atom	atom	distance	ADC(*)	atom	atom	distance	ADC(*)
O5	H5OA	3.426	3				
O6	H5OA	3.222	1				
O6	H5OB	3.440	1				
H5OA	H6OB	2.144	1				
H5OA	H5OB	2.442	3				
H5OA	H6OA	3.028	1				
H5OA	H5OA	3.438	3				
H5OB	H6OB	2.367	1				
H5OB	H5OB	2.469	3				

Contacts out to 3.60 angstroms. Estimated standard deviations in the least significant figure are given in parentheses.

Table A1.c. Bond Distances (Å) for NiL_2.

atom	atom	distance	ADC(*)	atom	atom	distance	ADC(*)
NI1	O1	2.072(4)	1	C3	C17	1.524(9)	1
NI1	O2	2.093(4)	1	C4	C5	1.528(8)	1
NI1	N1	2.094(5)	1	C6	C7	1.529(8)	1
NI1	N2	2.080(5)	1	C6	C20	1.505(9)	1
NI1	N3	2.084(5)	1	C7	C8	1.513(8)	1
NI1	N4	2.078(5)	1	C8	C26	1.525(8)	1
O1	C28	1.267(7)	1	C9	C10	1.511(8)	1
O2	C19	1.253(7)	1	C11	C12	1.386(8)	1
O3	C28	1.263(7)	1	C11	C16	1.388(9)	1
O4	C19	1.248(7)	1	C12	C13	1.393(9)	1
N1	C1	1.481(7)	1	C13	C14	1.36(1)	1
N1	C10	1.492(7)	1	C14	C15	1.37(1)	1
N2	C3	1.507(7)	1	C15	C16	1.399(9)	1
N2	C4	1.486(7)	1	C18	C19	1.519(8)	1
N2	C18	1.478(7)	1	C20	C21	1.34(1)	1
N3	C5	1.489(7)	1	C20	C25	1.38(1)	1
N3	C6	1.513(7)	1	C21	C22	1.43(1)	1
N4	C8	1.503(7)	1	C22	C23	1.34(1)	1
N4	C9	1.489(7)	1	C23	C24	1.41(2)	1
N4	C27	1.478(7)	1	C24	C25	1.36(1)	1
C1	C2	1.538(8)	1	C27	C28	1.519(8)	1
C1	C11	1.531(8)	1	O7	O7	1.4582(5)	65603
C2	C3	1.524(8)	1				

Distances are in angstroms. Estimated standard deviations in the least significant figure are given in parentheses.

Table A1.c. Bond Distances (Å) for NiL_2.

atom	atom	distance	atom	atom	distance
N1	H1N	1.051	C16	H16	0.945
N3	H3N	1.133	C17	H17A	0.923
C1	H1	0.969	C17	H17B	1.060
C2	H2A	1.054	C17	H17C	0.937
C2	H2B	0.918	C18	H18A	0.998
C3	H3	0.959	C18	H18B	0.867
C4	H4A	1.013	C21	H21	1.055
C4	H4B	1.020	C22	H22	1.060
C5	H5A	0.913	C23	H23	0.965
C5	H5B	0.966	C24	H24	0.966
C6	H6	1.003	C25	H25	1.153
C7	H7A	0.949	C26	H26A	1.028
C7	H7B	1.012	C26	H26B	1.012
C8	H8	1.010	C26	H26C	0.980
C9	H9A	0.974	C27	H27A	0.946
C9	H9B	0.984	C27	H27B	1.033
C10	H10A	0.967	O5	H5OA	1.052
C10	H10B	1.009	O5	H5OB	1.120
C12	H12	0.970	O6	H6OA	1.164
C13	H13	0.923	O6	H6OB	1.132
C14	H14	1.019	O7	H7OA	1.123
C15	H15	0.951	O7	H7OB	1.164

Distances are in angstroms. Estimated standard deviations in the least significant figure are given in parentheses.

Table A1.c. Bond Distances (Å) for NiL_2.

atom	atom	distance	ADC(*)	atom	atom	distance	ADC(*)
O1	C16	3.499(8)	55404	O4	O5	2.885(5)	65503
O3	N3	2.923(6)	55404	O4	C8	3.491(8)	55404
O3	N1	2.972(6)	55404	C14	O5	3.499(7)	4
O3	C4	3.304(7)	55404	C22	O6	3.58(1)	65501
O3	C5	3.380(7)	55404	O5	O6	2.696(2)	1
O4	O5	2.852(5)	65501				

Contacts out to 3.60 angstroms. Estimated standard deviations in the least significant figure are given in parentheses.

(*)footnote

The ADC (atom designator code) specifies the position of an atom in a crystal. The 5-digit number shown in the table is a composite of three one digit numbers and one two digit number: TA(1st digit) + TB(2nd digit) + TC(3rd digit) + SN(4th and 5th digit). TA, TB, & TC are the crystal lattice translation digits along cell edges a, b, and c. A translation digit of 5 indicates the origin unit cell. If TA=4, this indicates a translation of one unit cell length along the a axis in the negative direction. Each translation digit can range in value from 1 to 9 and thus (+/-)4 lattice translations from the origin (TA=5,TB=5,TC=5) can be represented.

The SN or symmetry operator number refers to the number of the symmetry operator used to generate the coordinates of the target atom. A list of the symmetry operators relevant to this structure are given below.

For a given intermolecular contact, the first atom (origin atom) is located in the origin unit cell (TA=5,TB=5,TC=5) and its position can be generated using the identity operator (SN=1). Thus, the ADC for an origin atom is always ADC=55501. The position of the second atom (target atom) can be generated using the ADC and the coordinates of that atom in the parameter table. For example, an ADC of 47502 refers to the target atom moved through operator two, then translated -1 cell translations along the a axis, +2 cell translations along the b axis, and 0 cell translations along the c axis.

An ADC of 1 indicates an intermolecular contact between two fragments (i.e.cation and anion) that reside in the same asymmetric unit.

Symmetry Operators:

(1)	+X	,	+Y	,	+Z	(2)	-X	,1/2+Y	,1/2-Z
(3)	-X	,	-Y	,	-Z	(4)	+X	,1/2-Y	,1/2+Z

Table A1.d. Bond Angles (°) for NiL_2

atom	atom	atom	angle	atom	atom	atom	angle
NI1	N1	H1N	114.85	H5A	C5	H5B	110.80
C1	N1	H1N	100.62	N3	C6	H6	101.40
C10	N1	H1N	107.09	C7	C6	H6	105.58
NI1	N3	H3N	110.12	C20	C6	H6	108.46
C5	N3	H3N	101.75	C6	C7	H7A	108.69
C6	N3	H3N	104.27	C6	C7	H7B	106.36
N1	C1	H1	108.22	C8	C7	H7A	110.83
C2	C1	H1	108.52	C8	C7	H7B	106.43
C11	C1	H1	108.07	H7A	C7	H7B	108.85
C1	C2	H2A	103.82	N4	C8	H8	105.39
C1	C2	H2B	108.66	C7	C8	H8	104.43
C3	C2	H2A	112.82	C26	C8	H8	108.33
C3	C2	H2B	105.46	N4	C9	H9A	114.96
H2A	C2	H2B	106.06	N4	C9	H9B	108.43
N2	C3	H3	105.27	C10	C9	H9A	110.59
C2	C3	H3	104.71	C10	C9	H9B	109.27
C17	C3	H3	109.17	H9A	C9	H9B	101.78
N2	C4	H4A	109.92	N1	C10	H10A	112.41
N2	C4	H4B	111.08	N1	C10	H10B	103.27
C5	C4	H4A	107.67	C9	C10	H10A	112.70
C5	C4	H4B	111.67	C9	C10	H10B	112.22
H4A	C4	H4B	104.32	H10A	C10	H10B	104.70
N3	C5	H5A	110.66	C11	C12	H12	117.75
N3	C5	H5B	111.52	C13	C12	H12	121.78
C4	C5	H5A	109.46	C12	C13	H13	117.02
C4	C5	H5B	106.09	C14	C13	H13	121.41

Angles are in degrees. Estimated standard deviations in the least significant figure are given in parentheses.

Table A1.d. Bond Angles (°) for NiL_2.

atom	atom	atom	angle	atom	atom	atom	angle
C13	C14	H14	121.60	C24	C25	H25	123.84
C15	C14	H14	119.68	C8	C26	H26A	112.62
C14	C15	H15	118.89	C8	C26	H26B	112.21
C16	C15	H15	119.94	C8	C26	H26C	115.45
C11	C16	H16	117.10	H26A	C26	H26B	102.03
C15	C16	H16	122.77	H26A	C26	H26C	106.82
C3	C17	H17A	108.75	H26B	C26	H26C	106.64
C3	C17	H17B	113.19	N4	C27	H27A	112.48
C3	C17	H17C	111.83	N4	C27	H27B	110.02
H17A	C17	H17B	102.60	C28	C27	H27A	111.65
H17A	C17	H17C	114.75	C28	C27	H27B	107.27
H17B	C17	H17C	105.44	H27A	C27	H27B	104.62
N2	C18	H18A	110.42	H5OA	O5	H5OB	105.52
N2	C18	H18B	104.27	H6OA	O6	H6OB	83.94
C19	C18	H18A	109.67	O7	O7	H7OA	139.98
C19	C18	H18B	109.07	O7	O7	H7OB	63.86
H18A	C18	H18B	108.93	H7OA	O7	H7OB	100.13
C20	C21	H21	122.71				
C22	C21	H21	116.32				
C21	C22	H22	111.26				
C23	C22	H22	132.08				
C22	C23	H23	120.03				
C24	C23	H23	114.91				
C23	C24	H24	115.05				
C25	C24	H24	128.30				
C20	C25	H25	112.43				

Angles are in degrees. Estimated standard deviations in the least significant figure are given in parentheses.

Table A1.d. Bond Angles (°) for NiL_2.

atom	atom	atom	angle	atom	atom	atom	angle
O1	NI1	O2	84.9(2)	NI1	N3	C5	102.8(3)
O1	NI1	N1	96.0(2)	NI1	N3	C6	117.4(4)
O1	NI1	N2	91.6(2)	C5	N3	C6	119.4(5)
O1	NI1	N3	174.6(2)	NI1	N4	C8	115.2(4)
O1	NI1	N4	80.8(2)	NI1	N4	C9	104.2(3)
O2	NI1	N1	178.6(2)	NI1	N4	C27	102.0(3)
O2	NI1	N2	82.8(2)	C8	N4	C9	111.0(5)
O2	NI1	N3	89.7(2)	C8	N4	C27	113.5(5)
O2	NI1	N4	94.8(2)	C9	N4	C27	110.3(5)
N1	NI1	N2	96.0(2)	N1	C1	C2	107.8(5)
N1	NI1	N3	89.4(2)	N1	C1	C11	114.4(5)
N1	NI1	N4	86.5(2)	C2	C1	C11	109.7(5)
N2	NI1	N3	87.3(2)	C1	C2	C3	119.3(5)
N2	NI1	N4	172.2(2)	N2	C3	C2	114.7(5)
N3	NI1	N4	100.1(2)	N2	C3	C17	113.0(5)
NI1	O1	C28	107.9(4)	C2	C3	C17	109.5(5)
NI1	O2	C19	113.0(4)	N2	C4	C5	111.9(5)
NI1	N1	C1	111.1(3)	N3	C5	C4	108.2(5)
NI1	N1	C10	106.3(3)	N3	C6	C7	112.6(5)
C1	N1	C10	117.1(5)	N3	C6	C20	114.6(5)
NI1	N2	C3	112.5(4)	C7	C6	C20	113.0(5)
NI1	N2	C4	104.4(3)	C6	C7	C8	115.4(5)
NI1	N2	C18	105.9(4)	N4	C8	C7	112.6(5)
C3	N2	C4	114.5(5)	N4	C8	C26	113.8(5)
C3	N2	C18	109.9(5)	C7	C8	C26	111.6(5)
C4	N2	C18	109.2(5)	N4	C9	C10	111.3(5)

Angles are in degrees. Estimated standard deviations in the least significant figure are given in parentheses.

Table A1.d. Bond Angles (°) for NiL_2

atom	atom	atom	angle	atom	atom	atom	angle
N1	C10	C9	111.0(5)				
C1	C11	C12	120.4(6)				
C1	C11	C16	121.3(6)				
C12	C11	C16	118.2(6)				
C11	C12	C13	120.4(7)				
C12	C13	C14	121.5(7)				
C13	C14	C15	118.6(7)				
C14	C15	C16	121.1(7)				
C11	C16	C15	120.1(7)				
N2	C18	C19	114.2(5)				
O2	C19	O4	125.9(6)				
O2	C19	C18	118.7(5)				
O4	C19	C18	115.4(6)				
C6	C20	C21	122.4(7)				
C6	C20	C25	118.0(8)				
C21	C20	C25	119.7(8)				
C20	C21	C22	120.8(9)				
C21	C22	C23	116(1)				
C22	C23	C24	125(1)				
C23	C24	C25	115(1)				
C20	C25	C24	123(1)				
N4	C27	C28	110.5(5)				
O1	C28	O3	124.2(6)				
O1	C28	C27	119.5(5)				
O3	C28	C27	116.3(6)				

Angles are in degrees. Estimated standard deviations in the least significant figure are given in parentheses.

Table A1.e. Torsion for NiL_2.

(1)	(2)	(3)	(4)	angle
C4	N2	C3	C17	-57.7(7)
C4	N2	C18	C19	-87.8(6)
C4	C5	N3	C6	-178.5(5)
C5	N3	C6	C7	112.7(6)
C5	N3	C6	C20	-18.3(8)
C5	C4	N2	C18	78.9(6)
C6	C7	C8	C26	149.7(5)
C6	C20	C21	C22	179.1(7)
C6	C20	C25	C24	-179(1)
C7	C6	C20	C21	-46.3(9)
C7	C6	C20	C25	132.2(7)
C7	C8	N4	C9	146.4(5)
C7	C8	N4	C27	-88.7(6)
C8	N4	C9	C10	-81.9(6)
C8	N4	C27	C28	161.8(5)
C8	C7	C6	C20	-157.9(5)
C9	N4	C8	C26	-85.3(6)
C9	N4	C27	C28	-73.1(6)
C10	N1	C1	C11	-50.5(7)
C10	C9	N4	C27	151.5(5)
C11	C12	C13	C14	2(1)
C11	C16	C15	C14	1(1)
C12	C11	C16	C15	0(1)
C12	C13	C14	C15	-1(1)
C13	C12	C11	C16	-1(1)
C13	C14	C15	C16	0(1)
C17	C3	N2	C18	65.6(7)
C20	C21	C22	C23	0(1)
C20	C25	C24	C23	-1(2)
C21	C20	C25	C24	0(1)
C21	C22	C23	C24	-2(2)
C22	C21	C20	C25	1(1)
C22	C23	C24	C25	2(2)
C26	C8	N4	C27	39.5(7)

The sign is positive if when looking from atom 2 to atom 3 a clockwise motion of atom 1 would superimpose it on atom 4.

Table A1.e. Torsion for NiL_2

(1)	(2)	(3)	(4)	angle	(1)	(2)	(3)	(4)	angle
NI1	O1	C28	O3	158.4(5)	O1	NI1	N4	C8	-161.1(4)
NI1	O1	C28	C27	-20.4(7)	O1	NI1	N4	C9	77.1(4)
NI1	O2	C19	O4	175.9(5)	O1	NI1	N4	C27	-37.7(4)
NI1	O2	C19	C18	-2.2(7)	O1	C28	C27	N4	-12.6(8)
NI1	N1	C1	C2	64.9(5)	O2	NI1	O1	C28	-62.2(4)
NI1	N1	C1	C11	-172.8(4)	O2	NI1	N1	C1	-85(7)
NI1	N1	C10	C9	31.4(5)	O2	NI1	N1	C10	147(7)
NI1	N2	C3	C2	-50.2(6)	O2	NI1	N2	C3	-139.6(4)
NI1	N2	C3	C17	-176.6(4)	O2	NI1	N2	C4	95.7(3)
NI1	N2	C4	C5	-33.9(5)	O2	NI1	N2	C18	-19.5(4)
NI1	N2	C18	C19	24.1(6)	O2	NI1	N3	C5	-60.0(4)
NI1	N3	C5	C4	-46.5(5)	O2	NI1	N3	C6	73.2(4)
NI1	N3	C6	C7	-12.6(6)	O2	NI1	N4	C8	-77.1(4)
NI1	N3	C6	C20	-143.6(5)	O2	NI1	N4	C9	161.1(3)
NI1	N4	C8	C7	28.3(6)	O2	NI1	N4	C27	46.3(4)
NI1	N4	C8	C26	156.6(4)	O2	C19	C18	N2	-15.8(8)
NI1	N4	C9	C10	42.7(5)	O3	C28	C27	N4	168.5(5)
NI1	N4	C27	C28	37.2(5)	O4	C19	C18	N2	165.9(5)
O1	NI1	O2	C19	-79.3(4)	N1	NI1	O1	C28	118.9(4)
O1	NI1	N1	C1	41.9(4)	N1	NI1	O2	C19	48(7)
O1	NI1	N1	C10	-86.6(4)	N1	NI1	N2	C3	41.2(4)
O1	NI1	N2	C3	-55.0(4)	N1	NI1	N2	C4	-83.5(3)
O1	NI1	N2	C4	-179.7(3)	N1	NI1	N2	C18	161.3(4)
O1	NI1	N2	C18	65.1(4)	N1	NI1	N3	C5	118.9(4)
O1	NI1	N3	C5	-56(2)	N1	NI1	N3	C6	-107.9(4)
O1	NI1	N3	C6	77(2)	N1	NI1	N4	C8	102.3(4)

The sign is positive if when looking from atom 2 to atom 3 a clockwise motion of atom 1 would superimpose it on atom 4.

Table A1.e. Torsion for NiL_2

(1)	(2)	(3)	(4)	angle	(1)	(2)	(3)	(4)	angle
N1	NI1	N4	C9	-19.5(4)	N3	NI1	N4	C27	136.9(4)
N1	NI1	N4	C27	-134.3(4)	N3	C6	C7	C8	70.2(7)
N1	C1	C2	C3	-73.5(7)	N3	C6	C20	C21	84.6(8)
N1	C1	C11	C12	140.0(6)	N3	C6	C20	C25	-96.9(8)
N1	C1	C11	C16	-42.0(9)	N4	NI1	O1	C28	33.5(4)
N1	C10	C9	N4	-51.9(7)	N4	NI1	O2	C19	-159.6(4)
N2	NI1	O1	C28	-144.9(4)	N4	NI1	N1	C1	122.3(4)
N2	NI1	O2	C19	12.9(4)	N4	NI1	N1	C10	-6.2(4)
N2	NI1	N1	C1	-50.3(4)	N4	NI1	N2	C3	-67(1)
N2	NI1	N1	C10	-178.8(4)	N4	NI1	N2	C4	168(1)
N2	NI1	N3	C5	22.9(4)	N4	NI1	N2	C18	53(2)
N2	NI1	N3	C6	156.0(4)	N4	NI1	N3	C5	-154.8(3)
N2	NI1	N4	C8	-149(1)	N4	NI1	N3	C6	-21.6(4)
N2	NI1	N4	C9	89(1)	N4	C8	C7	C6	-80.9(6)
N2	NI1	N4	C27	-26(2)	C1	N1	C10	C9	-93.4(6)
N2	C3	C2	C1	66.0(7)	C1	C2	C3	C17	-165.7(6)
N2	C4	C5	N3	57.2(6)	C1	C11	C12	C13	176.7(6)
N3	NI1	O1	C28	-66(2)	C1	C11	C16	C15	-177.9(7)
N3	NI1	O2	C19	100.3(4)	C2	C1	N1	C10	-172.8(5)
N3	NI1	N1	C1	-137.6(4)	C2	C1	C11	C12	-98.8(7)
N3	NI1	N1	C10	93.9(4)	C2	C1	C11	C16	79.3(8)
N3	NI1	N2	C3	130.3(4)	C2	C3	N2	C4	68.7(7)
N3	NI1	N2	C4	5.6(3)	C2	C3	N2	C18	-167.9(5)
N3	NI1	N2	C18	-109.6(4)	C3	N2	C4	C5	-157.3(5)
N3	NI1	N4	C8	13.5(4)	C3	N2	C18	C19	145.8(5)
N3	NI1	N4	C9	-108.3(4)	C3	C2	C1	C11	161.3(5)

The sign is positive if when looking from atom 2 to atom 3 a clockwise motion of atom 1 would superimpose it on atom 4.

Appendix 2

Table A2.a. Atomic Coordinate and Equivalent Isotropic Displacement Parameters for CoL_1^+.

	x	y	z	U(eq)
Co	10000	5000	10000	23(1)
O(1)	11176(3)	5379(2)	9600(3)	28(1)
O(2)	12112(3)	6527(2)	9438(4)	46(1)
N(1)	8831(3)	5301(3)	8622(3)	29(1)
N(2)	9888(3)	6187(2)	10448(3)	30(1)
C(1)	10189(5)	2756(4)	8214(5)	47(1)
C(2)	10068(4)	3694(3)	8468(4)	37(1)
C(3)	9007(5)	4055(3)	7664(4)	38(1)
C(4)	8859(5)	5001(3)	7598(4)	36(1)
C(5)	7706(5)	5204(4)	6747(4)	50(2)
C(6)	9806(6)	5438(4)	7329(5)	48(1)
C(7)	8615(5)	6228(3)	8646(4)	36(1)
C(8)	8748(4)	6448(3)	9731(4)	33(1)
C(9)	10802(4)	6687(3)	10268(4)	33(1)
C(10)	11407(4)	6177(3)	9720(4)	31(1)
Co'	5000	10000	5000	23(1)
O(1')	3839(3)	9975(2)	5525(3)	30(1)
O(2')	3242(3)	9343(3)	6649(3)	45(1)
N(1')	5941(3)	10810(3)	6103(3)	30(1)
N(2')	5722(3)	9056(3)	5973(3)	29(1)
C(1')	3352(6)	12381(4)	3730(6)	54(2)
C(2')	3970(4)	11724(3)	4514(4)	36(1)
C(3')	4974(5)	12115(3)	5338(4)	39(1)
C(4')	5512(4)	11656(3)	6339(4)	37(1)
C(5')	4654(5)	11551(4)	6866(5)	47(1)
C(6')	6509(6)	12176(4)	7025(5)	54(2)
C(7')	6511(5)	10296(4)	7026(4)	44(1)
C(8')	6784(4)	9451(4)	6700(4)	40(1)
C(9')	4937(4)	8832(3)	6514(4)	33(1)
C(10')	3924(4)	9422(3)	6221(4)	30(1)
Br	8587(4)	8710(2)	9239(3)	96(2)
Cl	8740(8)	8727(9)	9171(12)	75(4)

Table A2.b. Bond Lengths (Å) and Angles (°) for CoL_1^*.

Co-O(1)#1	1.880(3)
Co-O(1)	1.880(3)
Co-N(2)#1	2.004(4)
Co-N(2)	2.004(4)
Co-N(1)	2.020(4)
Co-N(1)#1	2.020(4)
O(1)-C(10)	1.294(6)
O(2)-C(10)	1.236(6)
N(1)-C(7)	1.495(6)
N(1)-C(4)	1.533(7)
N(2)-C(8)	1.489(6)
N(2)-C(9)	1.503(6)
N(2)-C(2)#1	1.518(7)
C(1)-C(2)	1.547(8)
C(2)-N(2)#1	1.518(7)
C(2)-C(3)	1.518(7)
C(3)-C(4)	1.507(7)
C(4)-C(5)	1.548(8)
C(4)-C(6)	1.551(8)
C(7)-C(8)	1.515(8)
C(9)-C(10)	1.508(7)
Co'-O(1')#2	1.879(3)
Co'-O(1')	1.879(3)
Co'-N(2')#2	2.007(4)
Co'-N(2')	2.008(4)
Co'-N(1')	2.030(4)
Co'-N(1')#2	2.030(4)
O(1')-C(10')	1.288(6)
O(2')-C(10')	1.232(6)
N(1')-C(7')	1.478(7)
N(1')-C(4')	1.528(7)
N(2')-C(8')	1.499(6)
N(2')-C(9')	1.504(6)
N(2')-C(2')#2	1.532(7)
C(1')-C(2')	1.510(8)
C(2')-C(3')	1.506(8)
C(2')-N(2')#2	1.532(7)
C(3')-C(4')	1.508(8)
C(4')-C(6')	1.521(8)
C(4')-C(5')	1.537(7)
C(7')-C(8')	1.496(8)
C(9')-C(10')	1.519(7)

O(1)#1-Co-O(1)	180.0
O(1)#1-Co-N(2)#1	87.3(2)
O(1)-Co-N(2)#1	92.7(2)
O(1)#1-Co-N(2)	92.7(2)
O(1)-Co-N(2)	87.3(2)
N(2)#1-Co-N(2)	179.998(1)
O(1)#1-Co-N(1)	88.7(2)
O(1)-Co-N(1)	91.3(2)
N(2)#1-Co-N(1)	91.8(2)
N(2)-Co-N(1)	88.2(2)
O(1)#1-Co-N(1)#1	91.3(2)
O(1)-Co-N(1)#1	88.7(2)
N(2)#1-Co-N(1)#1	88.2(2)
N(2)-Co-N(1)#1	91.8(2)
N(1)-Co-N(1)#1	179.998(1)
C(10)-O(1)-Co	116.0(3)
C(7)-N(1)-C(4)	113.2(4)
C(7)-N(1)-Co	106.6(3)
C(4)-N(1)-Co	124.6(3)

Table A2.b. Bond Lengths (Å) and Angles (°) for CoL_t^+.

C(8)-N(2)-C(9)	111.1(4)
C(8)-N(2)-C(2)#1	108.3(4)
C(9)-N(2)-C(2)#1	111.1(4)
C(8)-N(2)-Co	102.1(3)
C(9)-N(2)-Co	106.9(3)
C(2)#1-N(2)-Co	116.9(3)
N(2)#1-C(2)-C(3)	113.4(4)
N(2)#1-C(2)-C(1)	112.5(4)
C(3)-C(2)-C(1)	109.0(5)
C(4)-C(3)-C(2)	118.4(5)
C(3)-C(4)-N(1)	107.1(4)
C(3)-C(4)-C(5)	108.4(5)
N(1)-C(4)-C(5)	108.7(4)
C(3)-C(4)-C(6)	111.6(5)
N(1)-C(4)-C(6)	112.4(4)
C(5)-C(4)-C(6)	108.5(5)
N(1)-C(7)-C(8)	107.1(4)
N(2)-C(8)-C(7)	109.9(4)
N(2)-C(9)-C(10)	112.1(4)
O(2)-C(10)-O(1)	123.4(5)
O(2)-C(10)-C(9)	119.4(4)
O(1)-C(10)-C(9)	117.1(4)
O(1')#2-Co'-O(1')	180.0
O(1')#2-Co'-N(2')#2	86.8(2)
O(1')-Co'-N(2')#2	93.2(2)
O(1')#2-Co'-N(2')	93.2(2)
O(1')-Co'-N(2')	86.8(2)
N(2')#2-Co'-N(2')	180.0
O(1')#2-Co'-N(1')	87.8(2)
O(1')-Co'-N(1')	92.2(2)
N(2')#2-Co'-N(1')	92.6(2)
N(2')-Co'-N(1')	87.4(2)
O(1')#2-Co'-N(1')#2	92.2(2)
O(1')-Co'-N(1')#2	87.8(2)
N(2')#2-Co'-N(1')#2	87.4(2)
N(2')-Co'-N(1')#2	92.6(2)
N(1')-Co'-N(1')#2	180.000(1)
C(10')-O(1')-Co'	117.1(3)
C(7')-N(1')-C(4')	113.0(4)
C(7')-N(1')-Co'	106.6(3)
C(4')-N(1')-Co'	124.3(3)
C(8')-N(2')-C(9')	110.6(4)
C(8')-N(2')-C(2')#2	109.1(4)
C(9')-N(2')-C(2')#2	111.4(4)
C(8')-N(2')-Co'	103.1(3)
C(9')-N(2')-Co'	107.4(3)
C(2')#2-N(2')-Co'	114.9(3)
C(3')-C(2')-C(1')	110.3(5)
C(3')-C(2')-N(2')#2	113.1(4)
C(1')-C(2')-N(2')#2	112.1(5)
C(2')-C(3')-C(4')	119.2(4)
C(3')-C(4')-C(6')	108.6(5)
C(3')-C(4')-N(1')	107.1(4)
C(6')-C(4')-N(1')	109.3(4)
C(3')-C(4')-C(5')	110.2(5)
C(6')-C(4')-C(5')	109.0(5)
N(1')-C(4')-C(5')	112.6(4)
N(1')-C(7')-C(8')	108.5(4)
N(2')-C(8')-C(7')	109.3(4)
N(2')-C(9')-C(10')	111.9(4)
O(2')-C(10')-O(1')	124.4(4)
O(2')-C(10')-C(9')	118.9(4)
O(1')-C(10')-C(9')	116.7(4)

Table A2.c. Anisotropic Displacement Parameters for CoL_1^+.

	U11	U22	U33	U23	U13	U12
Co	20(1)	20(1)	32(1)	2(1)	12(1)	1(1)
O(1)	25(2)	27(2)	37(2)	1(1)	16(1)	-1(1)
O(2)	48(2)	30(2)	75(3)	5(2)	39(2)	-4(2)
N(1)	27(2)	27(2)	34(2)	3(2)	12(2)	2(2)
N(2)	28(2)	21(2)	44(2)	0(2)	18(2)	2(2)
C(1)	48(3)	47(3)	49(3)	-6(3)	21(3)	8(3)
C(2)	35(3)	38(3)	41(3)	-4(2)	18(2)	-1(2)
C(3)	41(3)	34(3)	39(3)	-6(2)	15(2)	-2(2)
C(4)	39(3)	38(3)	33(3)	-2(2)	14(2)	3(2)
C(5)	49(3)	58(4)	35(3)	7(3)	7(3)	13(3)
C(6)	63(4)	41(3)	55(4)	7(3)	39(3)	-2(3)
C(7)	38(3)	26(2)	44(3)	8(2)	13(2)	9(2)
C(8)	29(2)	24(2)	46(3)	3(2)	15(2)	5(2)
C(9)	34(2)	22(2)	45(3)	-1(2)	19(2)	-3(2)
C(10)	24(2)	27(2)	40(3)	6(2)	11(2)	2(2)
Co'	20(1)	27(1)	24(1)	2(1)	9(1)	0(1)
O(1')	25(2)	36(2)	31(2)	7(1)	13(1)	0(1)
O(2')	40(2)	58(3)	44(2)	15(2)	24(2)	7(2)
N(1')	26(2)	36(2)	27(2)	-4(2)	8(2)	-4(2)
N(2')	24(2)	34(2)	31(2)	6(2)	12(2)	2(2)
C(1')	54(4)	41(3)	69(4)	17(3)	25(3)	18(3)
C(2')	38(3)	31(2)	50(3)	11(2)	28(2)	8(2)
C(3')	46(3)	29(2)	47(3)	1(2)	23(3)	2(2)
C(4')	36(3)	38(3)	43(3)	-8(2)	21(2)	-5(2)
C(5')	55(3)	52(3)	42(3)	-13(3)	30(3)	-6(3)
C(6')	65(4)	48(3)	57(4)	-18(3)	33(3)	-18(3)
C(7')	43(3)	45(3)	32(3)	2(2)	1(2)	-3(2)
C(8')	27(2)	48(3)	35(3)	4(2)	1(2)	-1(2)
C(9')	34(2)	35(3)	38(3)	13(2)	24(2)	5(2)
C(10')	27(2)	37(3)	27(2)	1(2)	12(2)	-1(2)
Br	146(3)	38(1)	54(1)	7(1)	-21(2)	2(2)
Cl	38(3)	56(5)	88(8)	32(4)	-26(3)	-11(3)